

# Sheffield Hallam University

*Investigation of M2 and anti-segregation process HSS flat broaching tools.*

ALIM, Shahzad.

Available from the Sheffield Hallam University Research Archive (SHURA) at:

<http://shura.shu.ac.uk/19244/>

## A Sheffield Hallam University thesis

This thesis is protected by copyright which belongs to the author.

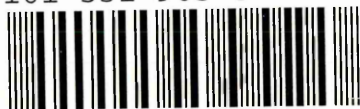
The content must not be changed in any way or sold commercially in any format or medium without the formal permission of the author.

When referring to this work, full bibliographic details including the author, title, awarding institution and date of the thesis must be given.

Please visit <http://shura.shu.ac.uk/19244/> and <http://shura.shu.ac.uk/information.html> for further details about copyright and re-use permissions.

SHEFFIELD HALLAM UNIVERSITY LIBRARY  
CITY CAMPUS POND STREET  
SHEFFIELD S1 1WB

101 531 903 3



BRN  
376673

Sheffield Hallam University

**REFERENCE ONLY**

ProQuest Number: 10694124

All rights reserved

INFORMATION TO ALL USERS

The quality of this reproduction is dependent upon the quality of the copy submitted.

In the unlikely event that the author did not send a complete manuscript and there are missing pages, these will be noted. Also, if material had to be removed, a note will indicate the deletion.



ProQuest 10694124

Published by ProQuest LLC (2017). Copyright of the Dissertation is held by the Author.

All rights reserved.

This work is protected against unauthorized copying under Title 17, United States Code  
Microform Edition © ProQuest LLC.

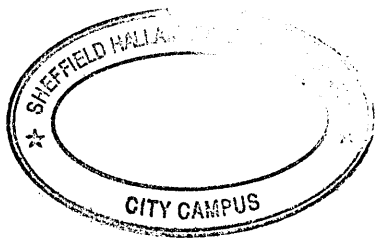
ProQuest LLC.  
789 East Eisenhower Parkway  
P.O. Box 1346  
Ann Arbor, MI 48106 – 1346

**Investigation of M2 and Anti-segregation  
Process HSS Flat Broaching Tools**

Shahzad Alim

A thesis submitted in partial fulfilment of the  
requirements of  
Sheffield Hallam University  
for the degree of Master of Philosophy

June 1994



## ABSTRACT

An investigation has been carried out to compare the cutting performance and tool life evaluation of high speed steel broach samples. The comparison has been done between conventional M2 and Anti-Segregation Process (ASP) ASP53 and ASP30 high speed steel broach samples. The ASP53 was a development material. The cutting performance was evaluated by measuring the cutting forces and calculating the specific cutting energy, an indicator of cutting performance. As the roughness of the machined surface is an important criterion in the evaluation of performance of a tool, the surface roughness of the workpiece was studied as a function of undeformed chip thickness. The workpiece material was 150M36 alloy steel used in manufacture of automobile engines. The performance tests were conducted at two cutting speeds, which were 0.7 m/min and 10.5 m/min respectively. This allowed a better understanding of the effect of cutting speed on tool performance. The wear tests were performed at a cutting speed of 10.5 m/min.

The cutting edges of ASP broach samples were finer compared to that of M2. There was no practical difference in the cutting forces and the specific cutting energy while cutting with M2, ASP30 and ASP53 broach samples. The ASP30 and ASP53 tools gave a better surface roughness on the machined surface than that of M2 at both cutting speeds. The ASP30 gave 2.25 times the life and an improved surface finish compared to M2 steel. The ASP53 gave 1.3 times the life of M2 steel.

# CONTENTS

	Page
ABSTRACT	ii
LIST OF FIGURES	vi
LIST OF TABLES	xii
ACKNOWLEDGEMENT	xiii
<b>CHAPTER ONE: INTRODUCTION</b>	<b>1</b>
1.1 High speed steel	3
1.1.1 Carbon	4
1.1.2 Chromium	4
1.1.3 Tungsten and molybdenum	4
1.1.4 Vanadium	5
1.1.5 Cobalt	6
1.2 Anti-segregation process high speed steels (ASP HSS)	7
<b>CHAPTER TWO: MECHANICS OF MACHINING AND TOOL WEAR</b>	<b>8</b>
2.1 Mechanics of metal cutting	9
2.2 Cutting forces	9
2.3 Specific cutting energy	10
2.4 Chip formation	12
2.4.1 Discontinuous chip	13
2.4.2 Continuous chip	14
2.4.3 Built-up edge	15
2.5 Tool life and tool wear	16
2.6 Tool wear mechanisms	17
2.6.1 Adhesion wear	17
2.6.2 Abrasive wear	18

2.6.3	Diffusion wear	19
2.7	Forms of wear in metal cutting	19
2.7.1	Crater wear	19
2.7.2	Flank wear	20
2.8	Tool life criteria	20
2.9	Premature tool failure	22
<b>CHAPTER THREE: BROACHING</b>		24
3.1	Advantages of broaching	25
3.1.1	Productivity	25
3.1.2	Quality of machining	25
3.1.3	Operational economy	25
3.2	Broach types	26
3.2.1	Internal broaching	26
3.2.2	External or surface broaching	27
3.3	Broaching characteristics and broach design	27
3.3.1	Tooth rise	29
3.3.2	Pitch	29
3.3.3	Chip space	30
3.3.4	Load on broach	31
<b>CHAPTER FOUR: TOOL PERFORMANCE TESTS</b>		35
4.1	Measurement of broach samples	36
4.1.1	Geometric features	36
4.1.2	Surface roughness	36
4.1.3	Heat treatment and hardness	37
4.1.4	Chemical composition	39
4.1.5	Carbide distribution	39
4.1.6	The cutting edge	41
4.2	Workpiece material	41

4.3	Cutting conditions	42
4.4	Instrumentation and test procedure	43
4.4.1	Measurement of cutting forces	44
4.4.2	Specific cutting energy	45
4.4.3	Roughness of machined surface	45
4.5	Discussion of results	46
<b>CHAPTER FIVE: WEAR TESTS</b>		51
5.1	Cutting conditions	51
5.2	Test procedure	51
5.2.1	Measurement of wear land	52
5.2.2	Roughness of machined surface	53
5.3	Discussion of results	53
<b>CONCLUSIONS</b>		56
<b>REFERENCES</b>		58
<b>FIGURES</b>		62
<b>TABLES</b>		113

## LIST OF FIGURES

Figure No.	Caption	Page No.
Figure 2.1	A perspective view of orthogonal cutting.	62
Figure 2.2	A metal cutting diagram showing the rake angle $\gamma$ , clearance angle $\beta$ , cutting speed $V$ , undeformed chip thickness UCT, chip thickness $t_c$ and chip velocity $V_c$ .	62
Figure 2.3	Forces acting on the tool in orthogonal cutting.	63
Figure 2.4	Fragmental or discontinuous chips.	63
Figure 2.5	Continuous chip with built-up edge.	64
Figure 2.6	A micrograph showing the built-up edge and the wear scar on the clearance face (x25).	64
Figure 2.7	Formation and failure of built-up edge leaving a poor machined surface. The built-up edge has been shaded dark only to illustrate.	65
Figure 2.8	A diagram showing the effect of illumination on the machined surface while cutting with a built-up edge.	66
Figure 2.9	A micrograph showing the machined surface while cutting with a built-up edge. The illumination is along the direction of cut (x45).	66
Figure 2.10	A micrograph showing the machined surface while cutting with a built-up edge. The illumination is opposite to the direction of cut (x40).	67
Figure 2.11	Typical wear on a tool in orthogonal cutting.	67
Figure 2.12	A micrograph showing a typical wear scar in orthogonal cutting (x75).	68

Figure 2.13	Development of flank wear with time for a carbide tool at a cutting speed of 1 m/s.	69
Figure 2.14	Some features of single-point tool wear in turning operations.	69
Figure 3.1	A diagram showing the significant features of a round internal broach.	70
Figure 3.2	A diagram showing a flat broach and the use of a tapered bar.	71
Figure 4.1	A side view of the broach sample showing the geometric features. $R_1$ is the rake angle radius and $R_2$ is the back-of-tooth radius.	72
Figure 4.2	A sketch showing the directions of measuring the roughness of significant surfaces of the broach samples.	73
Figure 4.3	Vickers hardness of M2 broach samples.	74
Figure 4.4	Vickers hardness of ASP53 broach samples.	75
Figure 4.5	Vickers hardness of ASP30 broach samples.	76
Figure 4.6	Carbide distribution of M2 HSS as seen under an optical microscope (x600).	77
Figure 4.7	Carbide distribution of ASP30 HSS as seen under an optical microscope (x600).	77
Figure 4.8	Carbide distribution of ASP53 HSS as seen under an optical microscope (x600).	77
Figure 4.9	Carbide distribution of M2 HSS (x960)	78
Figure 4.10	Carbide distribution of ASP30 HSS (x960)	78
Figure 4.11	Carbide distribution of <u>ASP30</u> HSS (x960) ?	78
Figure 4.12	X-ray analysis of the tungsten/molybdenum rich carbides of <u>ASP30</u> tool material.	79

Figure 4.13	X-ray analysis of the vanadium rich carbides of ASP30 tool material.	79
Figure 4.14	X-ray analysis of the vanadium rich carbides of ASP53 tool material.	80
Figure 4.15	Carbide distribution of M2 HSS (x120).	81
Figure 4.16	Carbide distribution of ASP30 HSS (x120)	81
Figure 4.17	A view of the cutting edge of an M2 broach sample (x110)	82
Figure 4.18	A view of the cutting edge of an M2 broach sample (x170)	82
Figure 4.19	A view of the cutting edge of an M2 broach sample (x340)	83
Figure 4.20	A view of the cutting edge of an M2 broach sample (x140)	83
Figure 4.21	A view of the cutting edge of an ASP30 broach sample (x150)	84
Figure 4.22	A view of the cutting edge of an ASP30 broach sample (x75)	84
Figure 4.23	A view of the cutting edge of an ASP53 broach sample (x260)	85
Figure 4.24	A view of the cutting edge of an ASP53 broach sample (x260)	85
Figure 4.25	A picture showing an overall setup of the test rig for performance tests at a cutting speed of 0.7 m/min.	86
Figure 4.26	A picture showing the dynamometer, workpiece vice, workpiece and the tool holder for performance tests at a cutting speed of 0.7 m/min.	86

Figure 4.27	A perspective view of the specially machined workpiece (150M36 alloy steel) for performance tests at a cutting speed of 0.7 m/min.	87
Figure 4.28	A picture showing an overall setup of the test rig for performance tests at a cutting a cutting speed of 10.5 m/min.	87
Figure 4.29	A picture showing the tool and the workpiece for performance tests at a cutting speed of 10.5 m/min.	88
Figure 4.30	A perspective view of the specially machined workpiece (150M36 alloy steel) for performance tests at a cutting speed of 10.5 m/min.	88
Figure 4.31	Typical traces of cutting and thrust forces obtained from the oscilloscope.	89
Figure 4.32	Effect of undeformed chip thickness on cutting forces (cutting speed : 0.7 m/min).	90
Figure 4.33	Effect of undeformed chip thickness on cutting forces (cutting speed : 10.5 m/min).	91
Figure 4.34	Effect of undeformed chip thickness on specific cutting energy (cutting speed : 0.7 m/min).	92
Figure 4.35	Effect of undeformed chip thickness on specific cutting energy (cutting speed : 10.5 m/min).	93
Figure 4.36	Effect of undeformed chip thickness on roughness average measured perpendicular to the direction of cut (cutting speed : 0.7 m/min).	94
Figure 4.37	Effect of undeformed chip thickness on roughness average measured parallel to the direction of cut (cutting speed : 0.7 m/min).	95
Figure 4.38	Effect of undeformed chip thickness on peak to valley height measured perpendicular to the direction of cut (cutting speed : 0.7 m/min).	96

Figure 4.39	Effect of undeformed chip thickness on peak to valley height measured parallel to the direction of cut (cutting speed : 10.5 m/min).	97
Figure 4.40	Effect of undeformed chip thickness on roughness average measured perpendicular to the direction of cut (cutting speed : 10.5 m/min).	98
Figure 4.41	Effect of undeformed chip thickness on roughness average measured parallel to the direction of cut (cutting speed : 10.5 m/min).	99
Figure 4.42	Effect of undeformed chip thickness on peak to valley height measured perpendicular to the direction of cut (cutting speed : 10.5 m/min).	100
Figure 4.43	Effect of undeformed chip thickness on peak to valley height measured parallel to the direction of cut (cutting speed : 10.5 m/min).	101
Figure 5.1	A picture showing the overall set-up of the test rig to perform the wear tests at a cutting speed of 10.5 m/min.	102
Figure 5.2	A picture showing the broach sample, broach sample holder and the tool post.	102
Figure 5.3	A perspective view showing overall dimensions of the specially machined workpiece to perform the wear tests.	103
Figure 5.4	A perspective view of the specially machined jig to hold the workpieces.	104
Figure 5.5	A micrograph showing the wear scar and the adhesion of work material on the clearance face of the M2 broach sample (x25).	105
Figure 5.6	A micrograph showing the wear scar on the clearance face of the ASP53 broach sample (x25).	105

Figure 5.7	A micrograph showing the wear scar on the clearance face of the ASP30 broach sample (x25).	105
Figure 5.8	Wear tests on M2, ASP53 and ASP30 broach samples.	106
Figure 5.9	Effect of tool-wear on roughness average of workpiece measured perpendicular to the direction of cut (cutting speed : 10.5 m/min).	107
Figure 5.10	Effect of tool-wear on roughness average of workpiece measured parallel to the direction of cut (cutting speed : 10.5 m/min).	108
Figure 5.11	Effect of tool-wear on peak to valley height of workpiece measured perpendicular to the direction of cut (cutting speed : 10.5 m/min).	109
Figure 5.12	Effect of tool-wear on peak to valley height of workpiece measured parallel to the direction of cut (cutting speed : 10.5 m/min).	110
Figure 5.13	A micrograph showing the wear scar on the clearance face of the ASP30 broach sample (x120).	111
Figure 5.14	A micrograph showing the adhesion of work material on the clearance face of the M2 broach sample (x120).	111
Figure 5.15	A micrograph showing the chippings on the clearance face of the M2 broach sample (x75).	112
Figure 5.16	A micrograph showing the chippings on the clearance face and adhesion of work material on the rake face of the ASP30 broach sample (x75).	112
Figure 5.17	A micrograph showing the chippings on the clearance face of the ASP30 broach sample (x120).	112

## LIST OF TABLES

<b>Table No.</b>	<b>Caption</b>	<b>Page No.</b>
Table 4.1	Clearance angle, rake angle, pitch and depth of tooth of M2 high speed steel broach samples measured on the Hilger Universal Projector (x25).	113
Table 4.2	Clearance angle, rake angle, pitch and depth of tooth of ASP53 high speed steel broach samples measured on the Hilger Universal Projector (x25).	114
Table 4.3	Clearance angle, rake angle, pitch and depth of tooth of ASP30 high speed steel broach samples measured on the Hilger Universal Projector (x25).	115
Table 4.4	Surface roughness of M2 high speed steel broach samples measured on the rake and clearance (flank) faces in the directions perpendicular and parallel to the cutting edge. Numbers in parentheses are Peak to Valley Roughness Height (Rt).	116
Table 4.5	Surface roughness of M2 high speed steel broach samples measured on the rake and clearance (flank) faces in the directions perpendicular and parallel to the cutting edge. Numbers in parentheses are Peak to Valley Roughness Height (Rt).	118
Table 4.6	Surface roughness of M2 high speed steel broach samples measured on the rake and clearance (flank) faces in the directions perpendicular and parallel to the cutting edge. Numbers in parentheses are Peak to Valley Roughness Height (Rt).	119

## ACKNOWLEDGEMENT

The author wishes to express his gratitude and sincere thanks to Professor M Sarwar director of studies, Dr. D Gillibrand supervisor and Dr. S Dugdale for their constant encouragement and guidance throughout the research programme. Thanks are also due to all the technicians and staff of the School of Engineering. In particular the author wishes to thank Mr. R C Wainwright, Mr. T J O'Hara, Mr. R C Wilkinson, Mr. M Jackson, Mr. M Kew, Mr. J Evans and Mrs. A M Mallon.

My very special and sincere thanks go to my parents, Mr. and Mrs. Alim for all the love, time and financial support they gave me upto this stage of my life. Last but not the least, I would like to register my gratitude to my wife, Shazia who constantly inspired me to work hard to achieve my objective.

## CHAPTER ONE

### INTRODUCTION

The materials from which the first steam engines were constructed were not very difficult to machine. Grey cast iron, wrought iron, brass and bronze were readily cut using hardened carbon steel tools. The methods of heat treatment of tool steel had been evolved by centuries of craftsmen, and reasonably reliable tools were available, although rapid failure of the tools could be avoided only by cutting at very low speed. Alloy steels in particular proved more difficult to machine than wrought iron, and cutting speeds had to be lowered even further to achieve a reasonable tool life. The incentive to reduce costs by cutting faster became more intense, evolving new tool materials.

The majority of industries concerned with machining have made a very valuable contribution to the improvement of metal cutting technology. The following developments have taken place in cutting tool materials over the last century.

High carbon steel : still used for hand tools

High speed steel : the most common material, can be machined in the annealed state

Tungsten carbides : in the form of sintered inserts

Other carbides : e.g. tantalum, titanium

Stellite : cast alloys - chromium carbides in cobalt and chromium

Cermets : mixed sintered oxides and sintered carbides

Coated carbides : hard coating on a tough substrate, usually with several intermediate layers

Ceramics : sintered oxides

Sialon : silicon nitride ceramic in solid or laminate form

Cubic Boron Nitride : very hard, in either solid or laminate form

Diamond : natural and synthetic - suitable for cutting non-ferrous materials

The newer techniques of applying wear resistant coatings have allowed cutting tools to be used at increased cutting speeds. This has forced machine tool manufacturers to develop their machines so as to make full use of the new tool materials through increased metal removal rates and improved productivity.

The machine operator, tool designer, the materials engineer are all seeking to find solutions to new problems in the form of cutting conditions, tool geometry, tool materials and treatments. In order to improve the efficiency of cutting and increase productivity, the cutting tool technologist must have an understanding of the fundamentals of metal cutting. It is what happens at the extreme cutting edge of the tool that determines the initial performance of the tool, the machinability of workpiece material and the quality of the machined surface.

The latest development in cutting tool technology is in the application of advanced surface engineering technologies to enhance/improve the cutting tool by modifying the surface to give better performance and longer tool life. Surface modification is carried out either by coating the substrate surface with a very thin film (2  $\mu\text{m}$  - 5  $\mu\text{m}$ ) of a hard substance or by implanting species into the substrate to a depth of approximately 100 Å. It is apparent that the major research effort associated with surface engineering has been concentrated on the film characteristics and little attention has been directed to the substrate suitability. In order for this latest technology to be successful the total system, i.e. substrate, interface and film characteristics have to be scientifically studied.

### **1.1 High Speed Steel**

High speed steels have been known in some form for over a century. The discovery was made by Robert F. Mushet in 1868 that a steel containing tungsten became hard when air cooled from a temperature from which most steels required water quenching for hardening [1]. It took its name from its capacity to retain a high level of hardness when cutting metals and other materials at high speed. The first real high speed steel as defined by modern standards was the 18-4-1 composition developed by Crucible Steel Company. This steel, now generally known by its specification number, T1, contains 18% tungsten, with 4% chromium, 1% vanadium, and 0.7% carbon. This steel remained popular until the 1950s, when it was overtaken by a tungsten-molybdenum steel, M2, in which two-thirds of the tungsten in T1 was replaced by 5% molybdenum and the vanadium content raised to 2% and the carbon to 0.85%.

The alloying elements impart certain properties to high speed steels. These elements and their effects are discussed below.

### 1.1.1 Carbon

Carbon is the most important of the elements and is very closely controlled. While the carbon content of any one high speed tool steel is usually fixed within narrow limits and variations within these limits can cause important changes in the mechanical properties and the cutting ability [1]. As the carbon content is increased, the working hardness also rises; the elevated temperature hardness is higher and the number of hard, stable, complex carbides increases. The latter contribute much to the wear resistance of the high speed tool steels.

### 1.1.2 Chromium

The presence of chromium in high speed steel from 3 to 5% has been the most consistent feature of most compositions throughout the history of these alloys. Chromium provides hardenability by slowing down reactions and the carbon necessary for hardening as its carbides dissolve in austenite [2]. It retards the formation of precipitates of carbides during tempering and improves cutting properties. The chromium carbide is readily soluble in the matrix on heat treatment, and thus chromium contributes to the deep hardening properties of the steel.

### 1.1.3 Tungsten and Molybdenum

Tungsten and molybdenum promote resistance to tempering, and cutting efficiency improves as the concentration of tungsten, or its equivalent in terms of molybdenum, is increased [3]. Molybdenum depresses the solidus

temperature more than tungsten, and hence the maximum permissible heat treatment temperature is reduced in the case of molybdenum steels.

These two elements perform similar functions and are interchangeable on an atomic basis. On a weight basis, 1% molybdenum is usually taken to be equivalent to between 1.6 and 2% tungsten. Economic considerations have in the past frequently been predominant in determining the selection of alloy, as both the metals are expensive.

The tungsten and molybdenum carbides are not soluble in the matrix on heat treatment, and thus contribute a little to the deep hardening properties of the steel. They do, however, slow down transformation reactions, thus contributing greatly to the temper resistance, or red hardness.

#### 1.1.4 Vanadium

Vanadium was first added to high speed tool steels as a scavenger to remove slag impurities and to reduce nitrogen levels in the melting operation, but it was soon found that the element materially increased the cutting efficiency of tools. In amounts up to 1%, its main function is to reinforce the secondary hardening. A small volume of hard particles of vanadium carbide of microscopic size is formed, and these are the hardest constituents of the alloy [4]. The hardness of vanadium carbide is 2500 Hv [5]. When steels contain more of the metal, there are many more of these hard particles and they play a significant role in resisting wear. On the other hand the presence of vanadium carbides causes difficulty in grinding.

### 1.1.5 Cobalt

Cobalt is present in amounts between 5 and 12%. The cobalt raises the temperature at which the hardness of the fully hardened steel starts to fall [6]. Although the increase in useful temperature is relatively small, the performance of tools under particular conditions is significantly improved. The cobalt restricts the growth of the precipitated carbide particles and does not itself form a carbide.

High speed steels having low thermal conductivity ( $21 \text{ W m}^{-1} \text{ K}^{-1}$  for M2) [7], which cause problems during solidification. Though high speed steels are reasonably homogeneous in the molten state, they are characterised by a very long freezing range. This causes the carbides to segregate [4] from the matrix during solidification and thus affects uniformity of hardness. A non-uniform and coarse microstructure [8] is inevitable, with variations in chemical composition. This causes the problem of dimensional stability during the heat treatment processes. Due to poor grindability of carbides, grinding of a cutting edge becomes difficult [9]. As the ingot contains a network of coarse carbides, during hot working this network is gradually broken down and large carbides are torn apart to form smaller ones. During recent years it has been learnt how to control the ingot structure in a more efficient way with molybdenum high speed steels. The measures include optimising the cooling rate [10] and solidification conditions [7] and the use of consumable electrode remelting processes such as electroslag refining (ESR) and vacuum arc remelting (VAR). The effect of these combined efforts is a considerable improvement in structure of the final product, but even after extensive hot working, rather coarse carbides abound in the structure and the carbide distribution is not uniform.

On the other hand development of powder metallurgy technology for the production of powder compacted high speed steels such as anti-segregation process has minimised the above problems to a great extent. This process is explained briefly in section 1.2.

## **1.2 Anti-Segregation Process High Speed Steels**

Since the early 1970's, several powder metallurgy techniques for producing high speed steel have been developed. One of the processes for producing an alloy powder is the Anti-Segregation Process (ASP), developed in Sweden [11, 12]. In this process, an alloy steel melt is atomised in an inert gas to give spherical powder particles. The powder is then poured into cylindrical sheet steel capsules, which are vibrated to pack the particles tightly. Air is removed before a cover is welded to the capsule. The capsule and its contents are cold isostatically pressed at 400 MPa (58,000 psi). The capsule is then hot isostatically pressed at 100 MPa (14,500 psi) at 1150 °C (2100 °F). After compaction, the steel is worked conventionally by forging and rolling to the desired dimensions. This processing results in a fine-grained material with a uniform distribution of small carbides. The homogeneous material, free from segregation, has a structure which is the same regardless of bar size and alloy content.

The high speed steels produced through the powder metallurgy process offer better properties than produced by conventional methods. The ASP high speed steels have much higher ultimate bend strength, better grindability and evenly distributed carbides independent of the bar size compared to M2 high speed steel [8, 13].

## CHAPTER TWO

### MECHANICS OF MACHINING AND TOOL WEAR

Considerable time and effort has been spent in studying the mechanics of metal cutting, associated with single point tools with the information obtained being applied to multi-point cutting tools. Although there has been some benefit to multi-point tools, a study of the dynamics of the chip once formed in restricted conditions (broaching) is also of fundamental importance, and should receive attention.

The characteristics of tool rake face and the geometrical features associated with retention and rejection of the chip (in tools such as broaches, circular saws and milling cutters), are also of prime importance.

Owing to the nature of the testing (i.e. time, tool and workpiece costs, manpower utilisation), metal cutting research is expensive and therefore mathematical modelling of the process is important. However, to date there is no accurate mathematical model for predicting loads, temperatures and stresses, which are absolutely essential quantities to the tool designer. With the development of computers, sophisticated electronic instrumentation and improved techniques, this task of collecting empirical data has been made somewhat easier.

## 2.1 Mechanics of Metal Cutting

The basic mechanism of metal cutting can be explained by analysing cutting with a single cutting edge. A simple case is known as orthogonal cutting, in which the cutting edge is perpendicular to the direction of motion relative to the workpiece and the cutting edge is wider than the chip. The wedge shaped tool consists of two planes intersecting to form the cutting edge (Figure 2.1). The surface along which the chip flows is known as the rake face and that surface ground back to clear the new or machined surface is known as the flank or clearance face (Figure 2.2). One of the most important variables of a cutting tool is the inclination of the rake face, known as the rake angle, which is specified in orthogonal cutting by the angle between the tool face and a line normal to the machined surface.

While the tool flank does not contribute to the process of chip removal, the rate of tool wear and quality of the machined surface can be influenced by the clearance angle.

## 2.2 Cutting Forces

Orthogonal cutting (Figure 2.1) is two-dimensional cutting and all the forces lie in one plane. The forces arising from this type of cutting action are shown in Figure 2.3. In order to determine the resultant force  $F_r$ , its two rectangular components are measured. The component of the resultant force acting along the direction of cut is called the cutting force  $F_c$  and the second component acting in the direction normal to the direction of cut, tending to push the tool away from the work is known as the thrust force  $F_t$ . The magnitude of cutting force is usually larger than that of the thrust force. The cutting force component determines the work required to remove the material. The thrust

force component has a minimal contribution to the work done, but both components produce deflection of the tool, the workpiece and the machine tool frame, which affects the accuracy of cutting.

A knowledge of these forces is useful for various reasons:

1. To ascertain the power requirements and selection of a motor for the machine tool.
2. To design the tool with sufficient rigidity to avoid excessive deflection and vibration.
3. To design the structure of machine tool having sufficient strength and rigidity.
4. To calculate the efficiency of metal removal.

Such requirements have led to the development of metal-cutting dynamometers capable of accurately measuring forces at the cutting tool.

### **2.3 Specific Cutting Energy**

This is defined as the amount of energy consumed in removing unit volume of metal. This parameter is an indicator of the efficiency of the cutting process, and this is of industrial importance. Rather than measure energy or power, it is easier and more practical to measure the force required during cutting. The rate of energy consumption during machining or power  $P$  is the product of cutting speed  $V$  and the cutting force  $F_c$ . Power is also the product of specific cutting energy  $E_{sp}$  and the metal removal rate  $M_{rr}$ .

$$P_w [\text{watt}] = F_c [\text{newton}] \times V \left[ \frac{m}{\text{sec}} \right] \quad \text{-----} \quad (2.1)$$

$$E_{sp} \left[ \frac{\text{watt} \cdot \text{sec}}{m^3} \right] = \frac{F_c [\text{newton}] \times V \left[ \frac{m}{\text{sec}} \right]}{M_{rr} \left[ \frac{m^3}{\text{sec}} \right]} \quad \text{-----} \quad (2.2)$$

Where,

$P_w$  = power

$F_c$  = cutting force

$V$  = cutting speed

$M_{rr}$  = metal removal rate

$E_{sp}$  = specific cutting energy

In orthogonal cutting, metal removal rate is a product of cross-sectional area of undeformed chip thickness  $A_c$  and the cutting speed  $V$ .

$$M_{rr} \left[ \frac{m^3}{\text{sec}} \right] = A_c [m^2] \times V \left[ \frac{m}{\text{sec}} \right] \quad \text{-----} \quad (2.3)$$

Where  $A_c$  = cross-sectional area of undeformed chip thickness

The unit, watt is a very small unit to represent the metal removal rate of one cubic meter. Hence its multiple unit is used for all practical purposes.

$$E_{sp} \left[ \frac{Gwatt - sec}{m^3} \right] = 10^9 \left[ \frac{watt - sec}{m^3} \right] \quad \text{-----} \quad (2.4)$$

Comparing equations (2.2) and (2.3), substituting the value of  $M_{IT}$  we get,

$$E_{sp} \left[ \frac{newton}{m^2} \right] = \frac{F_c [newton] \times V \left[ \frac{m}{sec} \right]}{A_c [m^2] \times V \left[ \frac{m}{sec} \right]} \quad \text{-----} \quad (2.5)$$

So specific cutting energy is dimensionally and numerically equal to specific cutting pressure. The units are [newton/m<sup>2</sup>] or [joule/m<sup>3</sup>] (one joule = one newton-meter). The numerical value is usually given as GJ/m<sup>3</sup> (one GJ=10<sup>9</sup>J).

## 2.4 Chip Formation

The majority of metal-cutting operations involve the separation of small segments or chips from the workpiece to achieve the required shape and size of manufactured parts. Chip formation involves three basic requirements which are as follows:

1. A cutting tool that is sufficiently strong and hard.
2. An interference between the tool and the workpiece in the shape of a thin layer.
3. A relative motion or cutting velocity between the tool and the workpiece with sufficient force to remove this thin layer.

When these three conditions exist, the thin layer of the material that interferes with free passage of the tool will be displaced to create a chip (Figure 2.2).

Many possibilities and combinations exist that may fulfil such requirements. Variations in tool material and tool geometry, feed and depth of cut, cutting velocity, and workpiece material have an effect not only upon the formation of the chip, but also upon cutting force, cutting temperatures, tool wear and tool life, dimensional stability, and the quality of the newly created surface.

Three basic types of chips are obtained during metal cutting with nominally sharp tools which are:

1. Discontinuous chip.
2. Continuous chip.
3. Continuous chip with built-up edge.

#### 2.4.1 Discontinuous Chip

If the workpiece material is brittle and has little capacity for deformation before fracture, when the fracture shear stress is reached, separation will take place along the shear plane to form a segmental chip (Figure 2.4). Discontinuous chips are formed when machining brittle materials such as cast iron.

### 2.4.2 Continuous Chip

The formation of the chip can be described as follows. Consider the wedge type of tool, Figure 2.2, to be stationary and the workpiece approaching the tool with a velocity  $V$ . Material in the vicinity of the cutting edge is compressed and plastically deformed along a shear plane or shear zone and continues to flow in a solid form as a chip with a velocity  $V_c$ , along the rake face of the tool. Ductile materials have sufficient plasticity to deform along the shear plane without rupture. Referring to Figure 2.2, the layer of material removed called undeformed chip thickness, UCT, is plastically deformed into chip thickness,  $t_c$ . In orthogonal cutting, thickness of the chip,  $t_c$ , is always greater than the undeformed chip thickness, UCT. A measure of efficiency of the cutting process is given by the cutting ratio  $C_r$ ,

$$C_r = \frac{\text{UCT} [mm]}{t_c [mm]} \quad \text{-----} \quad (2.6)$$

Where,

$C_r$  = cutting ratio

UCT = undeformed chip thickness

$t_c$  = chip thickness

The cutting ratio being dimensionless is always less than one and a convenient measure of cutting efficiency.

The nature of chip formation is approximately the same for orthogonal or oblique cutting with one or more cutting edges. The type of chip produced

during metal cutting depends on the material being machined, the cutting conditions, and the tool geometry.

### 2.4.3 Built-up Edge

As most of the cutting done by high speed steel tools is under conditions where a built-up edge is formed, some explanation is given below:

Consideration of chip flow along the face of the tool in the formation of continuous chips is of prime importance. If the friction force that resists the passage of the chip along the tool face is less than the force necessary to shear the chip material, the entire chip will pass off cleanly. In most cases, however, it is virtually impossible to prevent some amount of seizure between the chip and the tool face. Unless surfaces are perfectly flat, contact is made along the high spots over only a fraction of the total area. As the chip passes over the tool face, cutting forces give rise to an extremely high pressure, sufficient to form pressure welds. If these welds are stronger than the ultimate shear strength of workpiece material, that portion of the chip which is welded to the tool becomes what is called a built-up edge (Figure 2.5). A micrograph showing the formation of a built-up edge on the cutting edge of a high speed steel tool is presented in Figure 2.6.

The edge builds up to a point where it eventually breaks off, part of it going off with the chip along the rake face, and part of it being deposited on the work surface. This occurs at rapid intervals and degrades the quality of machined surface. Any change in cutting conditions that reduces or eliminates the built-up edge will usually improve the surface quality.

As the built-up edge grows, it takes over the cutting action from the actual tool tip (Figure 2.7) and hence cutting deeper than required. Part of the built-up

edge breaks off leaving the tool edge to begin cutting once again. This repetition of the process forms microscopic steps on the machined surface. This can be seen under a microscope with a single light source placed at an acute angle (Figure 2.8). The illumination causes shadows, if placed against the direction of cut and bright edges if placed along the direction of cut. Micrographs (Figures 2.9 and 2.10) show the machined surface while cutting with a built-up edge.

When one's finger is rubbed on a surface that has been machined under built-up edge conditions, the surface feels rough when it is rubbed in the direction of cutting, as the sharp edges of the steps are encountered, but it feels smooth when rubbed in the direction contrary to the direction of cutting.

Also, referring to Figures 2.9 and 2.10, the adhering pieces of built-up edge tend to be convex when viewed in the direction of cutting. This is because the highest point of the built-up edge adheres first, and the lower parts on either side shear a very short time later as the tool travels forward.

## **2.5 Tool Life and Tool Wear**

For satisfactory performance the shape of the cutting tool edge must be accurately controlled and is very critical in some applications. Much skill is required to develop and specify the optimum tool geometry, to grind the tools to the required accuracy and to inspect the tools before use.

In industrial machining operations the action of cutting gradually changes the shape of the tool edge so that in time the tool ceases to cut efficiently or fails completely. The following may be criteria for the end of tool life:

1. Temperature rises beyond a certain limit. Smoke and sparks are generated. The tool tip becomes thermally softened and is rubbed off. The tool then ceases to cut.
2. Machining operation becomes excessively noisy or vibrations become severe due to increased cutting forces.
3. Dimensions or surface finish of the workpiece fails to meet specified values or the tool profile becomes unsatisfactory.

The change of shape of the tool edge is very small and can not be observed adequately with the naked eye. A microscope with a suitable magnification is needed for the measurement of wear.

Cutting-tool life is one of the most important economic considerations in metal cutting so any improvement in tool or work-material that increases tool life is beneficial. The life of a tool can be brought to an end in two major ways:

- Gradual or progressive wearing away of certain regions of the face and flank of the cutting tool.
- Fracture, bringing the life of the tool to a sudden end.

## **2.6 Tool Wear Mechanisms**

In metal cutting three main mechanisms of wear are known to occur. These are discussed as follows:

### **2.6.1 Adhesive wear**

High speed steel tools are used at relatively low cutting speed and temperatures are low. The flow of metal past the cutting edge is more

irregular, less stream-lined or laminar (Figure 2.7), a built-up edge is formed and contact with the tool is less continuous. Under these conditions fragments of microscopic size are torn intermittently from the tool surface. This mechanism is called adhesion wear.

In continuous cutting operations using high speed steel tools, adhesion is usually a slow form of wear. More rapid destruction of the tool edge occurs in operations involving interruptions of cut and where vibration is severe due to lack of rigidity in the machine tool.

### 2.6.2 Abrasive wear

Abrasion wear occurs when hard particles pass over the tool, rake or flank face, and remove material by mechanical action. The source of these hard particles can be:

1. Highly strain-hardened fragments of an unstable built-up edge.
2. Fragments of the hard tool material removed by adhesion wear.
3. Hard constituents in the work material.

Abrasion is considered as a major cause of wear. Rapid wear by abrasion occurs where the work material contains greater concentrations of hard particles, such as pockets of sand on the surface of castings. In such concentrations the action is like that of a grinding wheel. The surface of castings should be treated to remove abrasive material in order to improve tool life.

### 2.6.3 Diffusion wear

In diffusion wear the surface structure of the tool weakens due to solid state diffusion. In this process, atoms in a metallic crystal lattice move from a region of high atomic concentration to one of low concentration. Diffusion wear is a sort of chemical attack on the tool surface, like etching, and is dependent on the solubility of the different phases of the tool material in the metal flowing over the surface, rather than on the hardness of these phases. During metal cutting high temperatures are achieved and the process of diffusion increases exponentially with the increase in temperature.

With high speed steel tools used in the usual cutting speed range, rates of wear by diffusion are relatively slow because the interface temperatures are relatively low. While using carbide tool inserts at high cutting speeds, higher temperatures are achieved and diffusion wear becomes a predominant mode of wear.

## **2.7 Forms of Wear in Metal Cutting**

The progressive wear of a tool takes place in two ways and are discussed as follows:

### 2.7.1 Crater Wear

Wear on the tool rake face occurs by formation of a crater, caused by the action of the chip flowing along the rake face. The crater conforms to the shape of the chip underside and is restricted to the chip-tool contact area (Figure 2.11). The highest temperature occurs some distance from the cutting edge along the rake face. At high cutting speeds a high enough temperature is

achieved to cause thermal softening in high speed steel. Hence the crater is formed by diffusion wear. As the crater grows bigger, the cutting edge becomes weaker and eventually fractures. A micrograph showing the crater and flank wear on a high speed steel broach sample is presented in Figure 2.12. It is obvious from the figure that the crater forms some distance from the cutting edge along the rake face. The deepest point of the crater is where the interface temperature reaches its maximum.

### 2.7.2 Flank Wear

Wear on the flank of a cutting tool is caused by friction between the newly machined workpiece surface and the contact area on the tool flank. The width of the wear land is measured using a microscope (Figure 2.12). A typical graph of the progress of flank wear land width  $V_B$  with cutting time is shown in Figure 2.13. The curve can be divided into three regions:

1. High initial wear due to breakdown of sharp edge, region AB.
2. Wear at a uniform rate, region BC.
3. Wear occurs at a gradually increasing rate, region CD.

Region CD indicates where the width of flank wear has become sensitive to the increased tool temperatures caused by such a large width of wear land. In practice, tools are sent for regrind before region CD is reached.

## 2.8 Tool Life Criteria

When the total volumetric amount of wear debris detached from a relevant surface (rake or flank) of the tool exceeds a specified value, the tool is at the

end of its useful life. The tool life is defined as a predetermined threshold value of a measurement of a wear land or crater. The failure occurs when the tool is no longer capable of producing parts within specification. The following factors may alone, or in combination, be used as criteria for tool failure:

1. Surface quality of the machined surface.
2. Dimensional tolerance of the workpiece.
3. Cutting forces and hence the cutting horsepower.
4. Production rate of the machined product.

Two criteria of tool failure are discussed below i.e. failure by measuring depth of crater and by measuring width of flank wear. In practical machining operations the wear of the rake and flank is not uniform along the active cutting edge. Figure 2.14 shows a typical worn single-point tool. The crater depth  $K_T$  is measured at the deepest point of the crater (section A-A). The largest permitted value of  $K_T$  for sintered carbide tools is specified in terms of the feed rate,

$$K_T [mm] = 0.06 + 0.3f \left[ \frac{mm}{rev.} \right] \quad \text{-----} \quad (2.7)$$

Where,

$K_T$  = maximum depth of crater

$f$  = feed rate

It can be seen that flank wear is usually greatest at the extremities of the active cutting edge. In the central portion of the cutting edge (zone B), the wear land is usually fairly uniform. The average width of wear land in this region is designated  $VB$ , and the maximum width of wear land is designated  $VB_{max}$ . The criteria recommended by International Standards Organisation (ISO3685:1977) to define the effective tool life for high speed steel tools are:

1. Catastrophic failure, or
2.  $VB = 0.3$  mm if the flank is regularly worn in zone B, or
3.  $VB_{max} = 0.6$  mm if the flank is irregularly worn, scratched, chipped, or badly grooved in zone B.

The high speed steel tools are subjected to relatively low cutting speeds, so temperature during cutting is not high enough to cause significant diffusion wear. The dominant mode of wear is the flank wear. Referring again to Figure 2.12, this micrograph was taken at the end of useful life of a high speed steel tool (tool life criterion being  $VB=0.3$  mm). The depth of crater is insignificant compared to the width of wear land.

## **2.9 Premature Tool Failure**

It is possible to make cutting tools from very hard materials because the tool is subjected to compressive stress while it is cutting. In fact, tools made from hard alloys can only sustain the stresses for which they are designed. Because of the low fracture toughness of these alloys, any accidental impact which gives rise to tensile stress is likely to break a chip off the cutting edge [15], for example, dropping the tool on the floor. As a further example, aluminium oxide tools have a controlled bevel ground on the cutting edge, of a size

related to the expected feed rate, to avoid chipping during cutting. Fortunately, high speed steel tools are fairly insensitive to rough treatment, but certain malpractices will cause chipping, such as stopping cutting when the tool is still engaged in the cut and then withdrawing the tool. The insensitivity of high speed steel to chipping makes it suitable for heavy roughing cuts on large forgings.

## CHAPTER THREE

### **BROACHING**

Broaching is a machining process in which a cutting tool having multiple transverse cutting edges is pushed or pulled over a surface or through a hole to remove metal by axial cutting. Broaching was originally developed for machining internal keyways and its obvious advantages (Section 3.1) quickly led to its development for the mass production machining of various surfaces, such as flat, interior and exterior cylindrical, and other irregular surfaces. Broaching produces better dimensional accuracy and surface finish of the workpiece than can be obtained by milling or reaming [16]. The most important part of the process is the broaching tool, in which the roughing, semifinishing, and finishing teeth are positioned along the axis of a single tool. Feed of the cutting edges is built into this tool. This permits an operation to be completed in a single pass. Several broaches are sometimes used in combination to form different surfaces on the workpiece simultaneously. As several teeth of a broach are cutting at the same time, the feeds and the cutting speeds may be reduced. With the introduction of powder metallurgy high speed steels, the broach tools give longer useful lives and better surface quality on the workpiece, making the broaching process more economical.

### **3.1 Advantages of Broaches**

The major advantages of broaching include high productivity, dimensional accuracy and good finish produced on the worksurface, and the economy in production. These are discussed as follows:

#### **3.1.1 Productivity**

The ability to rough and finish machine in one pass increases productivity. Broaching can produce finished product faster than other machining methods provided the process is properly applied using the correct tools and machines [17, 18, 19]. Several small parts may be stacked together and broached in a single pass.

#### **3.1.2 Quality of Machining**

Dimensional accuracy of the machined surface can be consistently maintained because of the inherent accuracy of the broach. Several surfaces on a workpiece can be located relative to each other, as this relationship is built into the tooling and does not depend on the machine. The surface produced is smooth compared with that of many other machining processes, as noncutting burnishing elements are provided on the finishing end of the broach, resulting in the elimination of any subsequent grinding operation [20].

#### **3.1.3 Operational Economy**

Although the capital cost of the tools is high compared with that of conventional tools, the cost per finished workpiece is low because of long tool life. The longer tool life is achieved because of low cutting speeds in broaching and because the amount of material removed by each tooth is small.

The reduced level of operational skill required for this process is one of the factors in economy [21].

### **3.2 Broach Types**

Broaching applications are of two types: internal broaching and external broaching. Both types are used for machining configurations ranging from flat surfaces to complex contours on or inside a workpiece. The workpieces can range from small precision components to very large parts. Broaching is generally not considered to be a heavy stock removal operation except in some applications of surface broaching. Because of the length of stroke and power requirements, broaching is seldom recommended for the removal of large amounts of metal. Where heavy stock must be removed, a preliminary roughing operation other than broaching is appreciated, or two or more roughing broaching passes are used to remove the required stock. Broaches are also classified by the way they are actuated i.e. pull or push type.

#### **3.2.1 Internal Broaching**

Workpieces with internal surfaces to be broached require a starting hole for insertion of the tool. Starting holes for internal broaching are generally produced by casting, forging, punching, drilling, or boring. Surfaces to be broached must be parallel to the direction of tool travel. Most common internal broached surfaces can be holes of different cross-sections such as: round, square, rectangular, and other shaped holes, the process is used to cut contoured surfaces, splines, keyways, serrations, and to rifle the bores of gun barrels. If a through hole is available to be broached then a pull-type broach is used. Figure 3.1 shows the features of a typical round pull-type broach. The pull end and front pilot are passed through a starting hole in the workpiece and

the pull end is locked to the pull head of the broaching machine. The front pilot on internal pull-type broaches ensures correct axial tool alignment with the starting hole and also serves as a check on the starting-hole size. The required size and shape of the hole is achieved in a single pass. If a through hole is not available then blind holes are broached by short push-type broaches. As the travel is limited so a series of broaches with increasing sizes are used. The final size and shape of the hole may be achieved in more than one pass. Pull broaches are much longer than the push-type since there is no problem of bending.

### 3.2.2 External or Surface Broaching

Surface broaching applications are practically unlimited. Any external form can be produced as long as the surfaces are in a straight line and unobstructed. Apart from a flat surface, slots, keyways, contoured surface, rack and gear teeth, and serrations are a few examples of external or surface broaching. Flat broaching is one of the examples of external broaching. In this process width of broach is more than that of workpiece. Flat broaches can have either oblique cutting edges or perpendicular to the direction of cut. The later type of flat broaches give rise to orthogonal cutting.

## **3.3 Broaching Characteristics and Broach Design**

The information on mechanics of metal cutting, tool wear and tool life is predominantly concerned with single-point tools. Whilst this information is transferable to multi-point tools, a full analysis of multipoint cutting requires additional information. Furthermore, owing to the broaching action and cutting conditions being very different from those normally applied to single-point tools, i.e.,

1. the process is complex owing to the geometry of the tool,
2. the feed mechanisms, i.e. feed is achieved by rise per tooth or tool inclination,
3. the tool requires accuracy in manufacture and setting in the machine,
4. the overall dimensions are a function of the length of cut, area of cut and shape and size of cut (relating to the work piece).

A major function of the broaching action is to efficiently produce the chip (i.e. tool edge geometry is important), allow the chip to flow freely up the rake face (requires an appropriate surface finish on the rake face) and to accommodate the chip in the gullet throughout the cut without damaging the machined surface.

Current broach design (i.e. cutting edges, length of broach and tooth geometry etc.) is purely on limited empirical data and broaching practice. Traditional methods of broach design are not scientifically based. With rapid developments of new workpiece materials the demands on the broaching operation are being increased in terms of productivity, machinability and component quality. In order to respond rapidly to these increased demands on the broach it is essential to provide the tool designer with,

1. a fundamental understanding of the broaching process,
2. clear design procedure,
3. scientific data associated with the tool and workpiece material.

Broaches in their simplest form consist of a slightly tapered flat or round bar with rows of cutting teeth located on one or more surfaces. As the teeth are stepped, additional metal is removed as each successive tooth contacts the

workpiece. The design of broaches is governed by the following general principles:

### 3.3.1 Tooth Rise

The progressive increase in tooth height between successive teeth is called the cut per tooth, step per tooth, or tooth rise. This height difference is greater along the roughing section than the semifinishing section. Harder materials require a smaller rise per tooth to avoid excessive stress on individual teeth. Another approach in the design of flat broach is to provide a tapered holder bar (Figure 3.2). The rise per tooth is incorporated in the holder bar rather than the broach itself, thus achieving convenience and simplicity in broach manufacture. All the teeth, except the finishing teeth, are ground to the same height. The finishing teeth are back stepped to prevent a rise. In this case, the clearance angle on the teeth is increased to compensate for the taper of the holder.

### 3.3.2 Pitch

The linear distance from the cutting edge of one tooth to the corresponding point on the next tooth is the pitch of a broach. This distance is determined by the following factors:

1. Length of cut.
2. Rise per tooth.
3. Type of workpiece material.

A large pitch means the gullet size is greater to accommodate more chip material. A relatively large pitch is required for roughing teeth, to provide

more chip space, for the roughing teeth have greater rise per tooth. The tooth pitch is smaller for semifinishing and finishing teeth to reduce the overall length of the broach. The longer cuts require more chip space, hence greater pitch. Similarly the type of workpiece material determines the type of chips being formed. Continuous chips require more space as compared to discontinuous chips. To prevent the broach from drifting and chattering it is necessary that at least two or preferably more teeth are cutting simultaneously. An empirical formula used to determine the pitch for short broaches, and not applicable to large horizontal broaches, is:

$$P [mm] = 1.764 \times \sqrt{L [mm]} \quad \text{-----} \quad (3.1)$$

Where,

P = pitch

L = length of cut

### 3.3.3 Chip Space

The chips produced during the broaching process are confined in the gullet, between the teeth, for the length of the cut. It is impossible to cut more metal with a broach tooth than the preceding gullet permits without causing tool breakage. The determination of gullet geometry and size depends on the following variables:

1. Rake angle.
2. Rake angle radius.
3. Back-of-tooth radius.

4. Cross-sectional area of gullet.
5. Surface finish on the rake face and the gullet.

These variables offer a compromise between the tooth strength, root diameter, and ideal chip carrying capacity [21].

### 3.3.4 Load on Broach

Pull on a broach can be calculated by rearranging equation (2.5), we get

$$P_L [\text{newton}] = A [m^2] \times E_{sp} \left[ \frac{\text{newton}}{m^2} \right] \text{-----} \quad (3.2)$$

In other words the total pull on the broach is numerically equal to the cutting force component times the number of teeth engaged in cutting.

The specific cutting energy values are required in the above load calculations. The specific cutting energy varies for different workpiece materials, tool geometry and is largely influenced by feed or rise per tooth.

Previously broach designers/users used a constant value for specific cutting energy and,

$$P_L = T \times R \times C \quad \text{-----} \quad (3.3)$$

Where,

T x R = area of metal removed by number of teeth in contact

R = rise per tooth

C = constant for workpiece material

and for surface broaching

$$T = N \times L \quad \text{-----} \quad (3.4)$$

Where,

L = effective width of broach

N = number of teeth engaged

In 1986, Vijayaraghavan [16] proved that better accuracy can be achieved by using internal broaching process. He also proved that higher cutting speed minimises dimensional deviation in broaching.

Cox [17] in 1988, showed that when several surfaces on a workpiece must be maintained in a precise parallel relationship to each other, external broaching is usually the fastest and most accurate method of machining.

Kuljanic [22] in 1975, showed that increase in cutting speed causes a decrease in the cutting forces and improved surface finish of the workpiece.

Beach [18] in 1987, claimed that broaching led to increased production. The workpiece was a cast-iron valve lever used in an automobile engine.

Motter [19] in 1989, argued that the Weldon Tool Company of Cleveland, Ohio had been able to improve production capability from a multiple-machine, multiple-person and multiple-shift operation to a one-person, one-machine and one-shift operation, after a broaching process had been installed to machine flats on cylindrical surfaces of end mill shanks.

Konig [20] in 1990, claimed that better surface finish can be achieved by the broaching process.

A specific objective of the present programme is to compare the performance of alternative tool steels. Literature treating this topic can now be considered.

Alvelid [23] in 1980, studied the wear mechanisms of M2, ASP23 and ASP30 high speed steel milling cutters. The ASP30 showed the longest life compared with M2 and ASP23 milling cutters.

Hellman [8] in 1984, showed that high speed steels produced through powder route has evenly distributed carbides and better bend strength. He also showed that broaches made from powder compacted steel give longer life and produced a larger number of pieces compared to broaches made from conventional high speed steel.

Lowder [9] in 1984, showed that powder compacted steels offer better grindability and increased performance in terms of tool life over conventional wrought steels. He also claimed that powder compacted steels can provide alloy combinations which were not possible before.

Bouzakis [24] in 1982, studied the effect of feed and speed on gear hobbing cutters. The tool materials were ASP23, ASP30 and ASP60 high speed steels. He showed that the ASP60 tool was more wear resistant than ASP30 and ASP23. He also studied the effect of austenitizing temperature on ASP30 steel and showed that hardening temperature of 1180 °C gave the best performance.

Ahman [25] in 1985, showed that ASP30 has uniformly distributed carbides. He investigated the wear mechanisms and performed wear tests at different cutting speeds.

Beard [4] in 1989, claimed that powder compacted high speed steels offer better machinability, consistency in heat treatment, better grindability and higher toughness than the conventionally produced high speed steels.

The general theme of these reports is that a better performance can be expected from powder compacted steel, but this advantage is rarely described in a quantitative way. In this thesis, performance is expressed numerically, to provide a basis for economic decisions.

## CHAPTER FOUR

### TOOL PERFORMANCE TESTS

An investigation has been carried out to compare the cutting performance and tool life evaluation of high speed steel broach samples. The wear tests will be discussed in chapter five. The comparison has been done between conventional M2 and powder metallurgy ASP30 and ASP53 high speed steel broach samples. The ASP53 was a development material.

The cutting performance was evaluated by measuring the cutting forces and calculating the specific cutting energy, an indicator of cutting performance.

As the roughness of the machined surface is an important criterion in the evaluation of performance of a tool, the surface roughness of the workpiece was studied as a function of undeformed chip thickness.

The tests were performed at two cutting speeds, which were 0.7 m/min and 10.5 m/min respectively.

Investigation was carried out on a set of six M2, five ASP53 and four ASP30 broach samples. All broach samples were measured prior to tests.

## 4.1 Measurement of Broach Samples

All the broach samples were measured as received and the following measurements were made.

### 4.1.1 Geometric Features

The broach samples had two teeth and a full gullet (Figure 4.1). A Hilger universal projector was used at a magnification of x25 to measure rake angle, clearance angle, pitch and depth of tooth of broach samples.

The nominal rake and clearance angles were 12 and 4 degrees respectively. The nominal pitch and depth of tooth were 9.6 and 4.6 mm respectively. Measurements of the geometric features are presented in Tables 4.1, 4.2 and 4.3, at total of 90 observations. Deviations from the nominal values were not considered to be significant.

The mean radius of the cutting edge of the broach samples was  $8\pm 3 \mu\text{m}$ .

### 4.1.2 Surface Roughness

A Rank Taylor Hobson Form Talysurf L-120 with a stylus having a nominal radius of  $2 \mu\text{m}$  was used to measure the surface roughness of the following surfaces (Figure 4.2):

1. Rake face (perpendicular and parallel to, and within 1.5 mm of the cutting edge).
2. Clearance face (perpendicular and parallel to, and within 1.5 mm of the cutting edge).

Each measurement consisted of five cut-off lengths of 0.25 mm. This cut-off length was chosen owing to the small space available on each of the above surfaces. Four measurements were made on each surface, in each direction, and the average was recorded (Tables 4.4, 4.5 and 4.6). Two parameters of surface roughness were taken into consideration, which were, Roughness Average (Ra) and Peak to Valley Roughness Height (Rt). The data shown in Tables 4.4, 4.5 and 4.6 represent 480 observations.

The roughness on the rake face measured perpendicular to the cutting edge is an important factor to determine broach tooth surface characteristics, as this surface is responsible for the chip flow resistance. The mean Ra values measured perpendicular to the cutting edge for ASP30, ASP53 and M2 broach samples were 1.42, 0.65 and 1.01  $\mu\text{m}$  respectively.

The surface roughness perpendicular to the direction of chip flow (or cutting edge) affects the friction characteristics and the restriction of the chip flow. Any improvements in surface roughness which will ease the chip flow will improve the efficiency of cutting. In single-point cutting operations the chip disposal is not as important compared with broaching. In broaching operations the chip flows over the rake face, accommodated in the gullet and is ejected at the end of the cut. The poor roughness on the rake face can cause adhesion of the chip, which can damage the surface of the workpiece or overload the tooth leading to a premature failure of the broach tool.

#### 4.1.3 Heat Treatment and Hardness

The following heat treatment cycle was followed by the manufacturers during the production of ASP30, ASP53 and M2 high speed steel tools:

First pre-heat	Dry air to 450°C - 500°C
Second pre-heat	Salt bath at 850°C - 900°C
Hardening	Salt bath at 1180°C (1220°C for M2)
Quench	Salt bath at 550°C

Allow tools to equalise at the above temperature then cool immediately in air to hand warm.

Tempering	Temper three times at 560°C for one hour each minimum.
-----------	--

It is essential to allow the tools to cool fully to room temperature between tempers.

The soaking time was the same for all the three high speed steels.

Vickers diamond pyramid indentation tests were performed to measure the hardness of the broach samples. A load of 50 kg was used for all tests to reduce the variation in measurements. At least ten measurements were taken from each broach sample.

The hardness measurements of all broach samples is presented in Figures 4.3, 4.4 and 4.5, representing 150 measurements. The average of measured values were:

Material	HV	Standard Deviation
M2	868	7.4
ASP53	910	9.7
ASP30	926	10.7

#### 4.1.4 Chemical Composition

The chemical composition (nominal) of the broach samples as supplied by the manufacturer is shown below:

Material	Carbon	Chromium	Molybdenum	Tungsten	Vanadium	Cobalt
M2	0.85	4.0	5.0	6.0	2.0	-
ASP53	2.5	4.2	3.0	4.0	8.0	-
ASP30	1.28	4.2	5.0	6.4	3.1	8.5

It is noted that the hardness of ASP53 is not so high as might be expected from its high vanadium content.

#### 4.1.5 Carbide Distribution

The broach sample materials were polished and then etched with a reagent having the following chemical composition to show the carbide distribution on an optical microscope:

Concentrated hydrochloric acid : 50 ml

Water : 50 ml

Ferric chloride : 10 g

The time of etching was 2 minutes.

The carbide distribution of M2, ASP30 and ASP53 high speed steel broach samples is shown in Figures 4.6, 4.7 and 4.8 respectively. The white spots represent the carbides and the black background is the steel matrix. The uniformity in carbide distribution of powder compacted material is obvious, as compared to the conventional M2 high speed steel.

The samples were polished again and a Philips Scanning Electron Microscope PSEM500 was used to identify the carbides of M2, ASP30 and ASP53 tool materials. Figures 4.9, 4.10 and 4.11 are back-scattered images which show the carbides and their distribution of M2, ASP30 and ASP53 high speed steel tool materials. The bright spots represent the tungsten/molybdenum carbides and the black spots represent the vanadium carbides.

Most of the carbides in M2 and ASP30 tool materials are of tungsten/molybdenum and the Energy Dispersive X-ray Analysis (EDAX) of these carbides is shown in Figure 4.12. The number density of vanadium carbides (dark spots) is very less, as it would suggest from the vanadium content of these two materials. The X-ray analysis (EDAX) of these vanadium carbides is shown in Figure 4.13.

The ASP53 tool material showed the presence of vanadium carbides only and its X-ray analysis (EDAX) is shown in Figure 4.14.

To compare the size and distribution of carbides between M2 and ASP30 tool materials, micrographs were taken at a relatively low magnification. Figures 4.15 and 4.16 represent the back-scattered images of M2 and ASP30 tool

materials respectively. The clusters, streaks and size of carbides in the M2 high speed steel is obvious in Figure 4.15. The uniformity in distribution and size of the carbides is the characteristic feature of the powder compacted high speed steels (Figure 4.16).

#### 4.1.6 The Cutting Edge

A Philips Scanning Electron Microscope SEM500 was used to examine the cutting edges of the broach samples. It was found that the M2 broach samples did not have a keen cutting edge as required for broaching. Figures 4.17 to 4.20 show some of the defects on the cutting edge of M2 broach samples. Figures 4.21 to 4.24 show the cutting edges of ASP30 and ASP53 broach samples.

## 4.2 **Workpiece Material**

The workpiece material was 150M36 alloy steel. This alloy steel is used to manufacture parts of an automobile engine. It had the following chemical composition obtained by chemical analysis and conforms to BS970:1991.

---

Carbon	Manganese	Silicon	Chromium	Nickel	Molybdenum	Sulphur
0.40	1.46	0.25	0.16	0.16	0.05	0.05

---

Vickers diamond pyramid indentation tests were performed on the workpiece material. The mean hardness value was 240 HV with a standard deviation of 4 HV. This analysis represents 50 measurements.

### 4.3 Cutting conditions

The cutting conditions were as follows:

Cutting speed	: 0.7 and 10.5 m/min.
Undeformed chip thickness	: 0.005 to 0.10 mm.
Width of cut	: 10 mm.
Length of cut	: 26 mm.
Cutting fluid	: 7-8% Quaker E750 in water.

The cutting speed of 0.7 m/min was selected to record the cutting process on video tapes. This provided a tool for better understanding of the broaching process. The performance tests at low cutting speed also provided the means to compare and understand the effects of cutting speed on tool performance. The cutting speed of 10.5 m/min was selected for it is the practical cutting speed for high speed steel broaches.

The undeformed chip thickness of 0.005 to 0.015 mm correspond to the tooth-rise for finishing teeth while cutting steels under flat broaching conditions [21]. Similarly the roughing teeth has a rise per tooth of 0.04 to 0.10 mm. This range of undeformed chip thickness also provided the means to understand the effect of undeformed chip thickness on specific cutting energy, an indicator of performance.

The width of the broach sample was 18 mm and a width of 10 mm was selected for the workpiece to achieve flat broaching conditions. The length of cut was calculated by using equation 3.1.

#### 4.4 Instrumentation and Test Procedure

A Kistler dynamometer type 9257A was used to measure the cutting forces during flat broaching experiments. It was a piezoelectric transducer for measuring forces in three components perpendicular to each other. For each of the three force components a proportional electrical charge is set up in the measuring platform. These charges were led into a charge amplifier where they were converted into proportional voltages. A Fylde charge amplifier FE-128-CA was used for this purpose. The output from the charge amplifier provided input for the oscilloscope. A four channel Gould 1604 digital storage oscilloscope having 10 kilobyte memory per channel, with a Gould 260 waveform processor, was used to store and record the data. This data was further processed to compute the cutting forces and the specific cutting energy required for the corresponding undeformed chip thickness.

A Precisa 125A sub-milligram balance was used to weigh the chips obtained during the cutting test. The chips were weighed for the calculation of undeformed chip thickness and specific cutting energy.

The cutting tests were performed at two cutting speeds which were 0.7 m/min and 10.5 m/min respectively. A Parkson vertical milling machine was used for the tests at a cutting speed of 0.7 m/min. A broach sample holder and workpiece vice were specially designed and made for the purpose. A general view of the test rig is shown in Figures 4.25 and 4.26. The workpiece was specially machined and its overall dimensions as shown in Figure 4.27.

A specially adapted Giewont universal milling machine was used to perform the tests at a cutting speed of 10.5 m/min. A minimum feed of 0.020 mm was the limitation of this machine. Figures 4.28 and 4.29 show the general set-up of the test rig. A specially machined workpiece is shown in Figure 4.30.

#### 4.4.1 Measurement of Cutting Forces

In order to compare the cutting performance of the broach samples the cutting force  $F_c$  and the thrust force  $F_t$  were measured by using the instrumentation explained in section 4.4. Figure 4.31 shows two typical traces, recorded during the measurement of forces, for different undeformed chip thicknesses. The traces in red and blue represent the cutting force  $F_c$  and the thrust force  $F_t$  respectively. The horizontal scale represents the time elapsed and each division is 500 millisecond. The vertical scale represents force factor  $Z$  and each division represents 200 newton per volt. The curve was integrated to give area under the curve in volt-sec. The following equation was used to calculate the average cutting force for the corresponding undeformed chip thickness:

$$F_c [\text{newton}] = A[\text{volt} - \text{sec}] \times Z \left[ \frac{\text{newton}}{\text{volt}} \right] \times \frac{1}{T[\text{sec}]} \quad \text{-----} \quad (4.1)$$

Where,

$F_c$  = cutting force

$A$  = area under the curve

$Z$  = force factor

$T$  = time taken to complete the cut

Similarly the thrust force  $F_t$  was calculated by integrating the corresponding curve and repeating the above calculations.

The following equation was used to calculate the undeformed chip thickness:

$$UCT[m] = \frac{W[kg]}{\rho \left[ \frac{kg}{m^3} \right] \times L[m] \times b[m]} \quad \text{-----} \quad (4.2)$$

Where,

$W$  = weight of chip

$\rho$  = density of workpiece material

$L$  = length of cut

$b$  = width of cut

In practice the units used for undeformed chip thickness are millimetres.

Figures 4.32 and 4.33 represent the cutting and thrust forces per unit width of the workpiece as a function of undeformed chip thickness at cutting speeds of 0.7 and 10.5 m/min respectively. These figures represent 109 measurements.

#### 4.4.2 Specific Cutting Energy

To compare the cutting efficiency of the broach samples the specific cutting energy was calculated by using the equation (2.5). The cutting force and the corresponding undeformed chip thickness was determined by using the equations (4.1) and (4.2) respectively. Figures 4.34 and 4.35 show the specific cutting energy as a function of undeformed chip thickness at cutting speeds of 0.7 and 10.5 m/min respectively. These curves are discussed in section 4.5.

#### 4.4.3 Roughness of Machined Surface

Owing to the importance of roughness of the machined surface an investigation was carried out to measure the surface roughness of the machined surface. Two parameters of surface roughness were considered i.e. Roughness Average (Ra) and Peak to Valley Roughness Height (Rt). The values of Ra and Rt were measured in both the directions, perpendicular and parallel, to the direction of cutting.

A Rank Taylor Hobson Form Talysurf 120-L was used to measure the roughness of machined surface. Each measurement consisted of seven cut-off lengths of 0.8 mm each. A set of four measurements were made on a broached surface, in each direction, and their average was recorded. Figures 4.36 to 4.39 show the Ra and Rt of the machined surface, measured perpendicular and parallel to the direction of cut, as a function of undeformed chip thickness at a cutting speed of 0.7 m/min. The effect of undeformed chip thickness on Ra and Rt of machined surface, measured perpendicular and parallel to the direction of cut, at a cutting speed of 10.5 m/min is shown in Figures 4.40 to 4.43. This analysis represent 436 measurements.

## **4.5 Discussion of Results**

1. The X-ray analysis (EDAX) and the back-scattered image (Figure 4.11) of the ASP53 tool material shows that it had only one type of coarse carbide i.e. vanadium carbide. The vanadium has a strong chemical affinity with the carbon [1] and apparently no carbon was left for tungsten and molybdenum to form their carbides. The presence of tungsten and molybdenum in the vanadium carbide can be seen in Figure 4.14. It suggests that these metals are dissolved in the vanadium rich carbides.
2. The size of the carbide cluster (~375  $\mu\text{m}$  long) in Figure 4.15 can be compared with the size of defect (~380  $\mu\text{m}$  long) on the cutting edge of an M2 broach sample shown in Figure 4.18. It can be inferred that a carbide cluster was knocked out during the grinding of the edge. Similarly the presence of a massive burr on the cutting edge of another M2 broach sample (Figure 4.17) suggests the existence of a carbide cluster. Figures 4.19 and 4.20

show similar defects on the cutting edges of the M2 broach samples.

3. The Figures 4.21 to 4.24 show the keen cutting edges of the ASP30 and ASP53 broach samples. Due to the uniform carbide distribution of these steels, a keen cutting edge can be obtained with certainty.

All graphs which are represented as a straight line have been obtained by a least square fit analysis.

Performance tests at a cutting speed of 0.7 m/min revealed the following:

4. The cutting and thrust forces were practically the same while cutting with ASP30, ASP53 and M2 broach samples and are shown in Figure 4.32. This was because the cutting force is largely influenced by tooth geometry and does not depend upon the material of the tool. These broach samples had the same nominal tooth geometry.
5. The slope of the lines (Figure 4.32) suggests that increasing the undeformed chip thickness caused a proportional increase in the cutting and thrust forces. This is because the shear stress required to plastically deform the material is approximately constant [14, 26].
6. There was no practical difference in the specific cutting energy while cutting with ASP30, ASP53 and M2 broach samples. Equation (2.5) shows that specific cutting energy is the workdone per second over metal removal rate. Figure 4.34 is a typical specific cutting energy curve as a function of undeformed chip thickness. At low values of undeformed chip

thickness the specific cutting energy is high and approaches infinity. In a broaching situation at very fine undeformed chip thickness the edge radius has a great influence on the cutting process. At these low values of undeformed chip thickness the total cutting force contains a large element of redundant forces which are made of ploughing force and friction force. At high feed values in the case of above 30  $\mu\text{m}$  the specific cutting energy is constant i.e. the edge radius of the tool has no effect. This has been explained in detail by [27, 28].

7. The roughness of the machined surface was less while cutting with ASP30 and ASP53 than that of M2 broach sample (Figures 4.36 to 4.39). The scatter of Ra and Rt values from the least square line was also less. This can be explained by the better cutting edges of the powder compacted material. A broken edge (Figures 4.17 to 4.20) leaves a very large edge radius which results in increased roughness of the machined surface [21]. The length of defect ( $\sim 380 \mu\text{m}$ ) on the cutting edge is too small compared to the width of cut (10 mm) to affect the average cutting force but leaves a comparatively rough surface.

Performance tests at a cutting speed of 10.5 m/min revealed the following:

8. There was no practical difference in the cutting force, thrust force and the specific cutting energy while cutting with ASP30, ASP53 and M2 broach samples (Figures 4.33 and 4.35). This has been explained above in paragraphs 4, 5 and 6.
9. Figures 4.40 to 4.43 show that the broach samples made from powder compacted steels, ASP30 and ASP53, gave consistently better surface finish, measured in both the directions, compared

with M2 steel. Adhesion between tool and workpiece in the form of built-up edge was observed in all cases. This is because M2 broach samples tend to have a larger built-up edge than the powder compacted broaches. Due to the uneven cutting edge of the M2 broach, the cutting pressure varies considerably along the edge. A higher local pressure promotes the formation of built-up edge, resulting in a poor surface [23].

10. All the curves shown in Figures 4.40 to 4.43 show a positive slope which suggests a decrease in surface quality with increasing undeformed chip thickness. Increasing the undeformed chip thickness is expected to increase the scale of the deformation, with an increase in all dimensions, including that of the built-up edge. This, in turn, gives increased roughness. The micrographs in Figures 2.9 and 2.10 show the machined surface produced while cutting with a built-up edge.
11. The effect of cutting speed on the Ra value of the machined surface can be seen by comparing the Figures 4.36 and 4.37 with 4.40 and 4.41 respectively. A similar effect on Rt can also be seen by comparing Figures 4.38 and 4.39 with 4.42 and 4.43 respectively. At extremely low cutting speeds, there is time available for the cutting fluid to penetrate into the tool-work interface. This reduces the width of the contact zone where adhesion occurs, and may eliminate built-up edge, with a beneficial effect on finish. As practical values of cutting speed are reached, there is no time for penetration of cutting fluid, and a built-up edge develops. The formation and collapse of the built-up edge leaves a rough surface. At even higher cutting speeds (approximately 100 m/min), the increased temperature at

the tool-work interface will not allow built-up edge to become established, and surface finish is found to improve [21, 22].

## CHAPTER FIVE

### WEAR TESTS

Simulation tests were carried out to investigate the useful life of the broach samples.

#### **5.1 Cutting Conditions**

The cutting conditions were as follows:

Cutting speed : 10.5 m/min.

Feed rate : 0.079 mm/rev.

Width of cut : 10 mm.

Length of cut : 30 mm.

Cutting fluid : 7-8% Quaker E750 in water.

#### **5.2 Test Procedure**

The wear tests were carried out on a specially modified fully variable-speed Churchill Denham SR10V centre lathe having a three-jaw chuck. The overall set-up is shown in Figure 5.1. A tool holder was designed and machined to

accommodate a broach sample and mounted on a standard tool post of the lathe, shown in Figure 5.2.

A perspective view of the specially machined workpiece is shown in Figure 5.3. A set of two workpieces were assembled into a specially machined workpiece holding jig (Figure 5.4). The workpiece had two legs **A** and **B** as shown. The workpieces were gripped at 180 degrees to each other and the legs marked **A** were cut first. A complete revolution of the chuck produced two cuts, one on each workpiece. An automatic feed rate of 0.079 mm/rev was selected for all wear tests, with a spindle speed of 15 rev/min. The workpieces were unbolted and fastened again so that the legs marked **B** could be subjected to cutting. In this manner the cutting speed was kept constant. A set of two workpieces gave a total length of cut of 21 meters in approximately 24 minutes.

Although this set-up did not give truly orthogonal cutting, this was the closest possible solution for performing the extensive wear tests.

### 5.2.1 Measurement of Wear Land

The broach sample was removed intermittently for measurement of the wear land width. A tool maker's microscope at a magnification of x30 was used for this purpose. The wear land width  $VB = 0.3$  mm was the criterion of useful tool life. Progress of the wear scar was recorded by using an optical and a scanning electron microscope. Figures 5.5, 5.6 and 5.7 show the wear scar on the flank face at the end of useful tool life of M2, ASP53 and ASP30 broach samples respectively. The progress of tool life of the broach samples is shown in Figure 5.8, representing 67 measurements.

### 5.2.2 Roughness of Machined Surface

The surface roughness of the workpiece was also recorded throughout the life of the broach sample. The selection of cut-off length and the surface roughness parameters were the same as explained in Section 4.2. The roughness of the machined surface was measured after suitable intervals of cutting. The effect of tool-wear on the machined surface is shown in Figures 5.9 and 5.10. This analysis represents 144 measurements.

## 5.3 Discussion of Results

1. Adhesion between tool and work in the form of built-up edge was observed in all cases and there is strong evidence of sliding between tool and workpiece (Figure 5.13). The slip at the interface was intermittent and probably there was slip at the beginning of each cut and sticking occurred later. Adhesion of workpiece on the flank face can be seen in Figures 5.5 and 5.14. This adhered material was analysed and identified as workpiece material by using energy dispersive X-ray analysis on the scanning electron microscope. During the period when the tool is not cutting, it cools and when the new cut starts the adhering work material is torn off and sliding occurs until a new zone of stagnant material is built up, and slip at the interface stops. Figures 5.15 and 5.16 show the adhered work material on the rake face and the scars caused by chipping on the flank faces of M2 and ASP30 broach samples respectively. The chips were small in the case of powder compacted steel and can be seen at a relatively high magnification in Figure 5.17. The sliding wear

mechanisms found in these cases are both adhesion and abrasion.

2. The differences in the gradual wear between the different tool materials for the same work material thus depend on differences in the strength of the adhesion and the toughness of the tool material. A closer look into the Figures 5.5, 5.6 and 5.7 shows that the M2 steel has a greater tendency for adhesion compared to the powder compacted steels.
3. While strong adhesion protects the edge from wearing away it also causes a greater risk of chipping. Adhesion appears to be stronger in the case of M2 steels. To avoid the chipping, the tool should have high toughness. The toughness of the tool material depends upon uniformity in distribution and size of carbides [5]. The powder compacted materials have proved to possess high toughness and hence have a longer tool life as shown in Figure 5.8. This conclusion has also been reached by others [8, 9, 23, 24].
4. The ASP30 broach showed an increase in life of 225% over that of M2 broach. It may be noted that the scars due to microscopic chipping on the flank faces were larger for M2 than for ASP30 (see Figures 5.13 and 5.15).
5. The ASP30 and ASP53 broaches gave better surface finish on the workpiece compared to that of M2 broach (Figures 5.9 to 5.12). This has been explained in section 4.5 paragraph 9.
6. Surface finish produced by the tool throughout its useful life is an important factor to consider. The slope of the lines in Figures

5.9 to 5.12 suggests that roughness of the machined surface was not affected as the life of the tool progressed. In the case of M2 broach the scatter of Ra values from the least square fit line is relatively larger compared with that of broaches made from powder compacted steel. This suggests that wear of the M2 broach occurred in jumps rather than gradually, as can be seen in Figure 5.8. The adhesion of relatively large amount of workpiece material in the form of built-up edge causes large pieces of tool material to be torn away, resulting in erratic performance in terms of wear rate and quality of finish of the machined surface.

## CONCLUSIONS

The following conclusions drawn from the work in this thesis are hoped to broaden the understanding of why the performances of alternative high speed steels vary, and how this understanding can be used to improve the performance of high speed steel broaches.

1. The surface roughness of the workpiece depends upon the quality of the cutting edge. The M2 broach samples possessed a poor edge which resulted in a rough surface ( $\sim Ra=1.1 \mu\text{m}$ ) even at very low cutting speed (0.7 m/min). Whereas, the ASP broach samples gave better finish at the same cutting speed ( $\sim Ra=0.6 \mu\text{m}$ ).
2. A keen cutting edge cannot be produced on a conventional high speed steel tool because of irregular distribution of carbides, which causes problems during grinding.
3. The anti-segregation process high speed steel has greater toughness with respect to hardness, this allows the tool to wear slower than the M2 steel. The ASP30 gave 2.25 times the life of M2 broach sample. This is due to the uniform distribution of carbides in the powder compacted steels.
4. The cost of ASP30 and ASP53 is twice that of M2 steel, and as the ASP30 gave in excess of double the life and an improved surface finish compared to M2 steel. The extra cost is therefore justified.

5. The ASP53, being a development material, although gave a better surface finish but the tool life was only 1.3 times that of M2 steel and is therefore not cost-efficient.
6. The ASP broach samples had a reliable cutting edge which could prove to be a better material for surface engineering applications (e.g. TiN coating).

## REFERENCES

1. Hoyle G. High Speed Steels. Butterworth and Co. (Publishers) Limited. 1988.
2. Rong W, et al. The Role of Alloy Composition in the Precipitation Behavior of High Speed Steels. ACTA Metalurgia et Materialia. vol. 7, p.1727, 1992.
3. Kremnev L S, Geller Yu A. Effect of Tungsten on the Properties of High Speed Steels. Metall. Mining. vol. 1, p.136, 1964.
4. Beard T. PM Tool Steels Keep the Edge. Modern Machine Shop. vol. 62(3), p.56, 1989.
5. Kremnev L S. Theory of Alloying of High Speed Steels. Trans. Metal Science and Heat Treatment. vol. 33(5-6), p.428, 1991.
6. Santhanakrishnan G, Krishnamurthy R, Malhotra S K. High Speed Steel Tool Wear Studies in Machining of Glass-fibre-reinforced Plastics. Wear. vol. 132(2), p.327, 1989.
7. Andrews R E, Groves J, Jacobs M H. High Pressure and High Velocity Gas Quenching of Tool Steels After Vacuum Heat Treatment. Heat Treatment Conference. p.41.1, 1984.
8. Hellman P. High Speed Steels for Broaching. S.M.E. Manufacturing Engineering Transactions and 12th North American Manufacturing Research Conference. p.14, 1984.

9. Lowder S H, Bhardwaj J. Cutting Tools for State-of-the-art Machining. 2nd Biennial International Machine Tool Technical Conference. vol. 3, p.7(189), 1984.
10. Jacobs M H. Family of Designs Seeks Balance of Cooling Rate, Capacity, Cost. Heat Treatment. vol. 9, p.30, 1985.
11. Hellman P, Billgren P. Commercial Gas Atomisation of High Speed Steels. Met. Powder Report. vol. 40(1), p.38, 1985.
12. Hellman P, et al. The ASEA-STORA-Process. Modern Developments in Powder Metallurgy. vol. 4, p.573, 1970.
13. Hellman P, Wisell H. Toughness of Powder Metallurgy High Speed Steels. 5th European Powder Metallurgy Symposium. p.216, 1978.
14. Boothroyd G. Fundamentals of Metal Machining and Machine Tools. Scripta Book Company. 1975.
15. Ghani A K, Barrow G. Tool Failure at Exit During Interrupted Cutting. Annals of the CIRP. vol. 34(1), p.71, 1985.
16. Vijayaraghavan L, Krishnamurthy R. Dimensional Accuracy in Internal Broaching. 12th AIMTDR conference IIT Delhi. p.285, 1986.
17. Cox W. Why Use Straddle Broaching? Modern Machine Shop. vol. 60(10), p. 82, 1988.
18. Beach J. New twist ... Broaching on The Fly. Machine and Tool Blue Book. vol. 82(4), p.75, 1987.

19. Van De Motter C, Haupthoff W. Broaching Flats Leads to Productivity and Quality Improvements. Tooling and Production. vol. 55(9), p.43, 1989.
20. Konig W, et al. Machining hard materials with geometrically defined cutting edges - Field of applications and limitations. Annals of the CIRP. vol. 39(1), p.61, 1990.
21. Forst Handbook - Hints on Broaching. 1973. Oswald Forst Gesellschaft Mit Beschränkter Haftung.
22. Kuljanic E. Cutting Forces and Surface Roughness in Broaching. Annals of the CIRP. vol. 24(1), p.77, 1975.
23. Alvelid B, Wisell H. Wear of High Speed Steel in Orthogonal Milling. Scandinavian Journal of Metallurgy. vol. 9, p.59, 1980.
24. Bouzakis K D, Konig W. Use of Powder Metallurgical High Speed Steel in Gear Hobbing and Gear Shaping. Annals of the CIRP. vol. 31(1), p.25, 1982.
25. Ahman L, et al. Wear of High Speed Steel Milling Tools. Scandinavian Journal of Metallurgy. vol. 14, p.60, 1985.
26. Kapolinsky E M, Oxley P L B. An Investigation of the Influence of Feed and Rake Angle on the Ratio of Feed Force to Cutting Force when Machining with Negative Rake Angle Tools. Annals of the CIRP. vol. 33(1), p.43, 1984.
27. Lucca D A, Seo Y W. Effect of Tool Edge Geometry on Energy Dissipation in Ultraprecision Machining. Annals of the CIRP. vol. 42(1), p.83, 1993.

28. Sarwar M. and Thompson P J. Cutting Action of Blunt Tools.  
International MTDR Conference, Manchester. p.295, 1981.

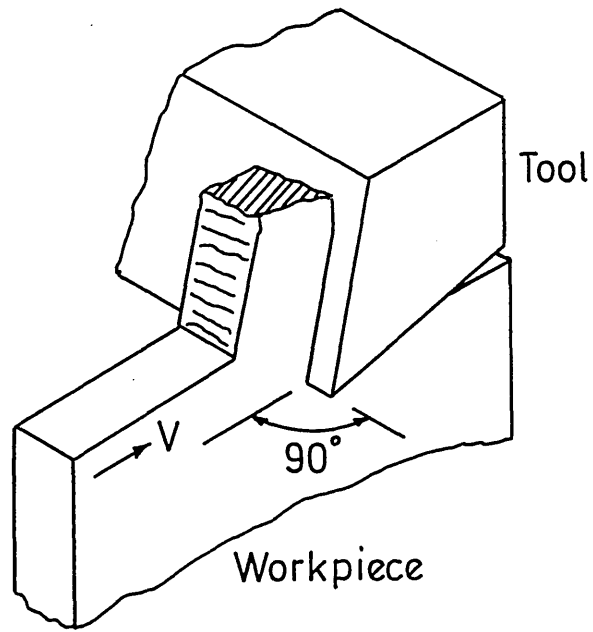


**Figure 2.1** A perspective view of orthogonal cutting.

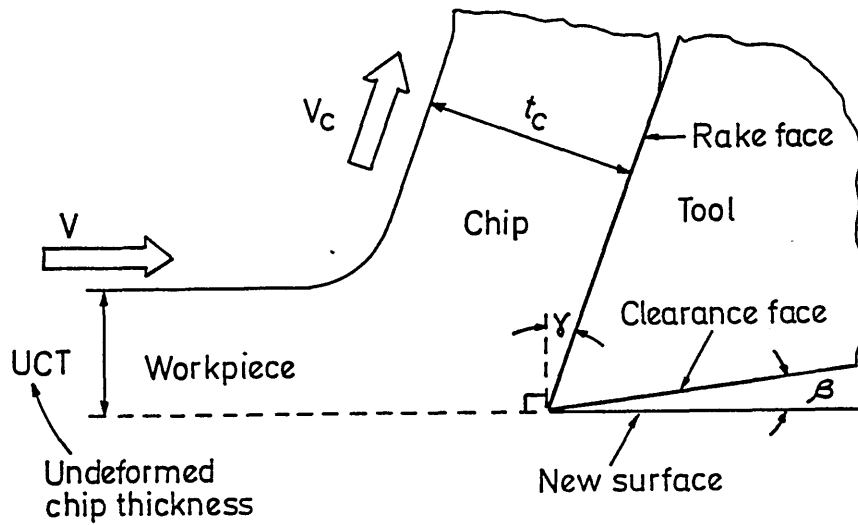


**Figure 2.2** A metal cutting diagram showing the rake angle  $\gamma$ , clearance angle  $\beta$ , cutting speed  $V$ , undeformed chip thickness UCT, chip thickness  $t_c$  and chip velocity  $V_c$ .

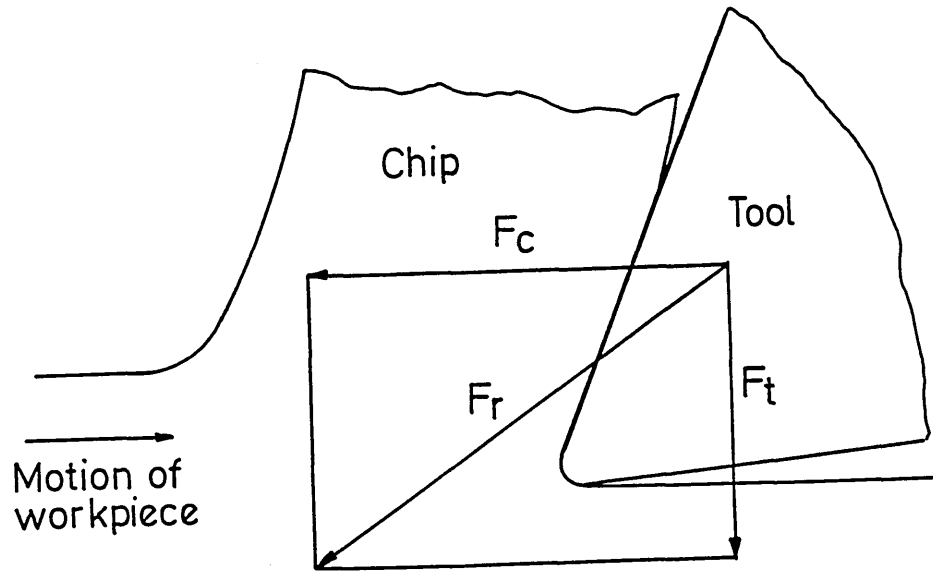


**Figure 2.3** Forces acting on the tool in orthogonal cutting.

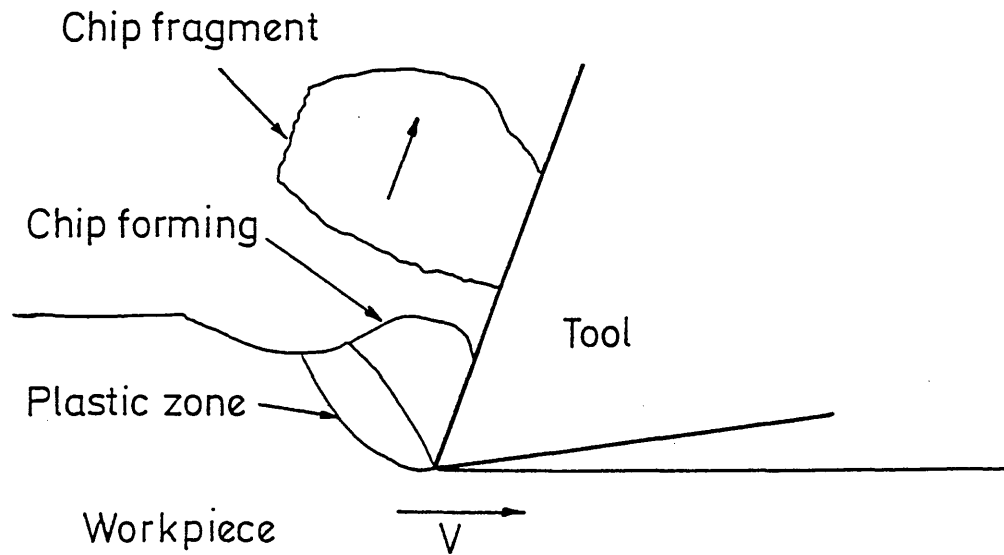


**Figure 2.4** Fragmental or discontinuous chips.

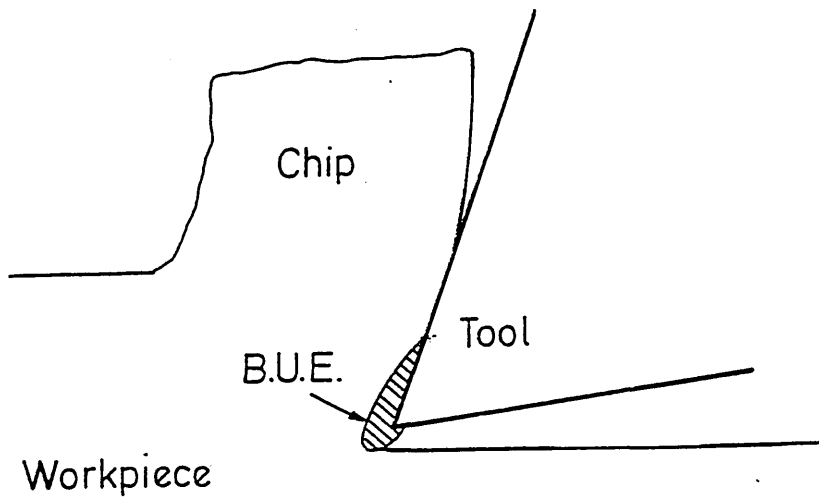


**Figure 2.5** Continuous chip with built-up edge.

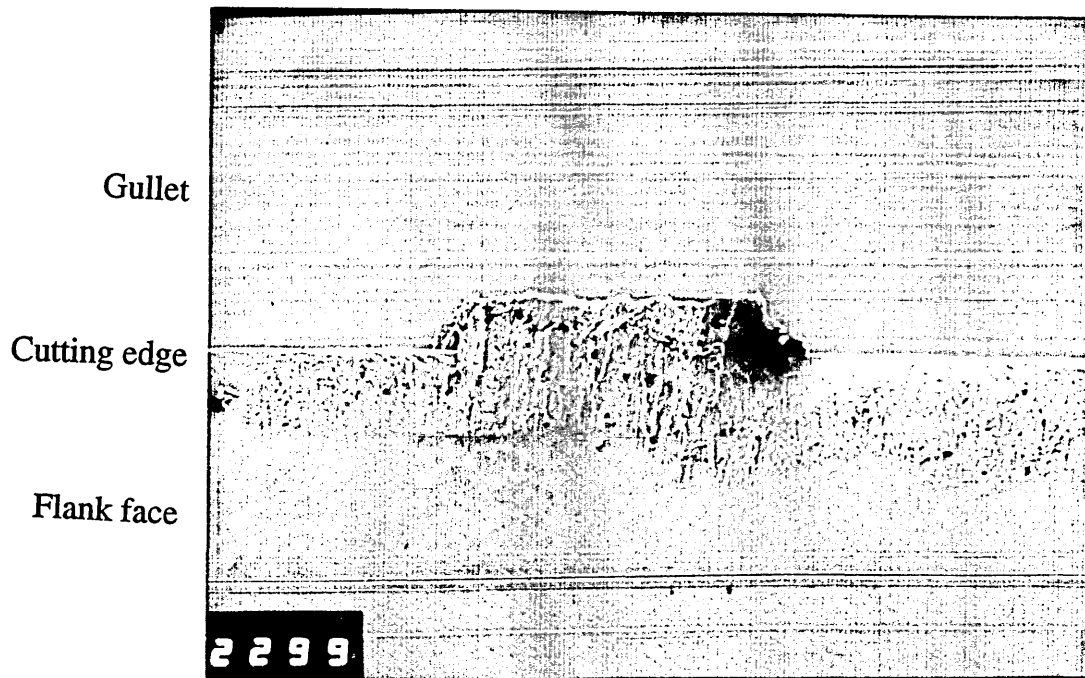


**Figure 2.6** A micrograph showing the built-up edge and the wear scar on the clearance face (x25).

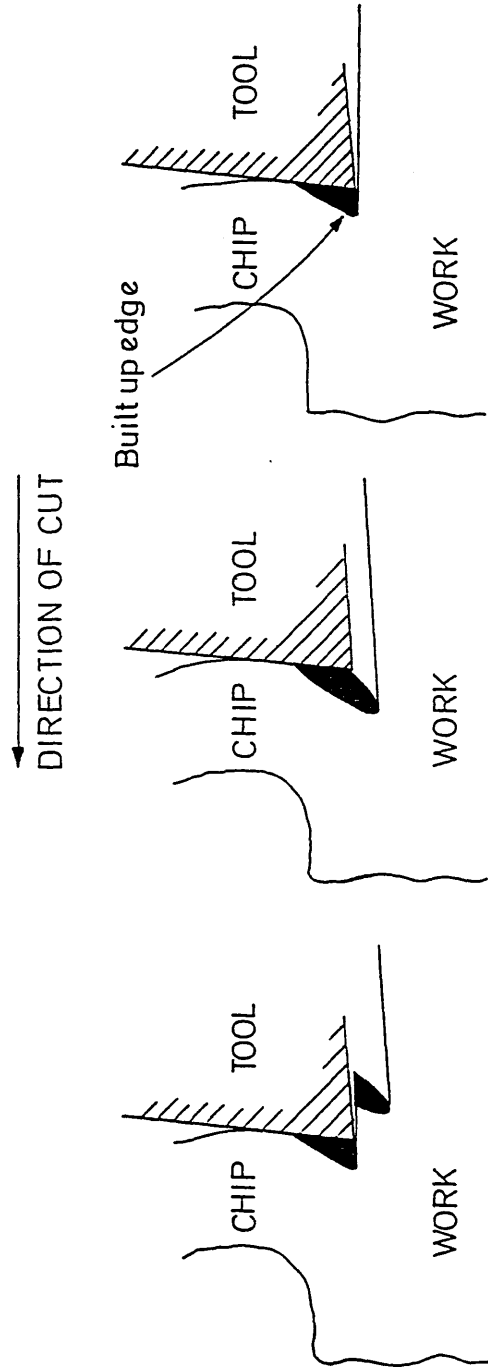


**Figure 2.7** Formation and failure of built-up edge leaving a poor machined surface. The built-up edge has been shaded dark only to illustrate.

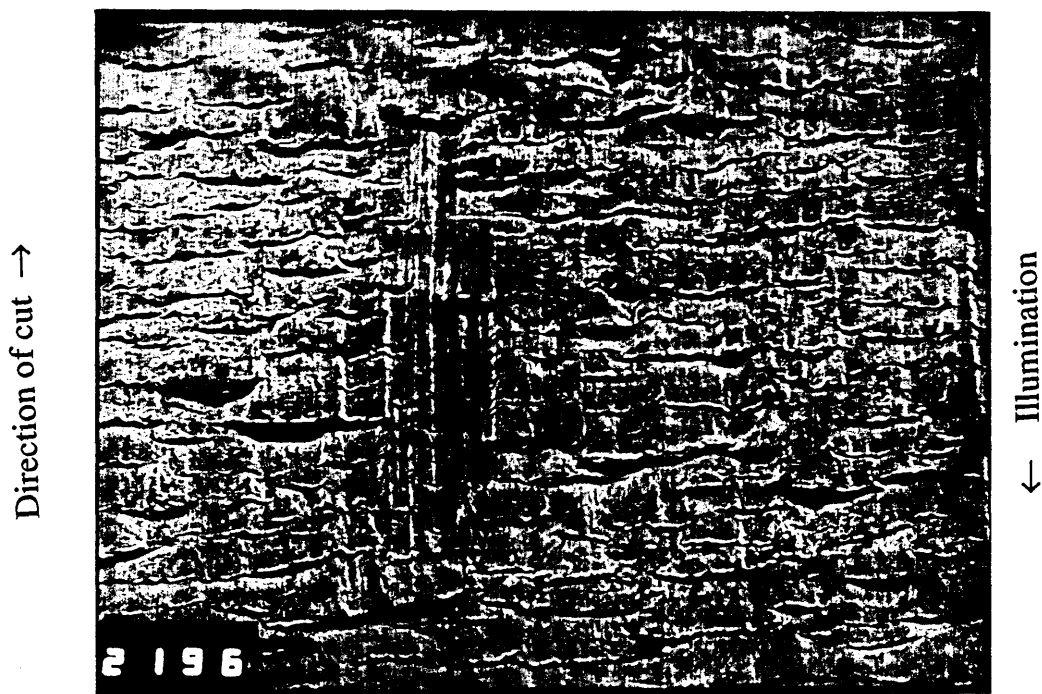


**Figure 2.10** A micrograph showing the machined surface while cutting with a built-up edge. The illumination is opposite to the direction of cut (x40).

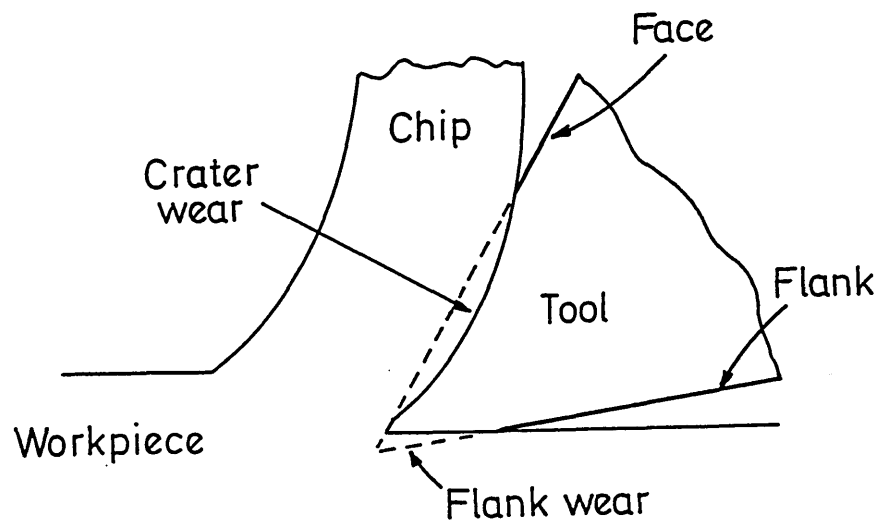


**Figure 2.11** Typical wear on a tool in orthogonal cutting.

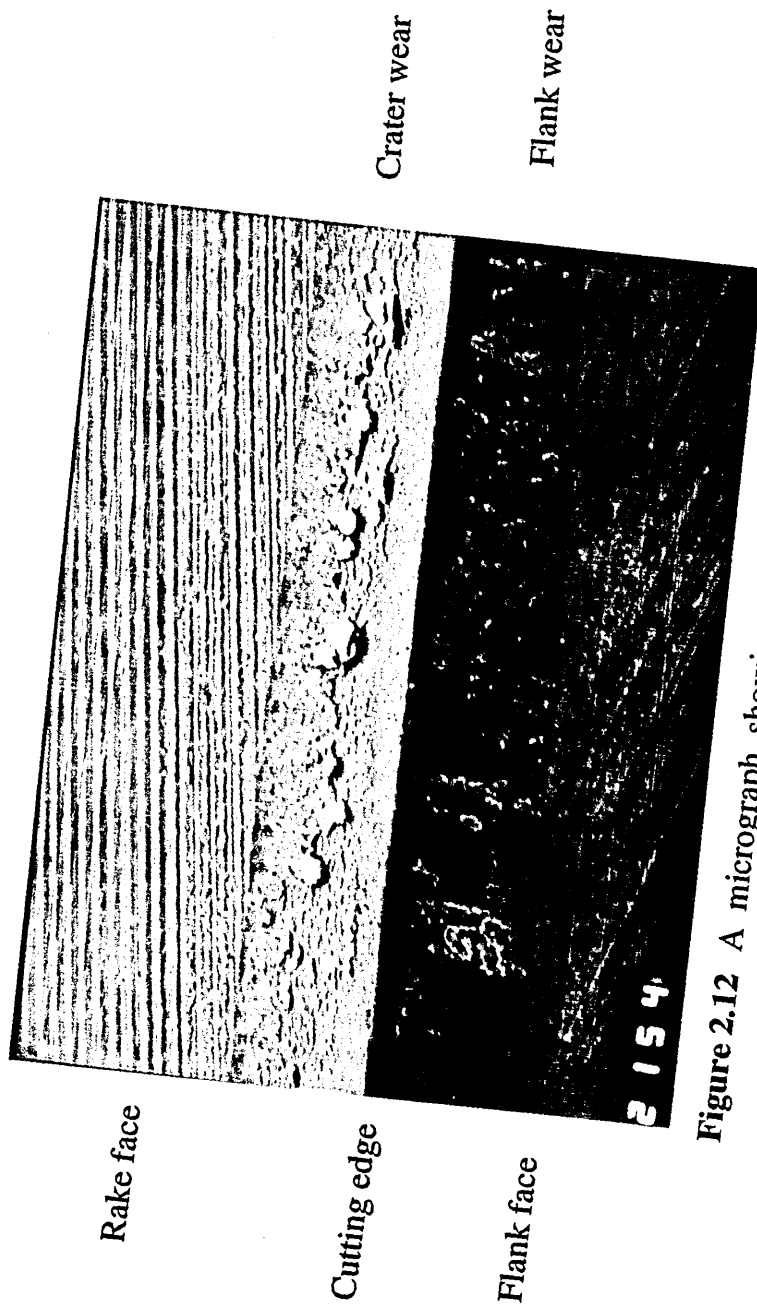
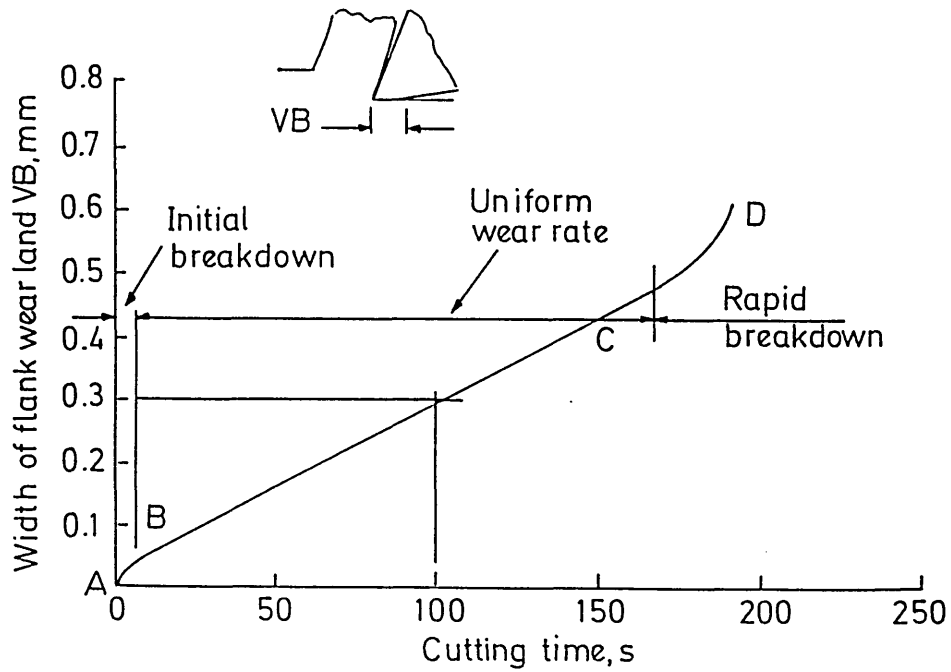
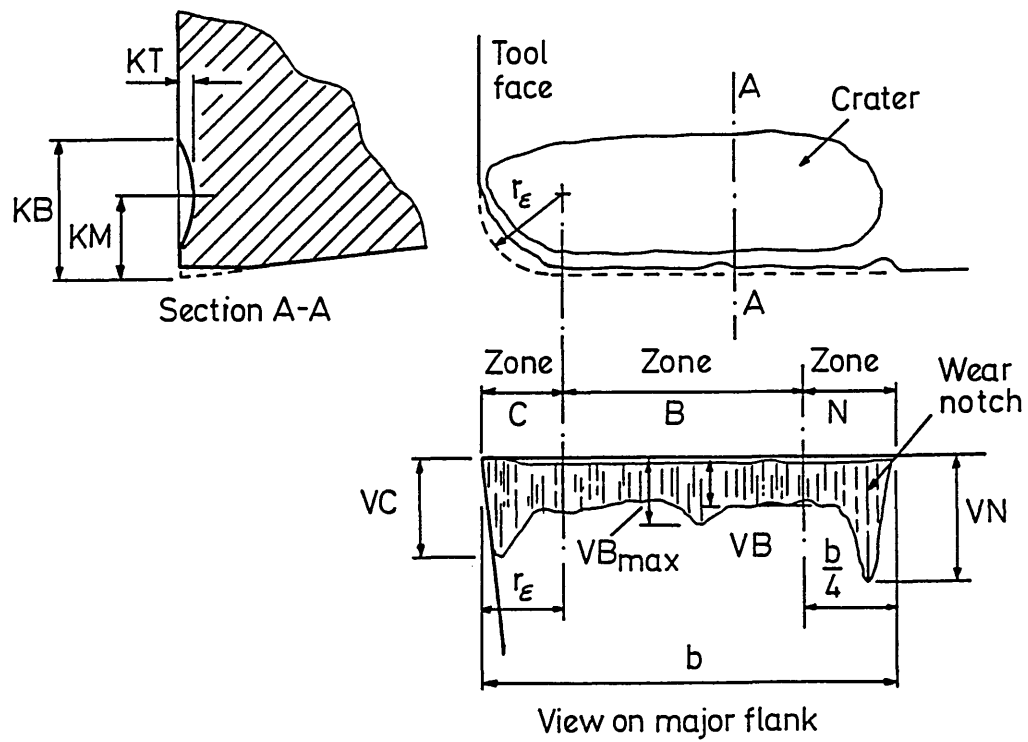


Figure 2.12 A micrograph showing a typical wear scar in orthogonal cutting (x75).



**Figure 2.13** Development of flank wear with time for a carbide tool at a cutting speed of 1 m/s [18].



**Figure 2.14** Some features of single-point tool wear in turning operations [18].

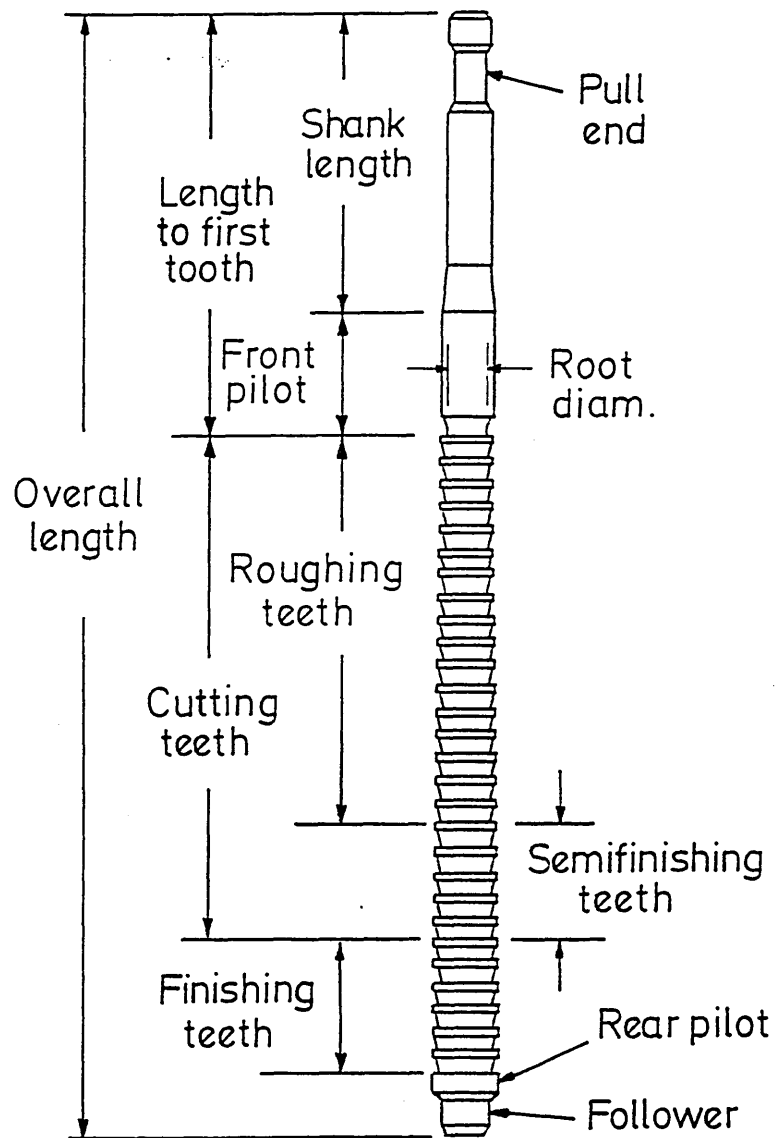


**Figure 3.1** A diagram showing the significant features of a round internal broach.

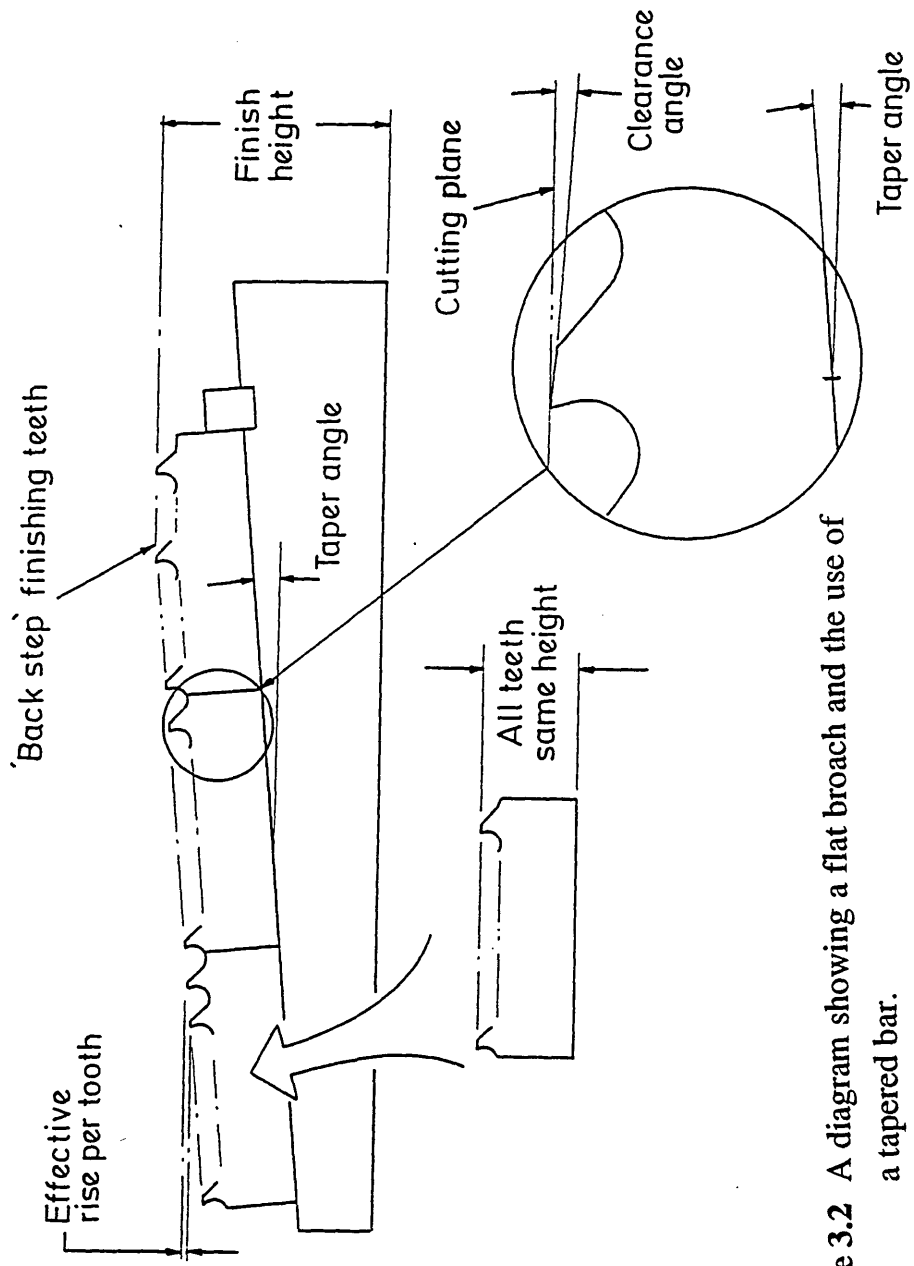


**Figure 3.2** A diagram showing a flat broach and the use of a tapered bar.

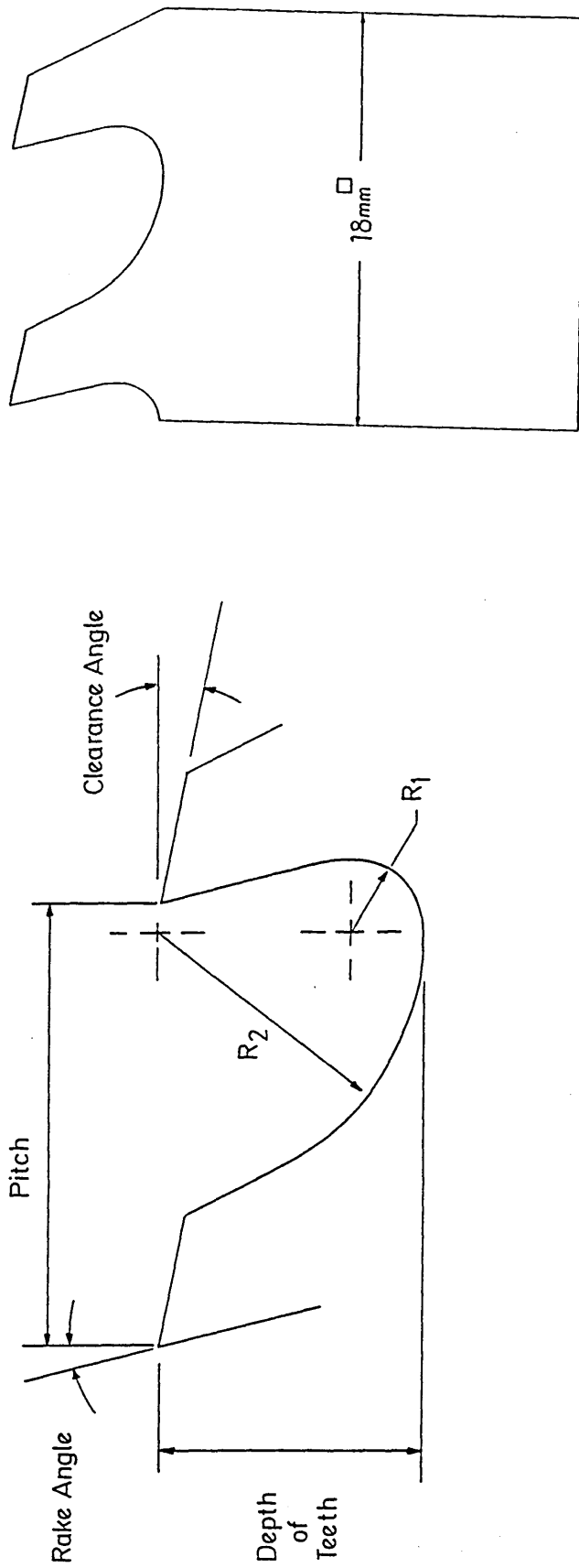


**Figure 4.1** A side view of the broach sample showing the geometric features.  $R_1$  is the rake angle radius and  $R_2$  is the back-of-tooth radius.

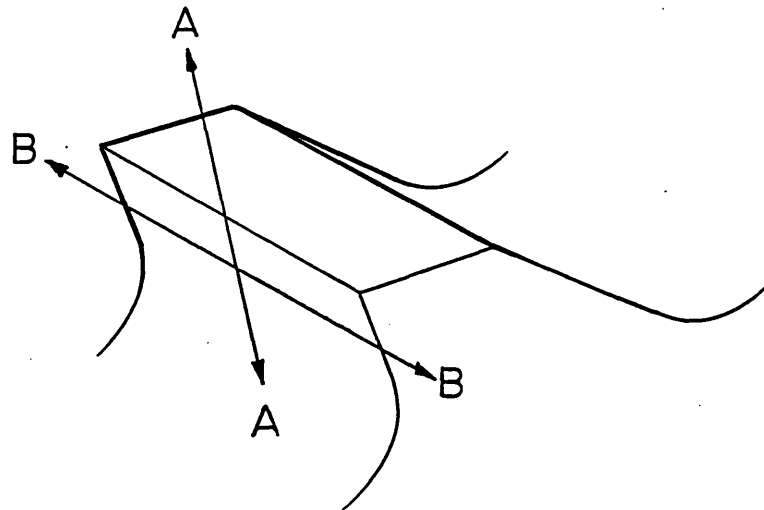
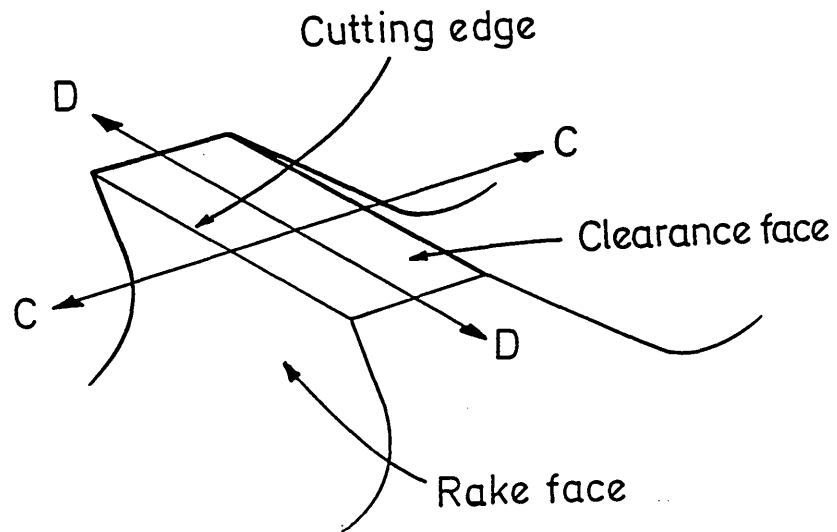


**Figure 4.2** A sketch showing the directions of measuring the roughness of significant surfaces of the broach samples.

# Vickers hardness of M2 broach samples

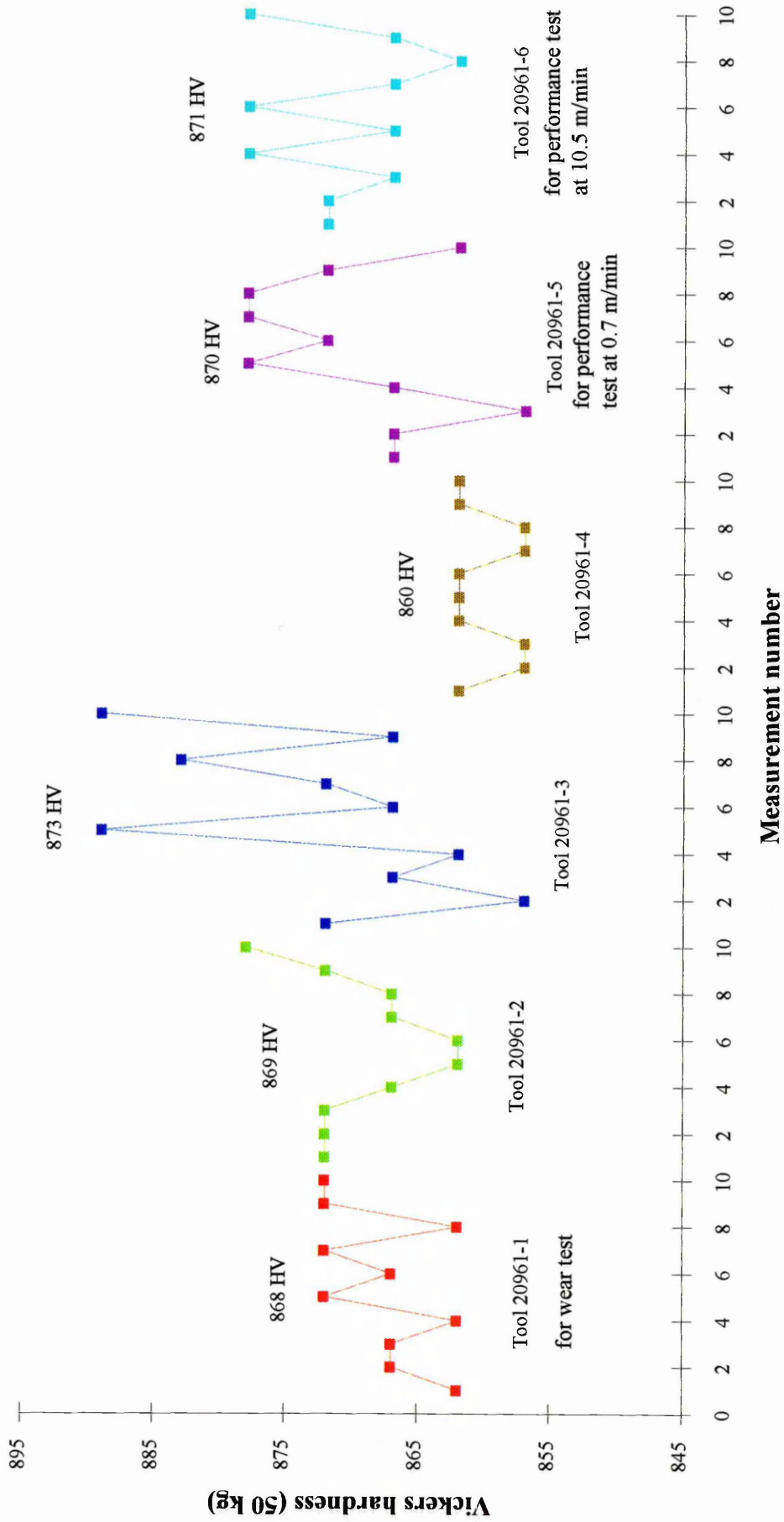


Figure 4.3

# Vickers hardness of ASP53 broach samples

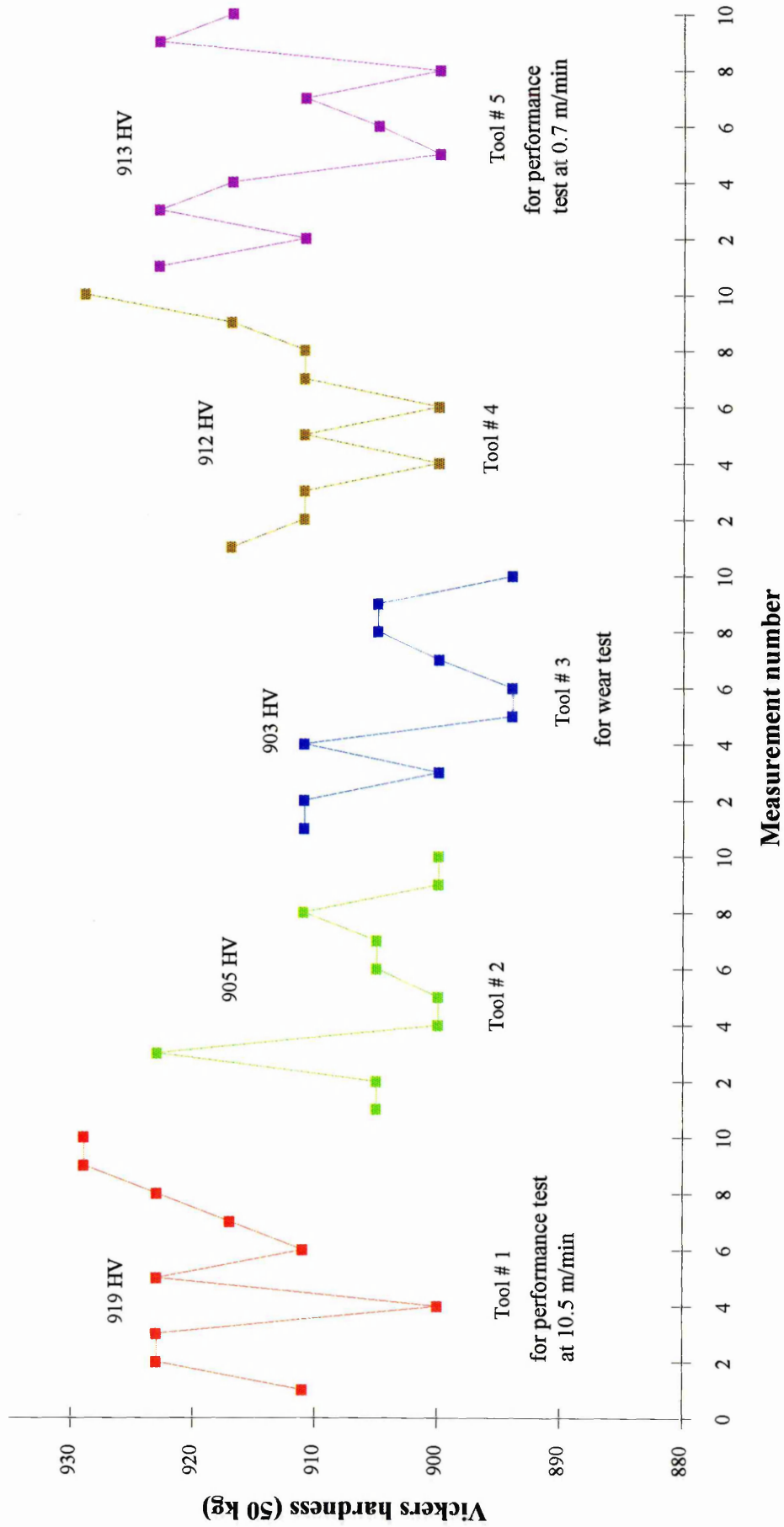


Figure 4.4

# Vickers hardness of ASP30 broach samples

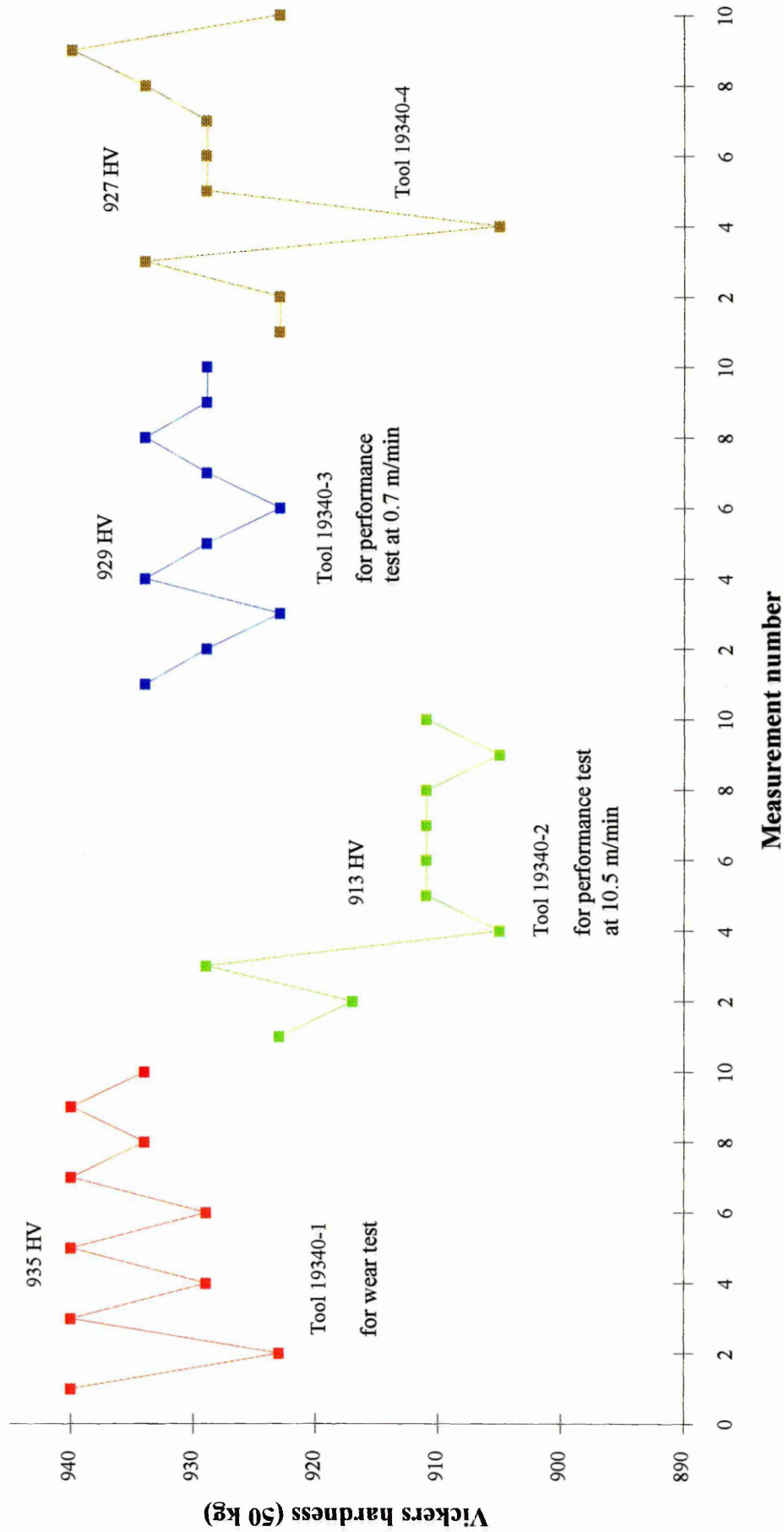


Figure 4.5



**Figure 4.6** Carbide distribution of M2 HSS as seen under an optical microscope (x600).



**Figure 4.7** Carbide distribution of ASP30 HSS as seen under an optical microscope (x600).

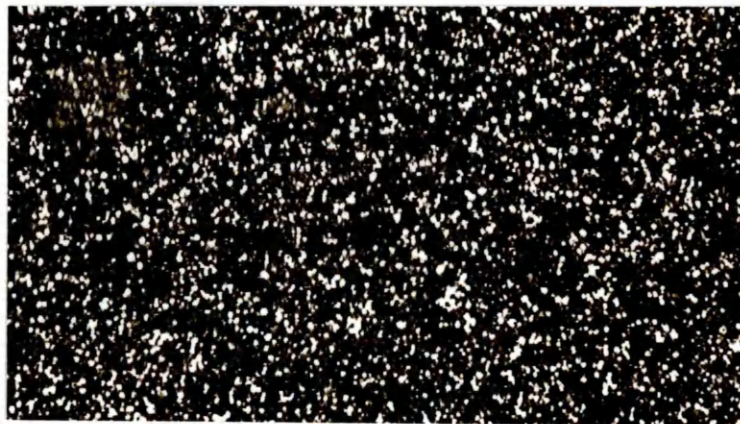


**Figure 4.8** Carbide distribution of ASP53 HSS as seen under an optical microscope (x600).

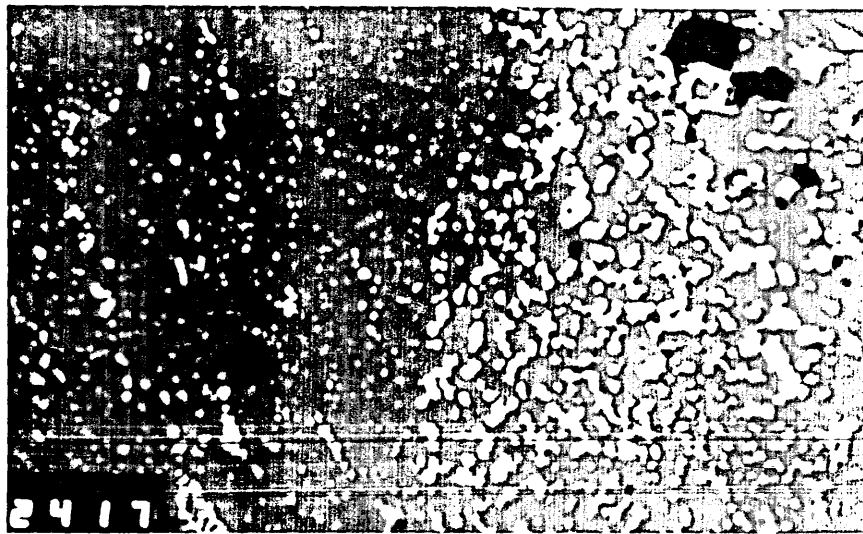


Figure 4.9 Carbide distribution of M2 HSS (x960).

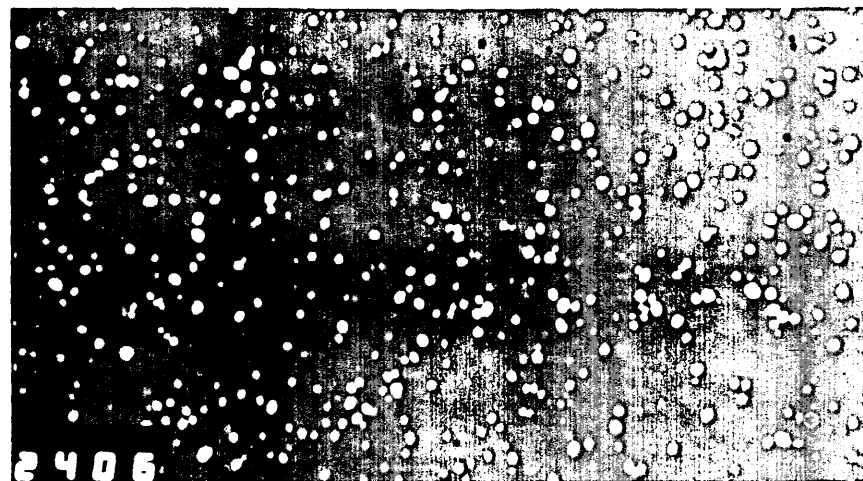


Figure 4.10 Carbide distribution of ASP30 HSS (x960).

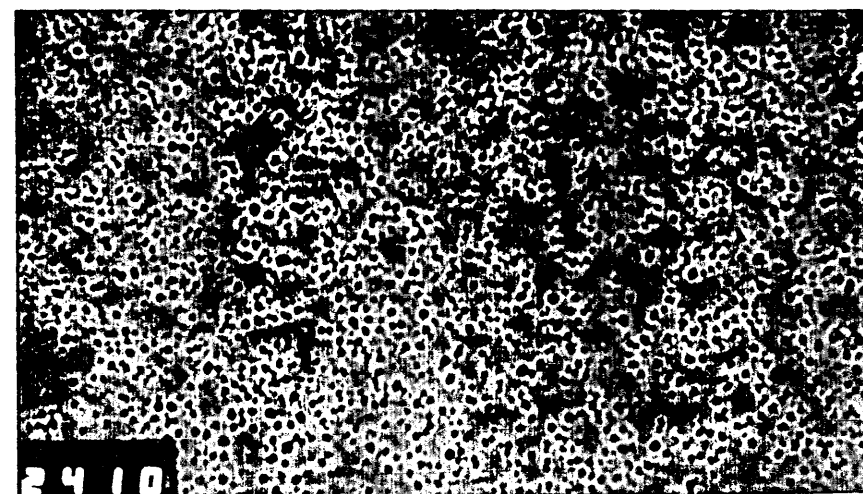


Figure 4.11 Carbide distribution of ASP53 HSS (x960).

Analysis of ASP30  
Tungsten/Molybdenum Rich  
Carbide

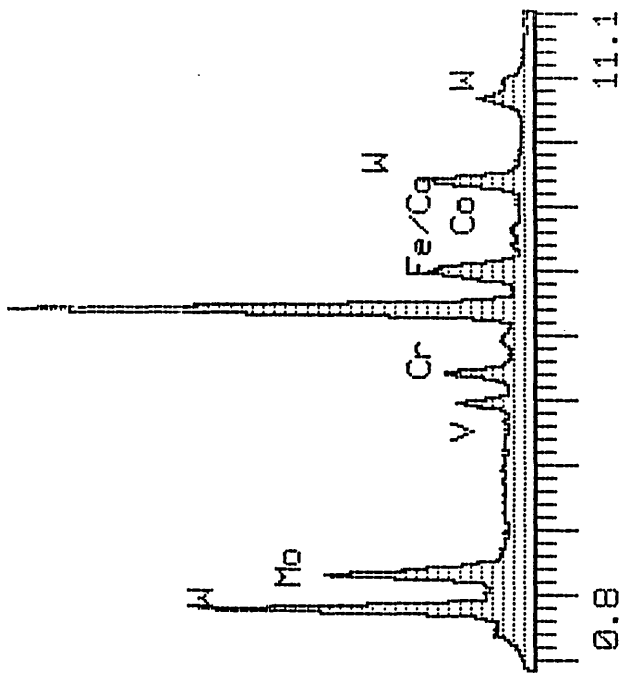


Figure 4.12 X-ray analysis of the tungsten/molybdenum rich carbides of ASP30 tool material.

Analysis of ASP30  
Vanadium Rich Carbide

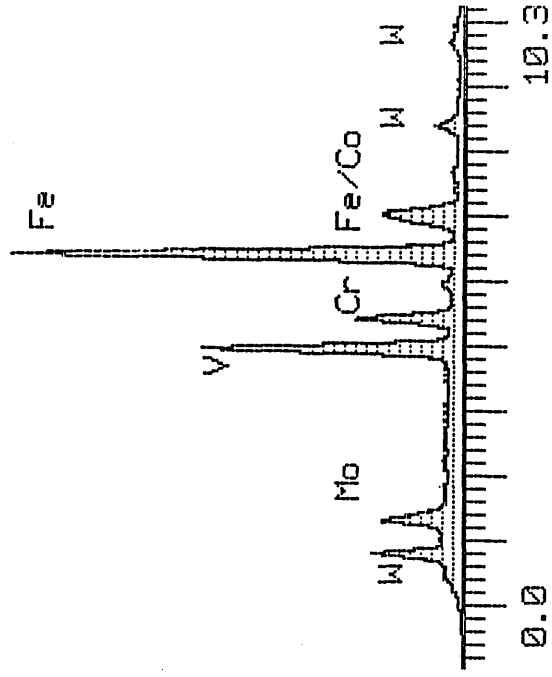
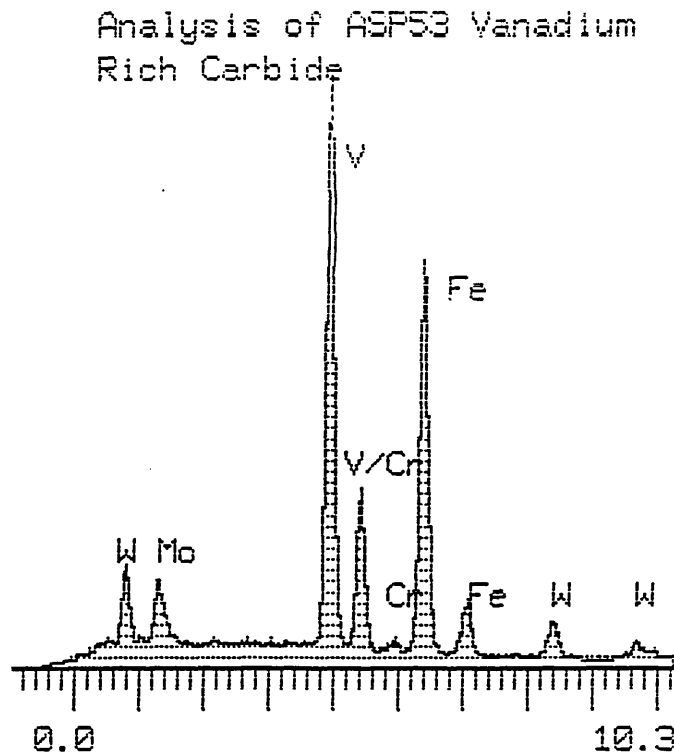


Figure 4.13 X-ray analysis of the vanadium rich carbides of ASP30 tool material.

5160 EV 20 EV/CHAN



**Figure 4.14** X-ray analysis of the vanadium rich carbides of ASP53 tool material.

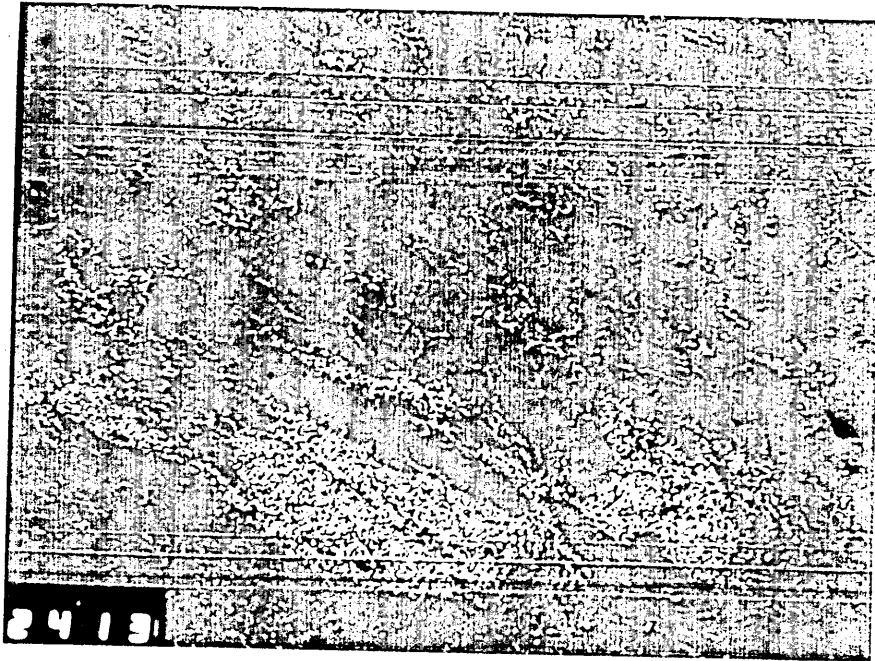


Figure 4.15 Carbide distribution of M2 HSS (x120).

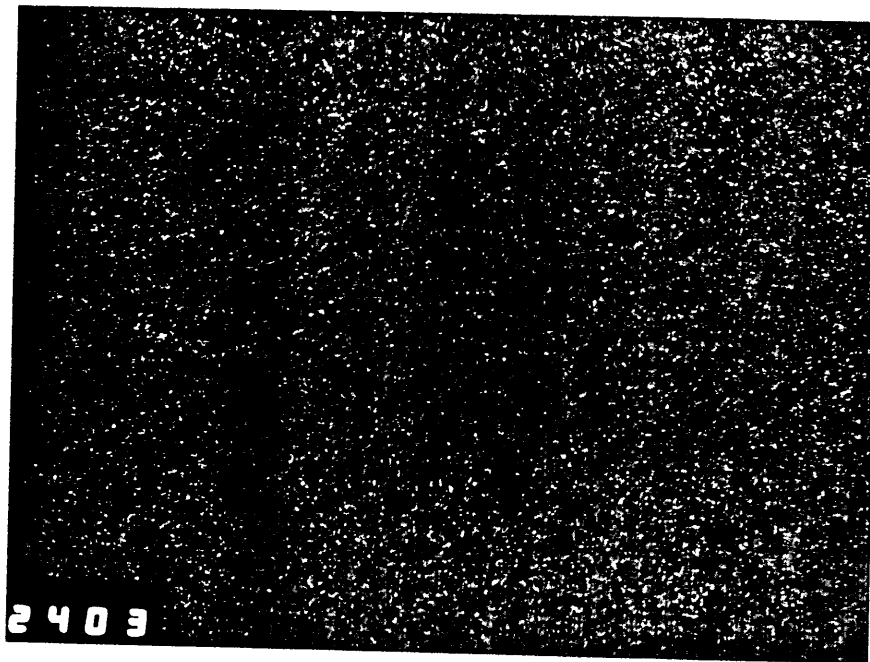
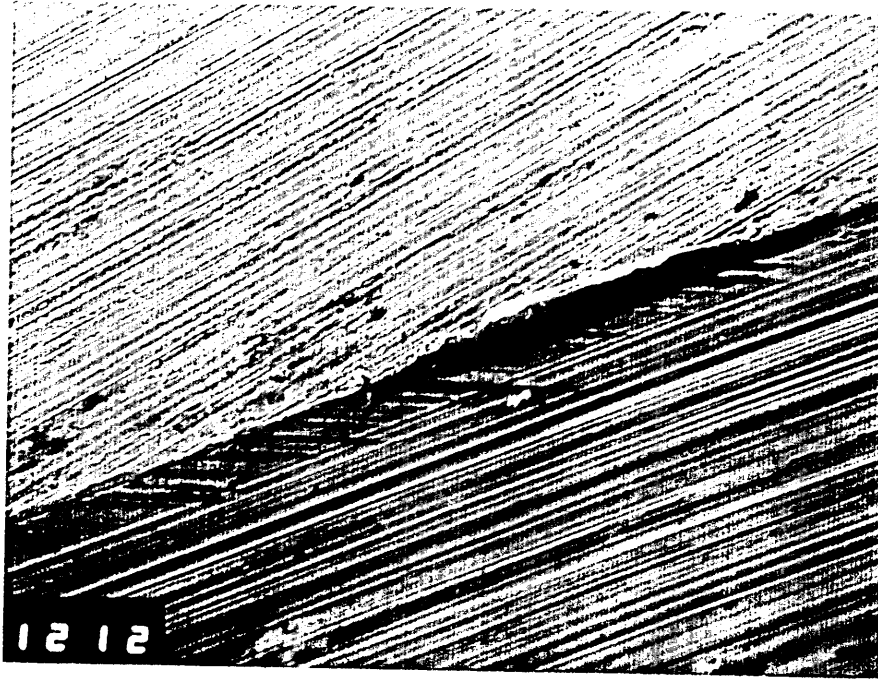
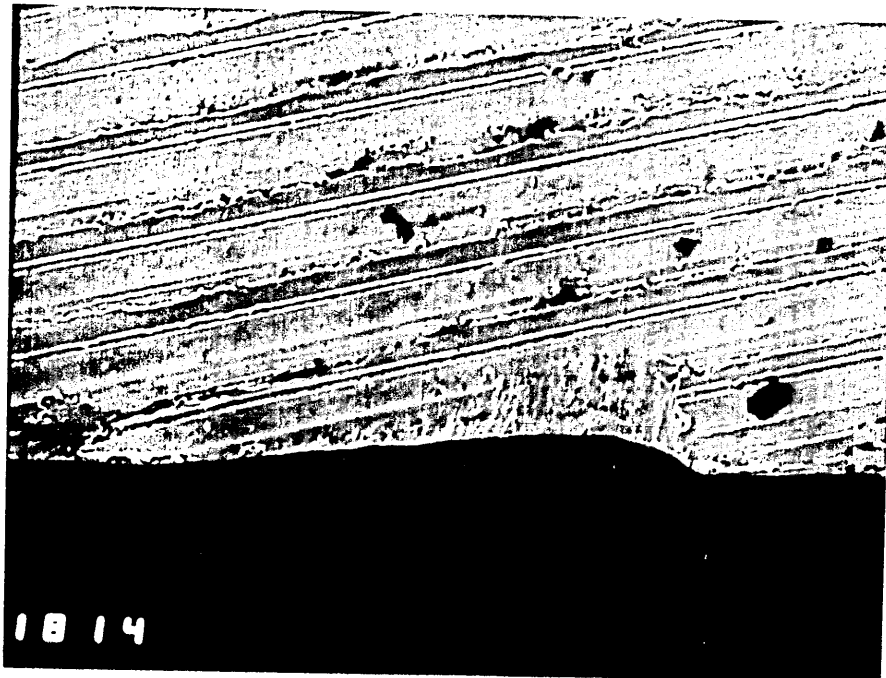


Figure 4.16 Carbide distribution of ASP30 HSS (x120).



**Figure 4.17** A view of the cutting edge of an M2 broach sample (x110)



**Figure 4.18** A view of the cutting edge of an M2 broach sample (x170)

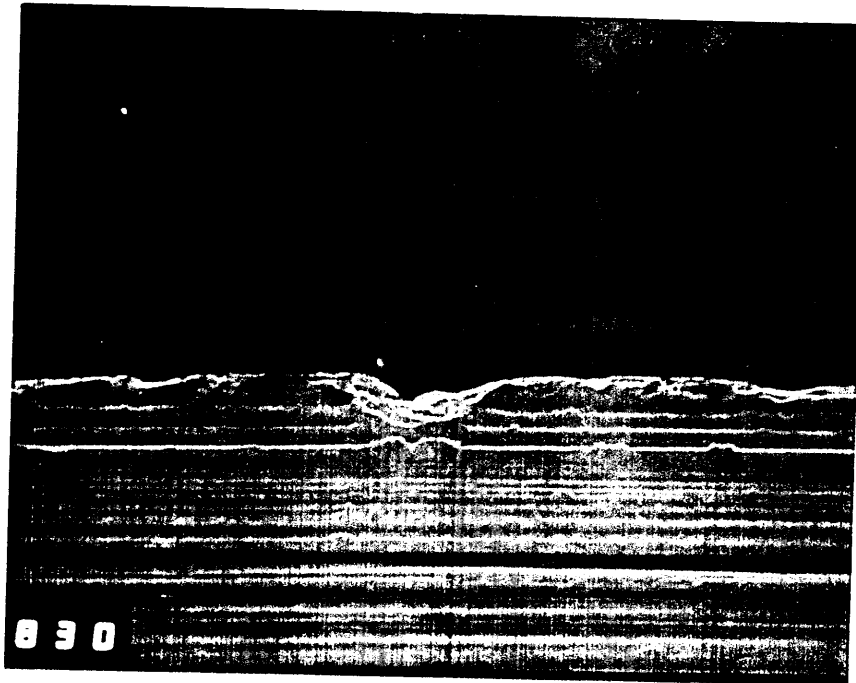


**Figure 4.19** A view of the cutting edge of an M2 broach sample (x340)



**Figure 4.20** A view of the cutting edge of an M2 broach sample (x140)

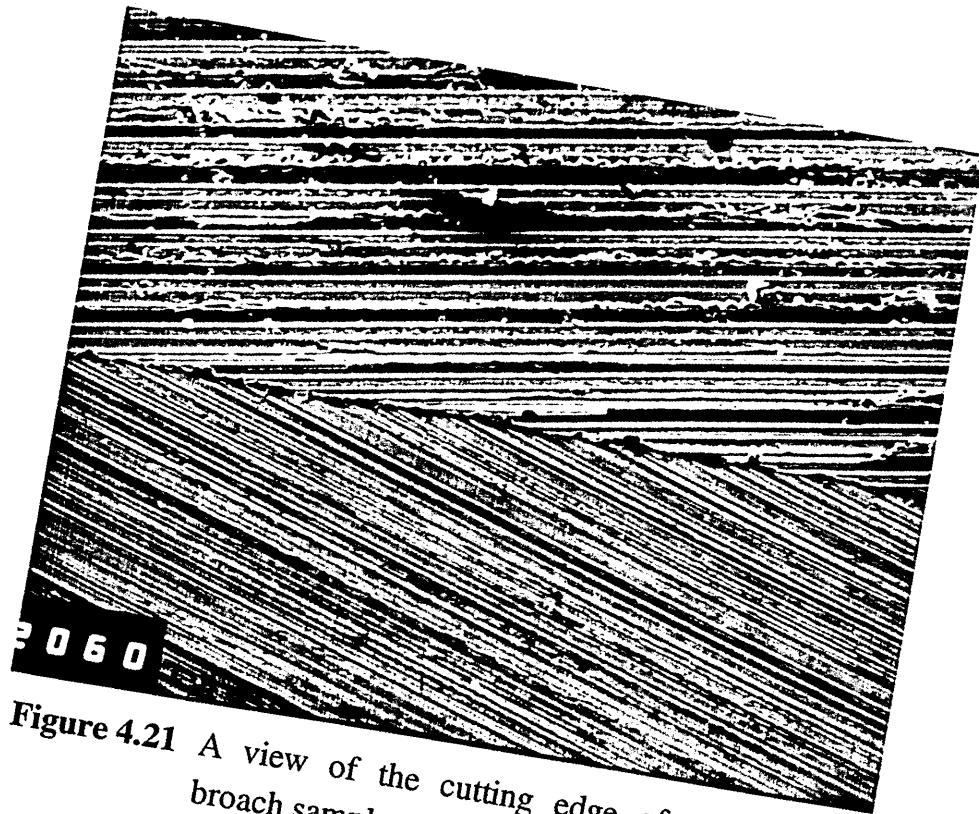


Figure 4.21 A view of the cutting edge of an ASP30 broach sample (x150)

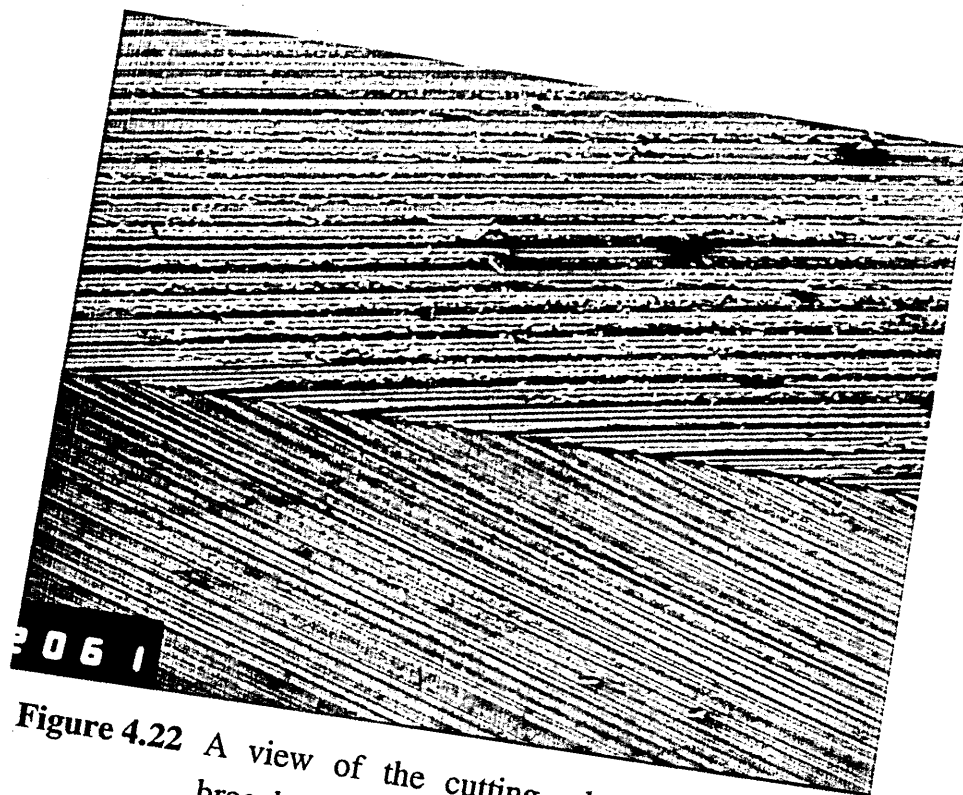
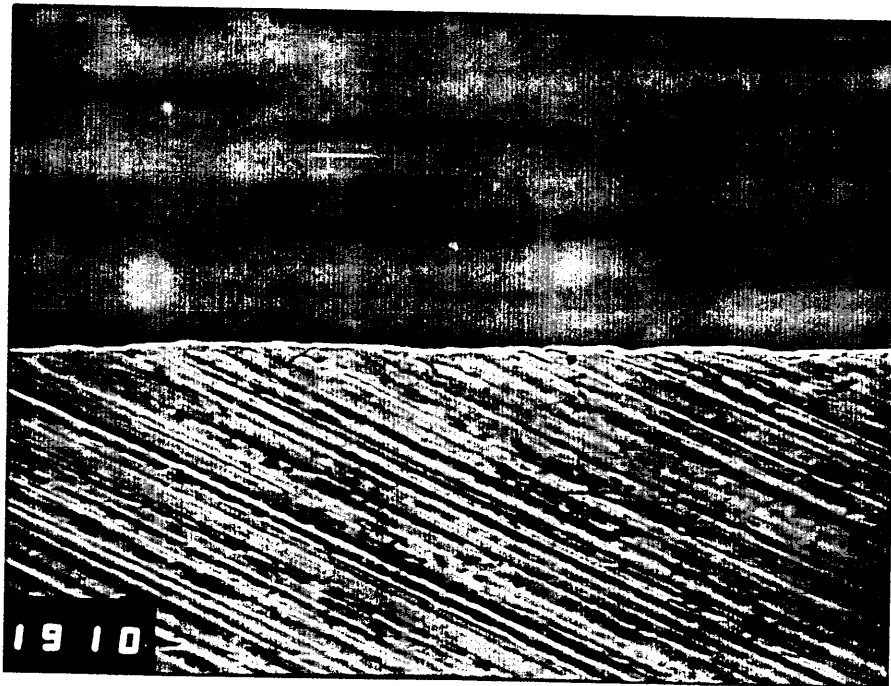
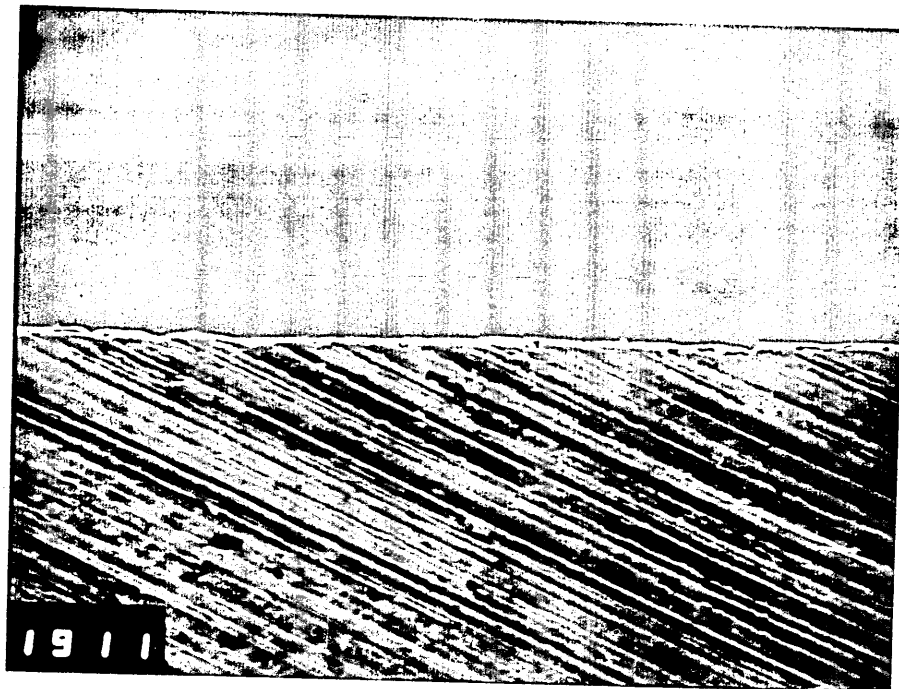


Figure 4.22 A view of the cutting edge of an ASP30 broach sample (x75)



**Figure 4.23** A view of the cutting edge of an ASP53 broach sample (x260)



**Figure 4.24** A view of the cutting edge of an ASP53 broach sample (x260)

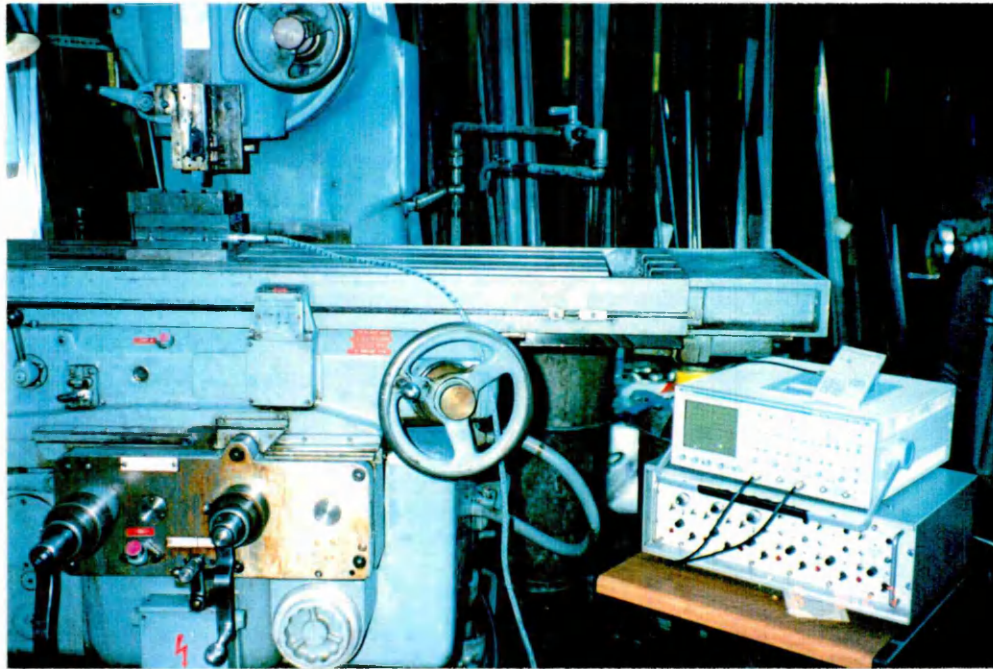


**Figure 4.25** A picture showing an overall setup of the test rig for performance tests at a cutting speed of 0.7 m/min.

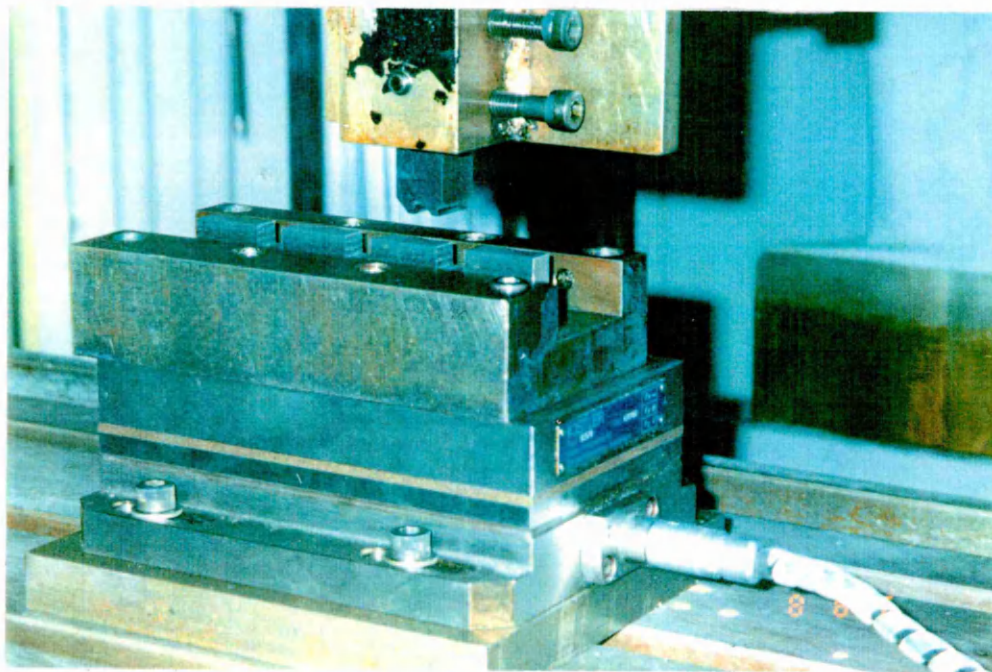


**Figure 4.26** A picture showing the dynamometer, workpiece vice, workpiece and the tool holder for performance tests at a cutting speed of 0.7 m/min.

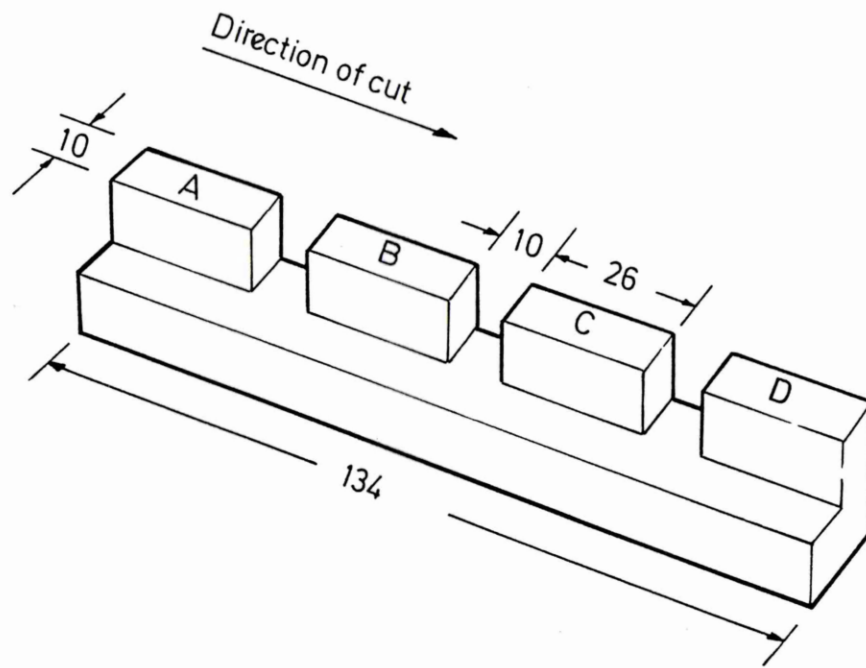


**Figure 4.27** A perspective view of the specially machined workpiece (150M36 alloy steel) for performance tests at a cutting speed of 0.7 m/min.



**Figure 4.28** A picture showing an overall setup of the test rig for performance tests at a cutting speed of 10.5 m/min.

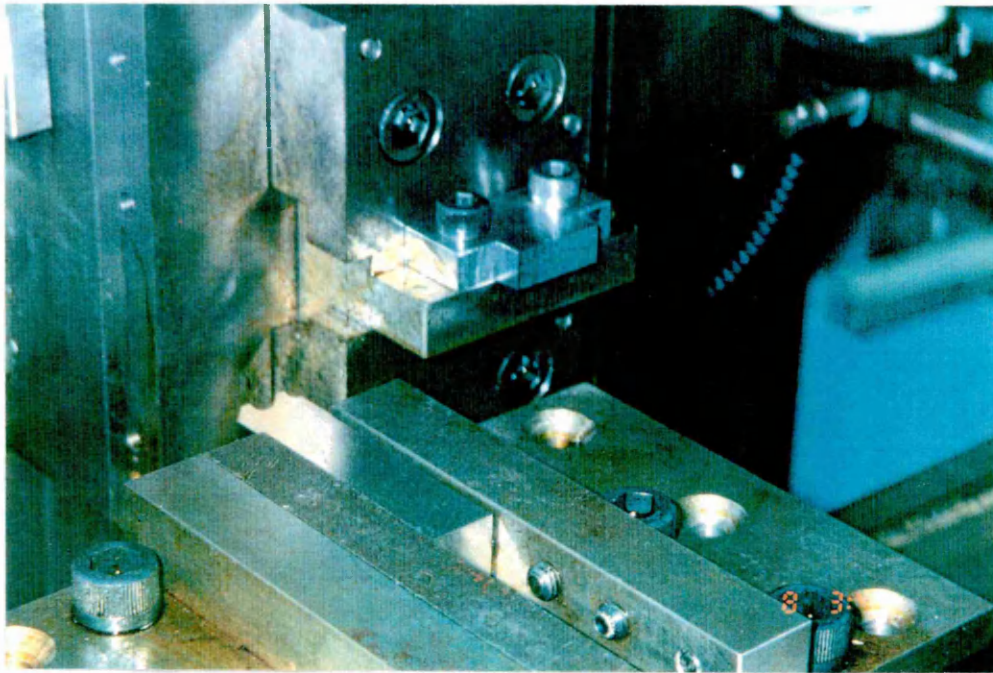


**Figure 4.29** A picture showing the tool and the workpiece for performance tests at a cutting speed of 10.5 m/min.

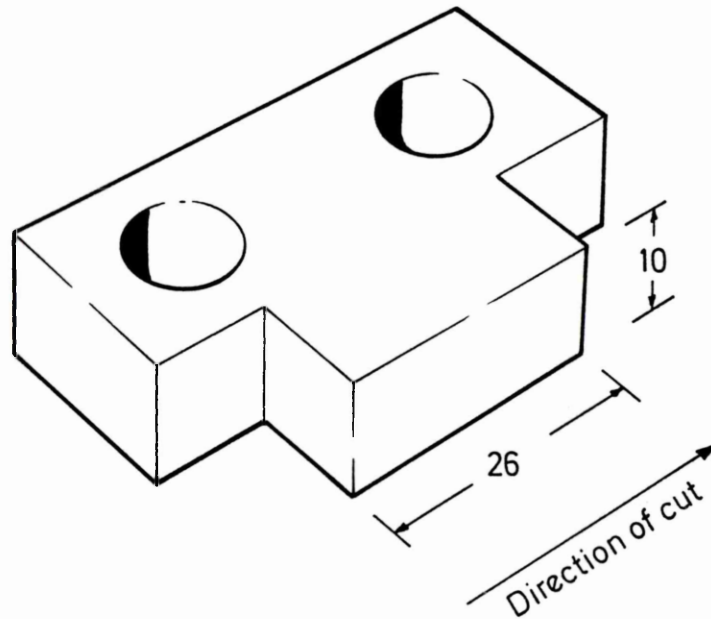
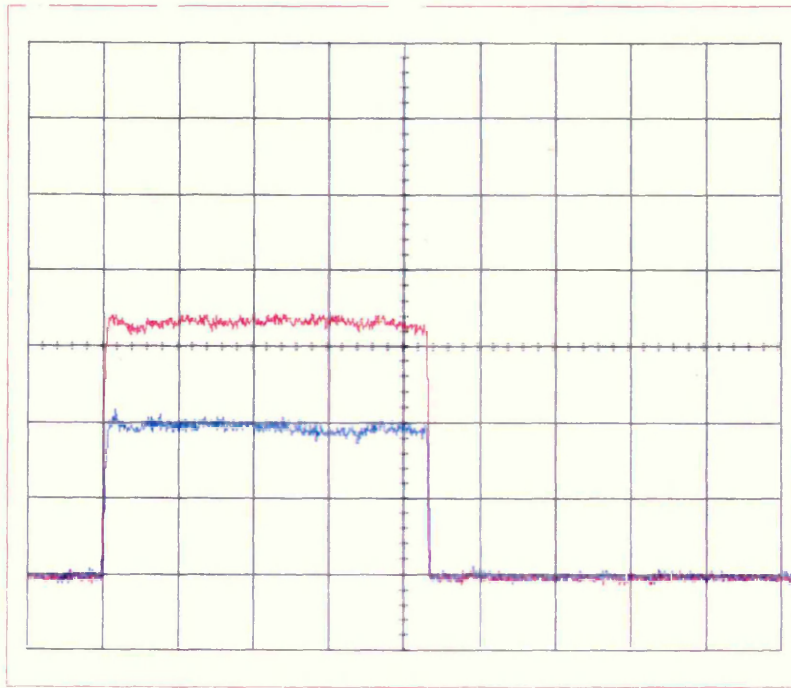


**Figure 4.30** A perspective view of a specially machined workpiece (150M36 alloy steel) for performance tests at a cutting speed of 10.5 m/min.

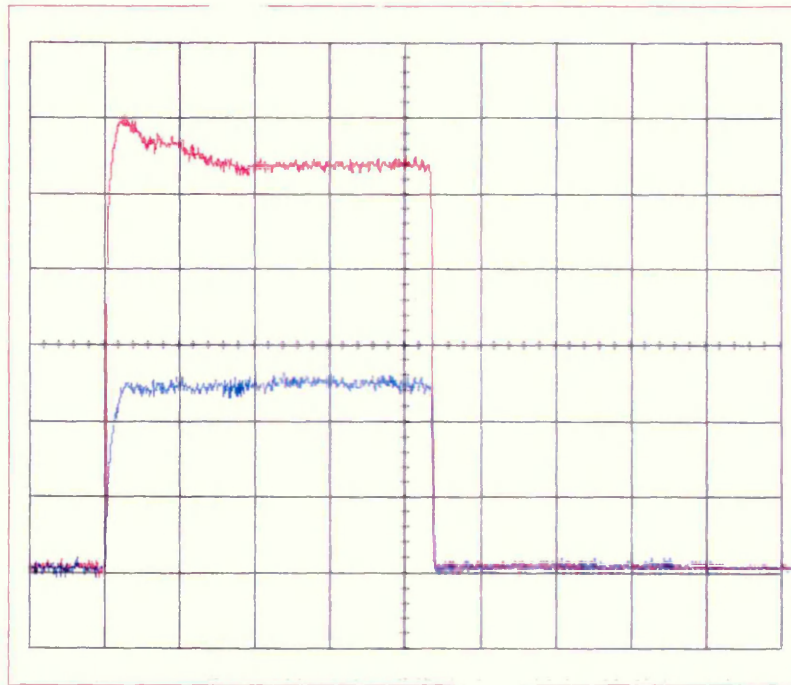


DATE: Jul 27/93

TIME: 23:55:22

CH1: 1.00V :500ms

CH2: 1.00V :500ms



DATE: Jul 27/93

TIME: 17:49:01

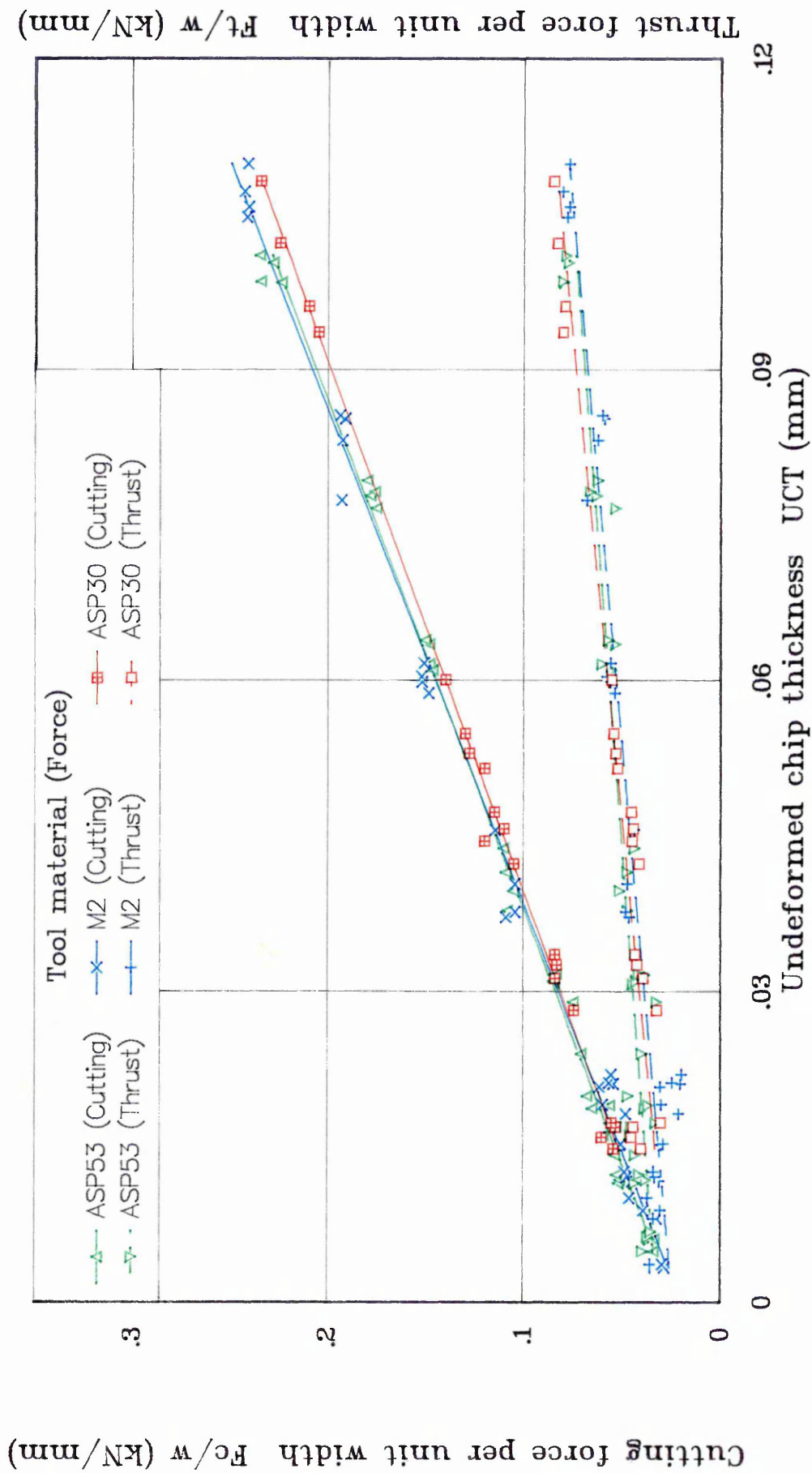
CH2: 1.00V :500ms

CH3: 1.00V :500ms

**Figure 4.31** Typical traces of cutting and thrust forces obtained from the oscilloscope.

# Effect of Undeformed Chip Thickness on Cutting Forces

(cutting speed 0.7 m/min)

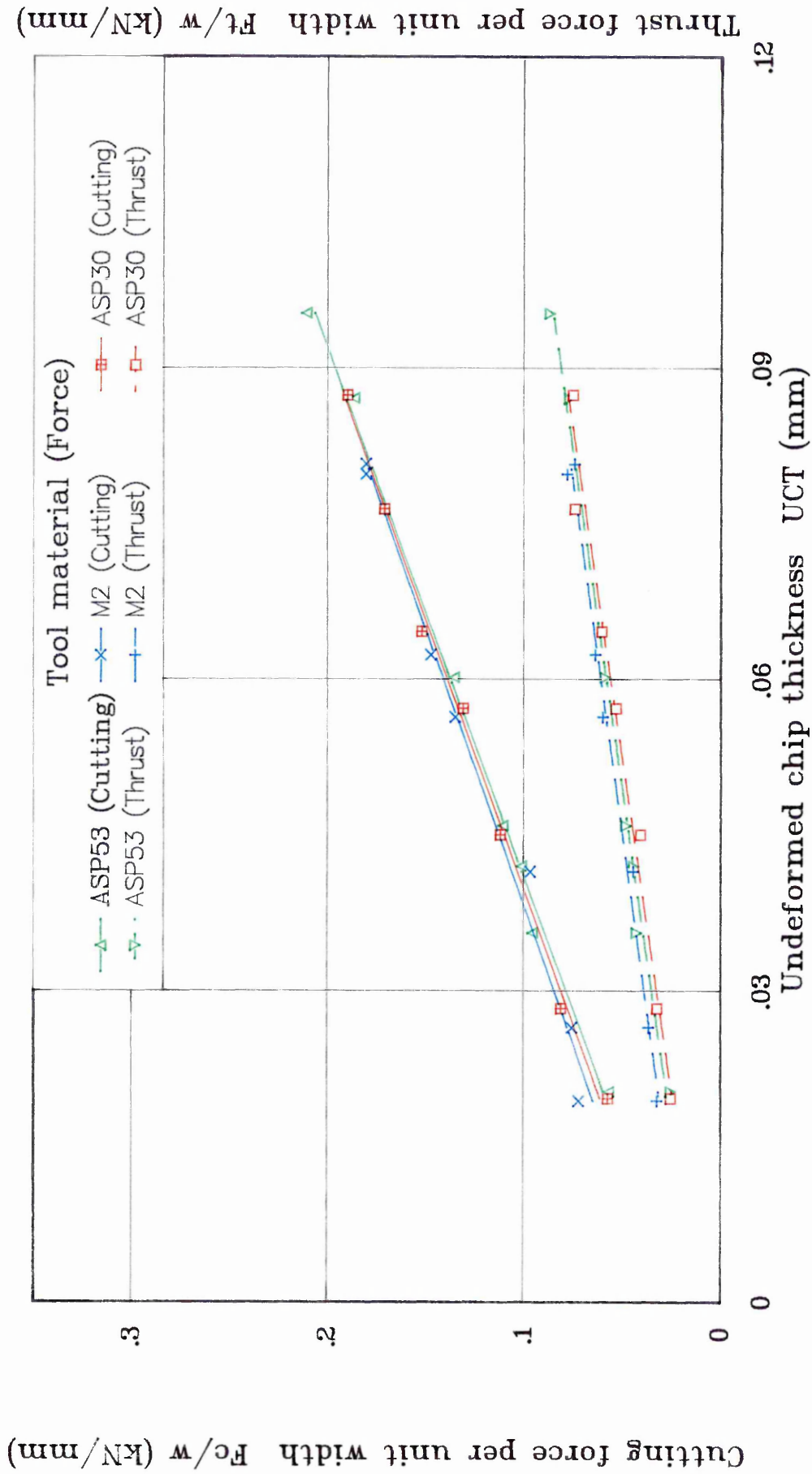


AS-553(940405)

Figure 4.32

# Effect of Undeformed Chip Thickness on Cutting Forces

(cutting speed : 10.5 m/min)



AS-162(940413)L

Figure 4.33

# Effect of Undeformed Chip Thickness on Specific Cutting Energy

(cutting speed : 0.7 m/min)

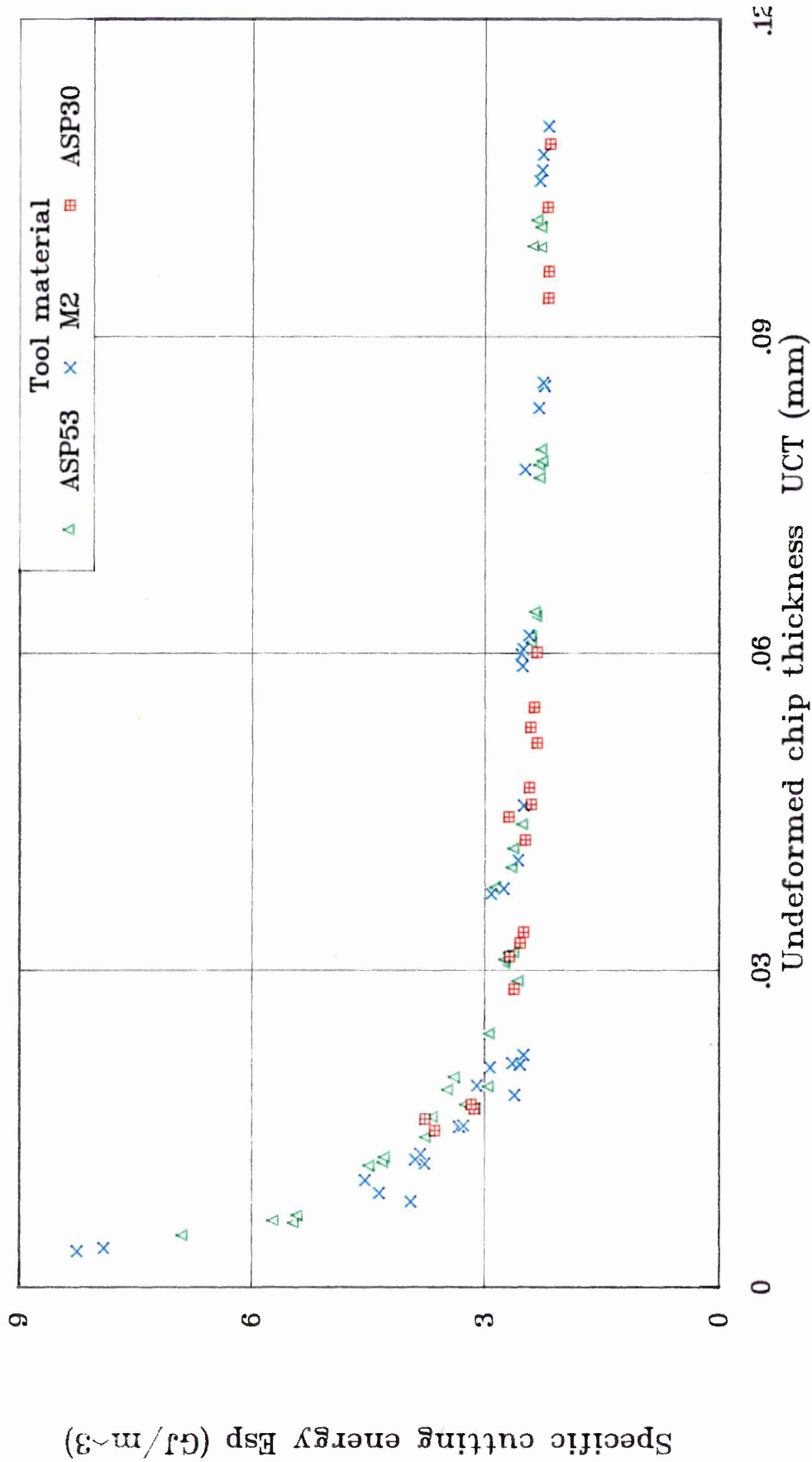
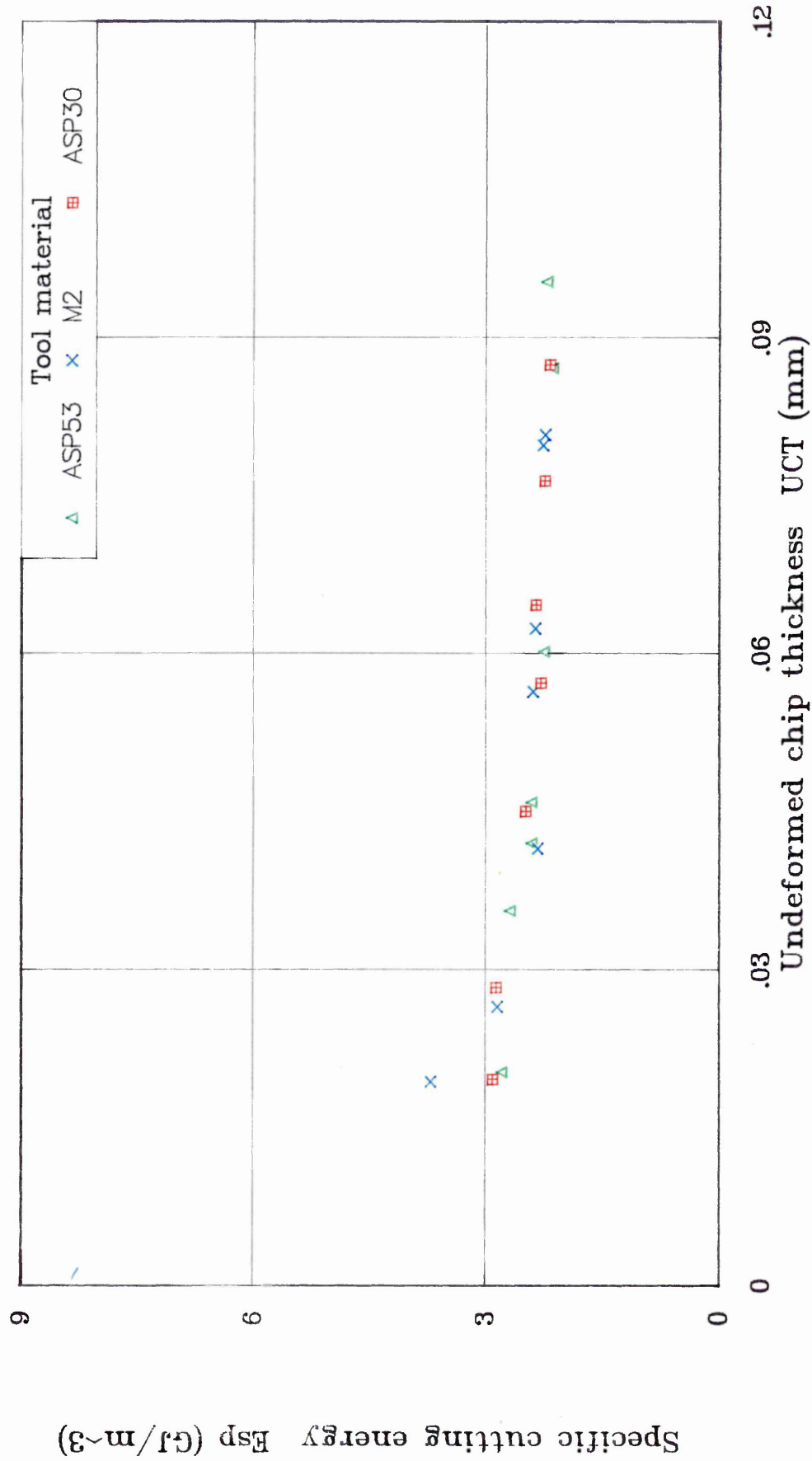


Figure 4.34

# Effect of Undeformed Chip Thickness on Specific Cutting Energy

(cutting speed : 10.5 m/min)



AS-162(940413)L

Figure 4.35

# Effect of Undeformed Chip Thickness on Roughness Average

Measured Perpendicular to the Direction of Cut (cutting speed : 0.7 m/min)

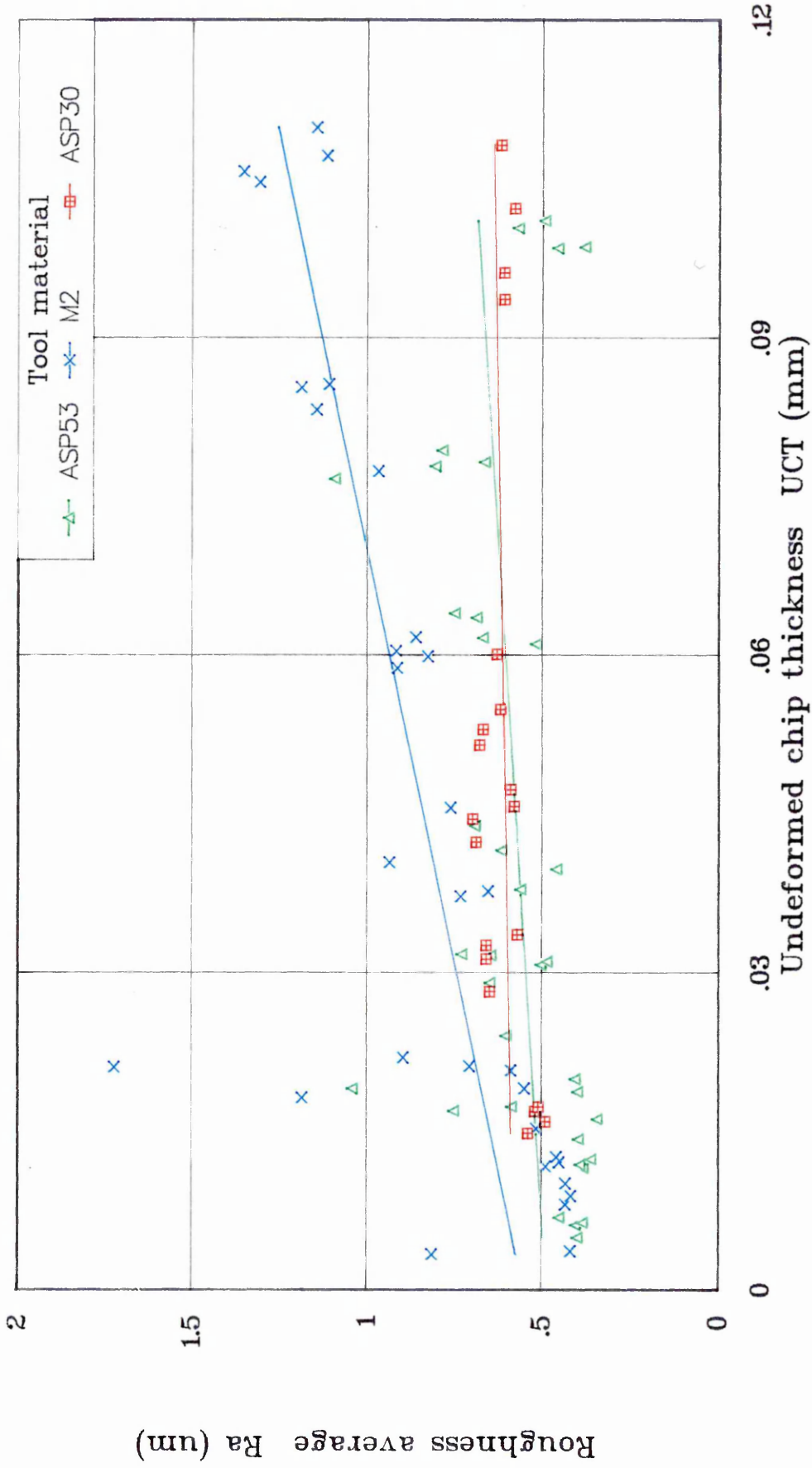
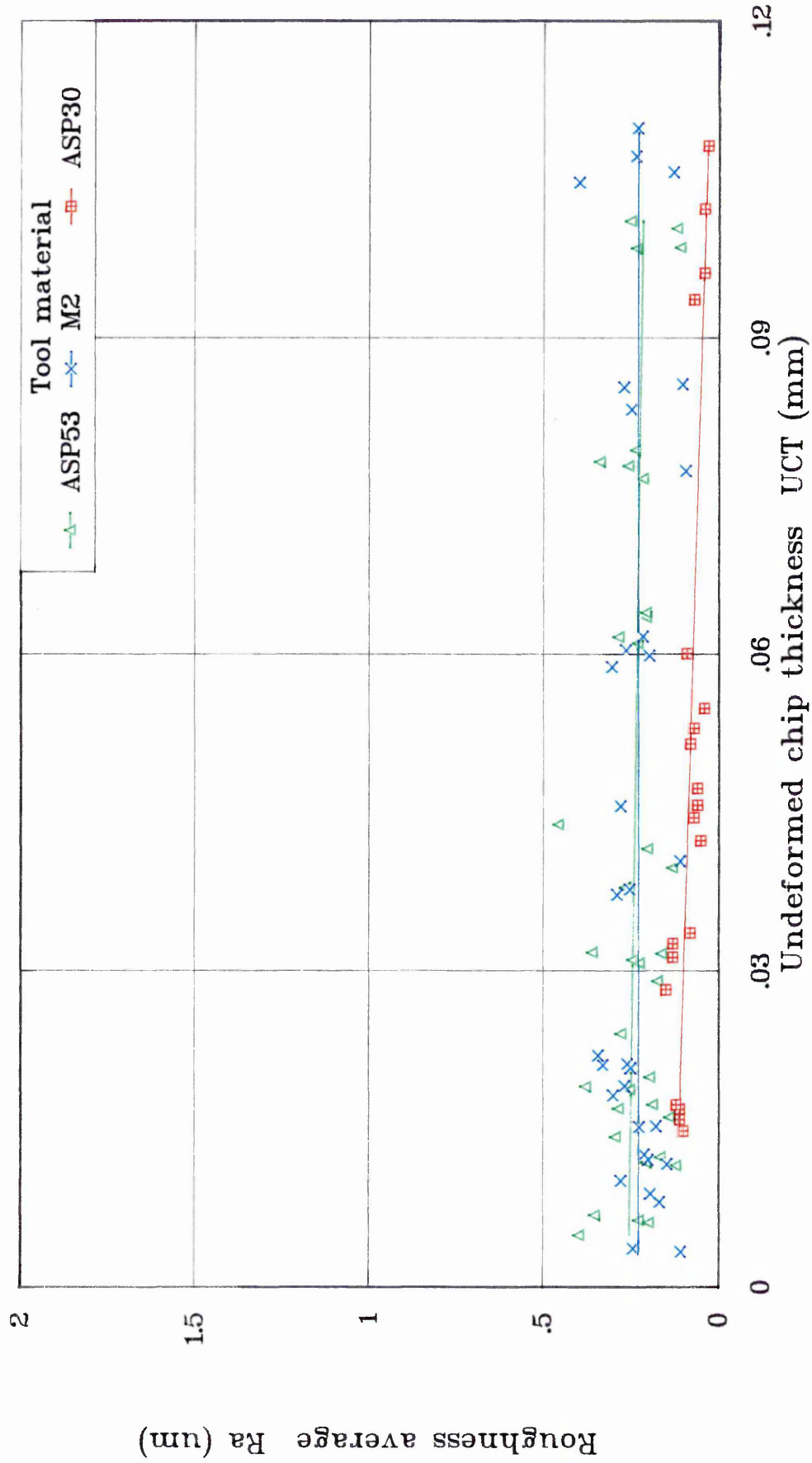


Figure 4.36

# Effect of Undeformed Chip Thickness on Roughness Average

Measured Parallel to the Direction of Cut (cutting speed : 0.7 m/min)

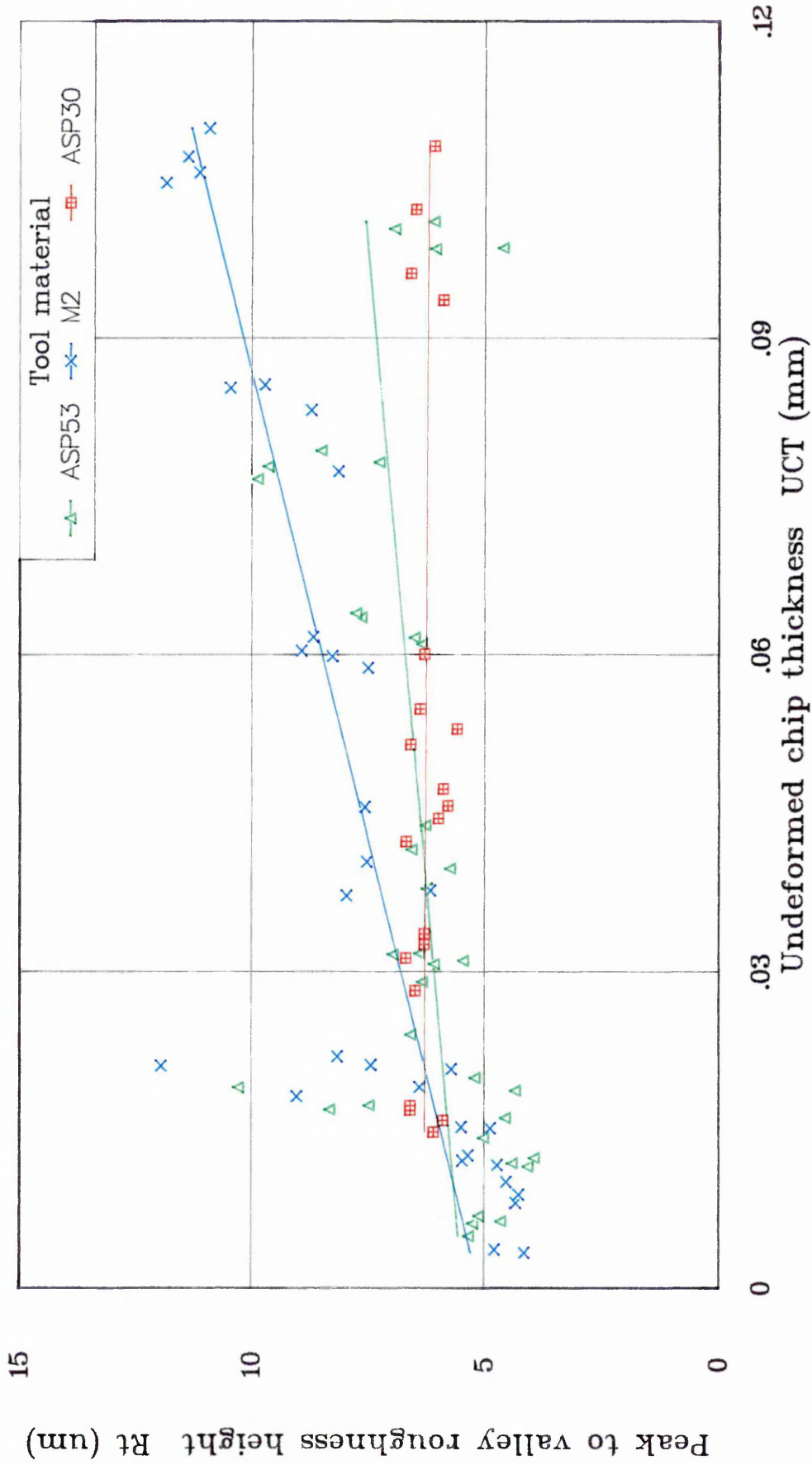


AS-553(940405)L

Figure 4.37

# Effect of Undeformed Chip Thickness on Peak to Valley Height

Measured Perpendicular to the Direction of Cut (cutting speed : 0.7 m/min)

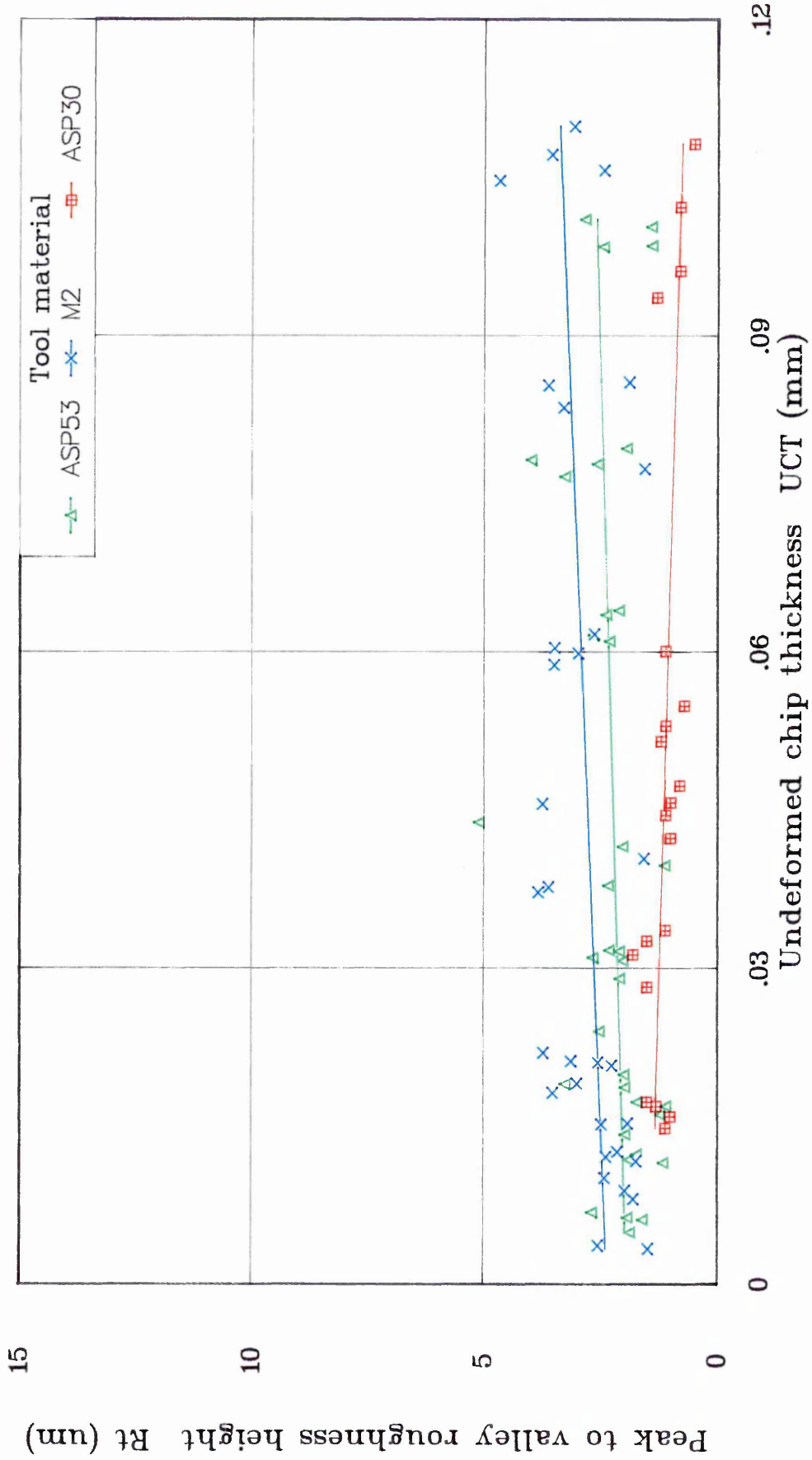


AS-553(940405)L

Figure 4.38

# Effect of Undeformed Chip Thickness on Peak to Valley Height

Measured Parallel to the Direction of Cut (cutting speed : 0.7 m/min)

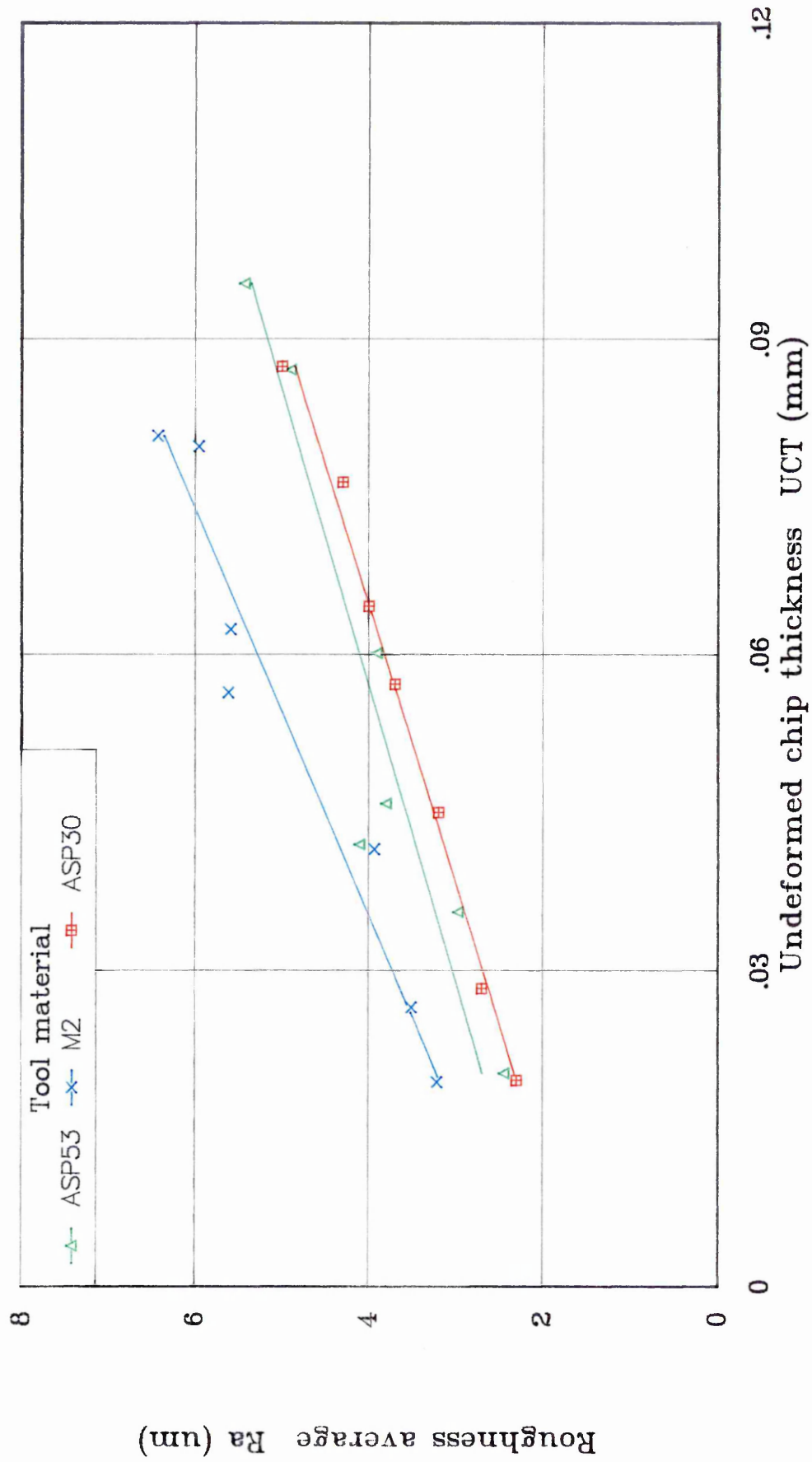


AS-553(940405)L

Figure 4.39

# Effect of Undeformed Chip Thickness on Roughness Average

Measured Perpendicular to the Direction of Cut (cutting speed : 10.5 m/min)

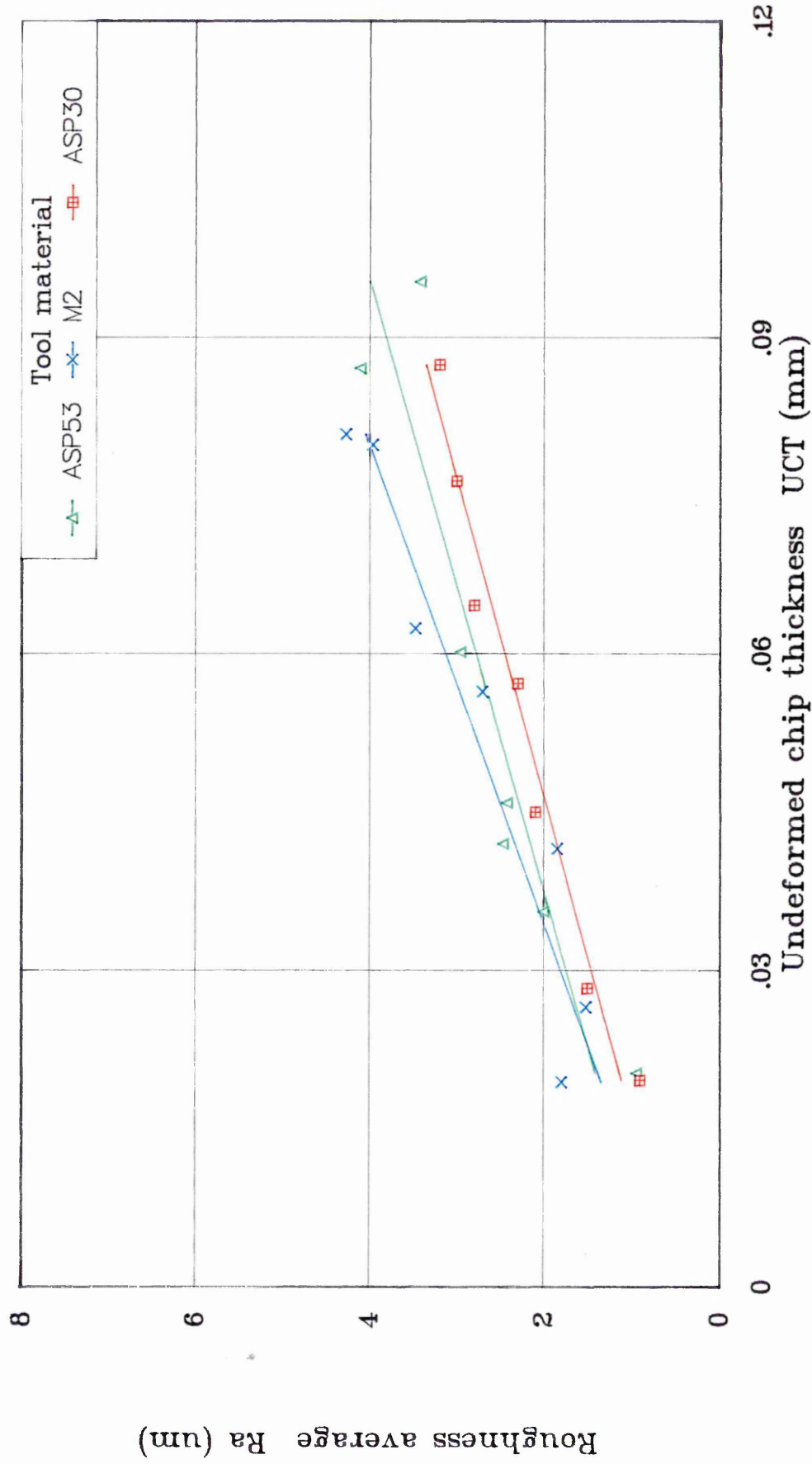


AS-162(940413)L

Figure 4.40

# Effect of Undeformed Chip Thickness on Roughness Average

Measured Parallel to the Direction of Cut (cutting speed : 10.5 m/min)

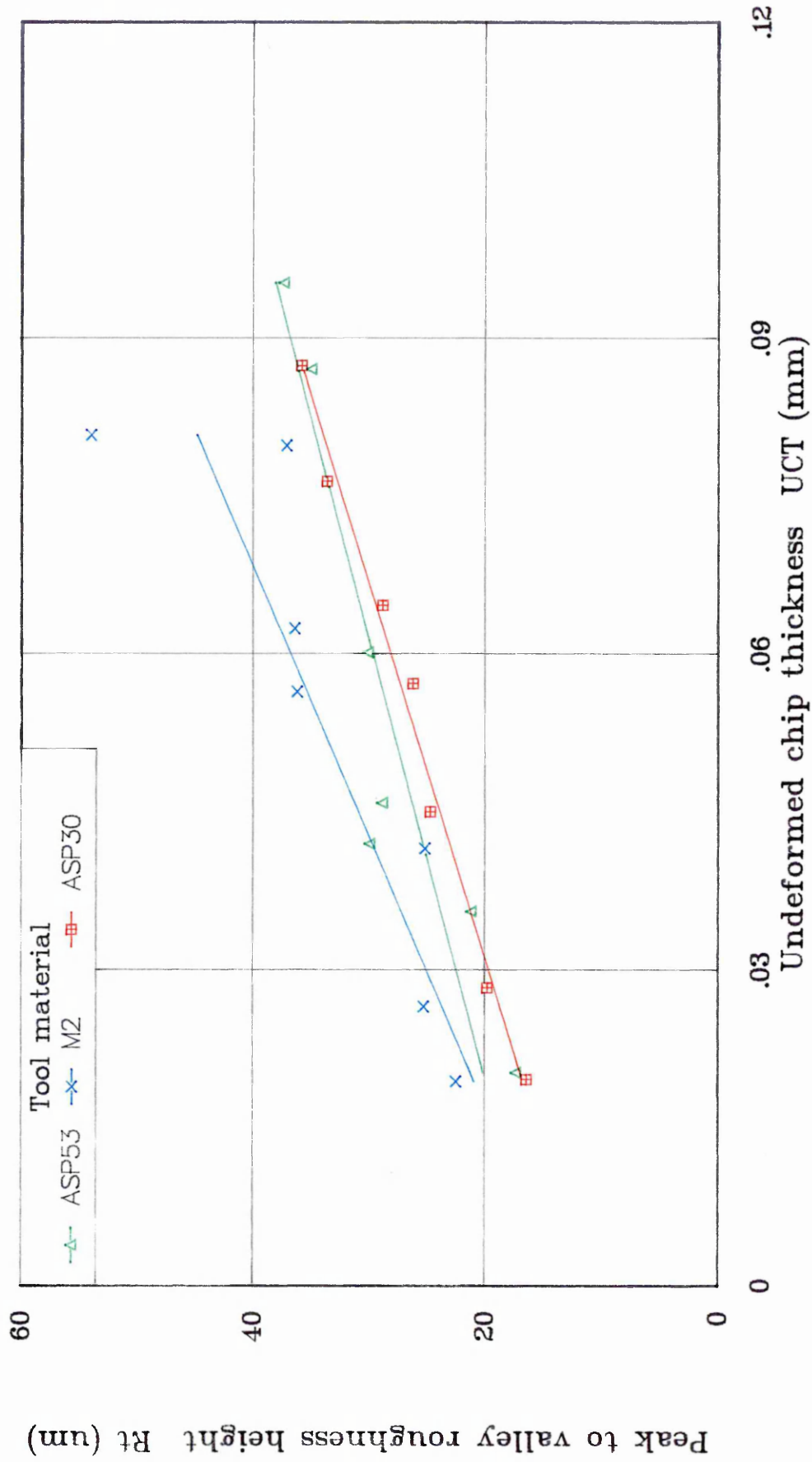


AS-162(940413)L

Figure 4.41

# Effect of Undeformed Chip Thickness on Peak to Valley Height

Measured Perpendicular to the Direction of Cut (cutting speed : 10.5 m/min)

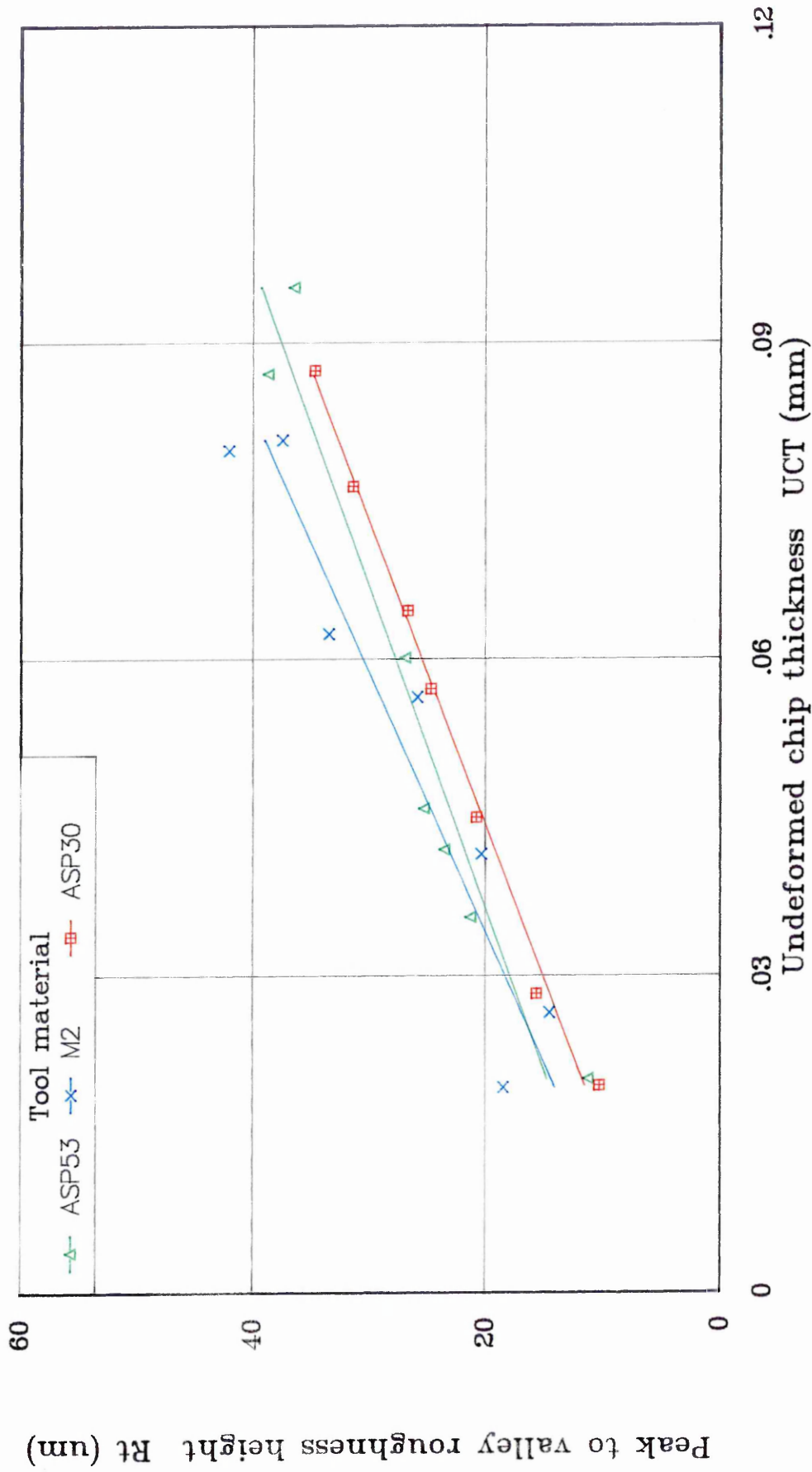


AS-162(940413)-L

Figure 4.42

# Effect of Undeformed Chip Thickness on Peak to Valley Height

Measured Parallel to the Direction of Cut (cutting speed : 10.5 m/min)



AS-162(940415)

Figure 4.43

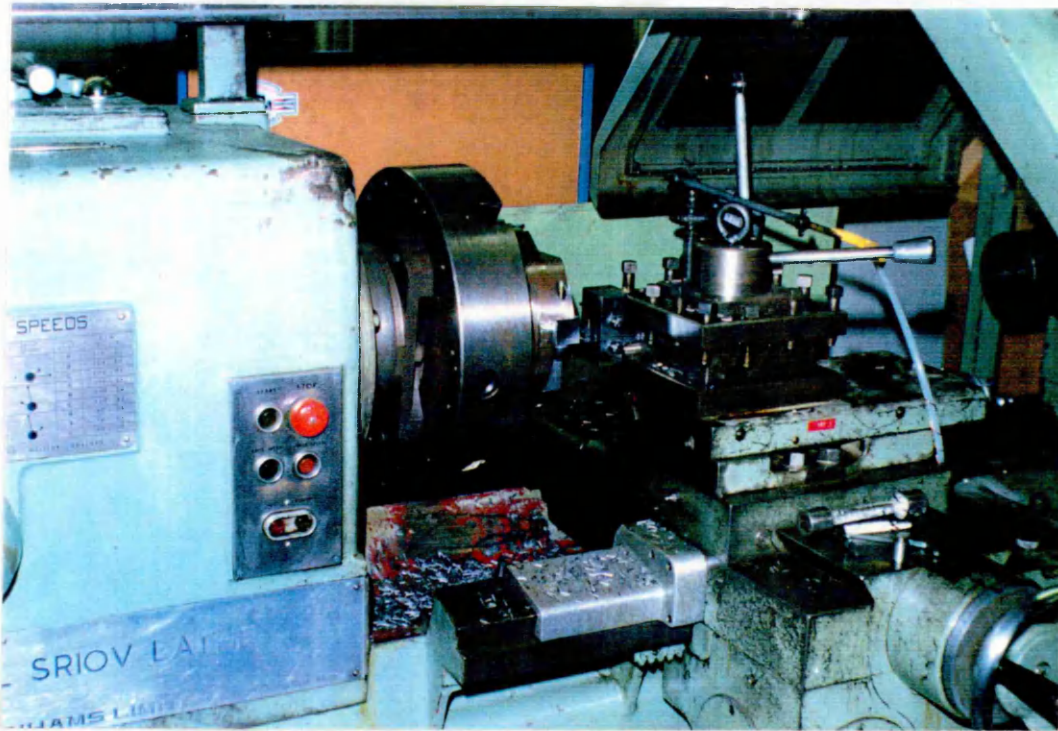


**Figure 5.1** A picture showing the overall set-up of the test rig to perform wear tests at a cutting speed of 10.5 m/min.

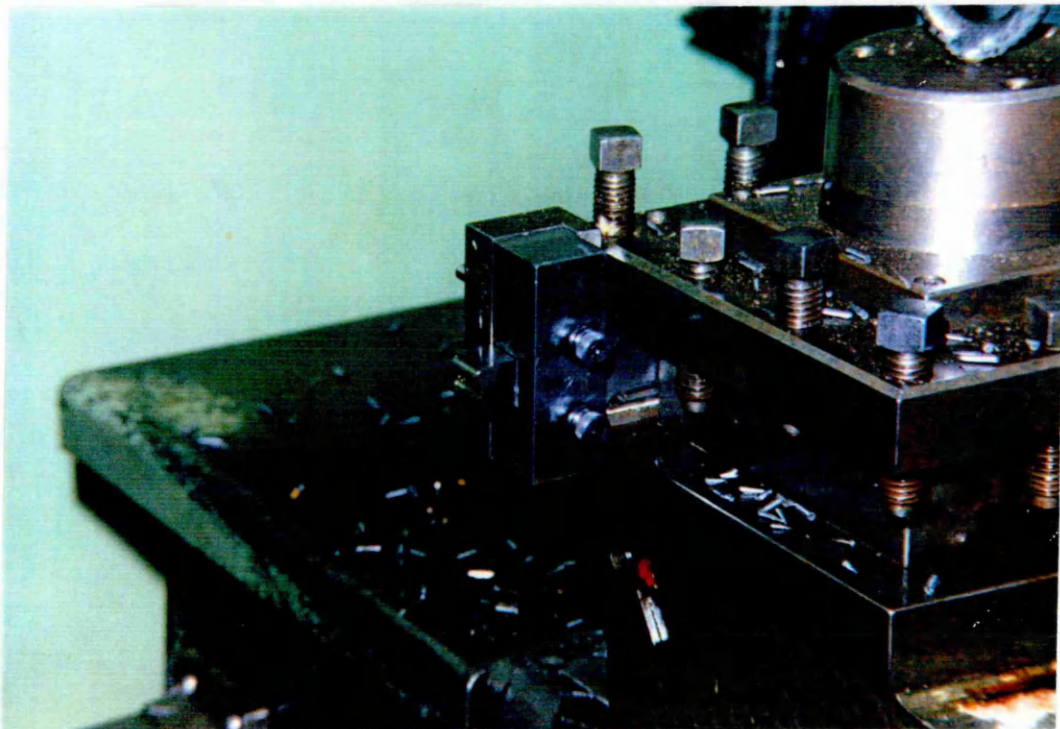


**Figure 5.2** A picture showing the broach sample, broach sample holder and the tool post.

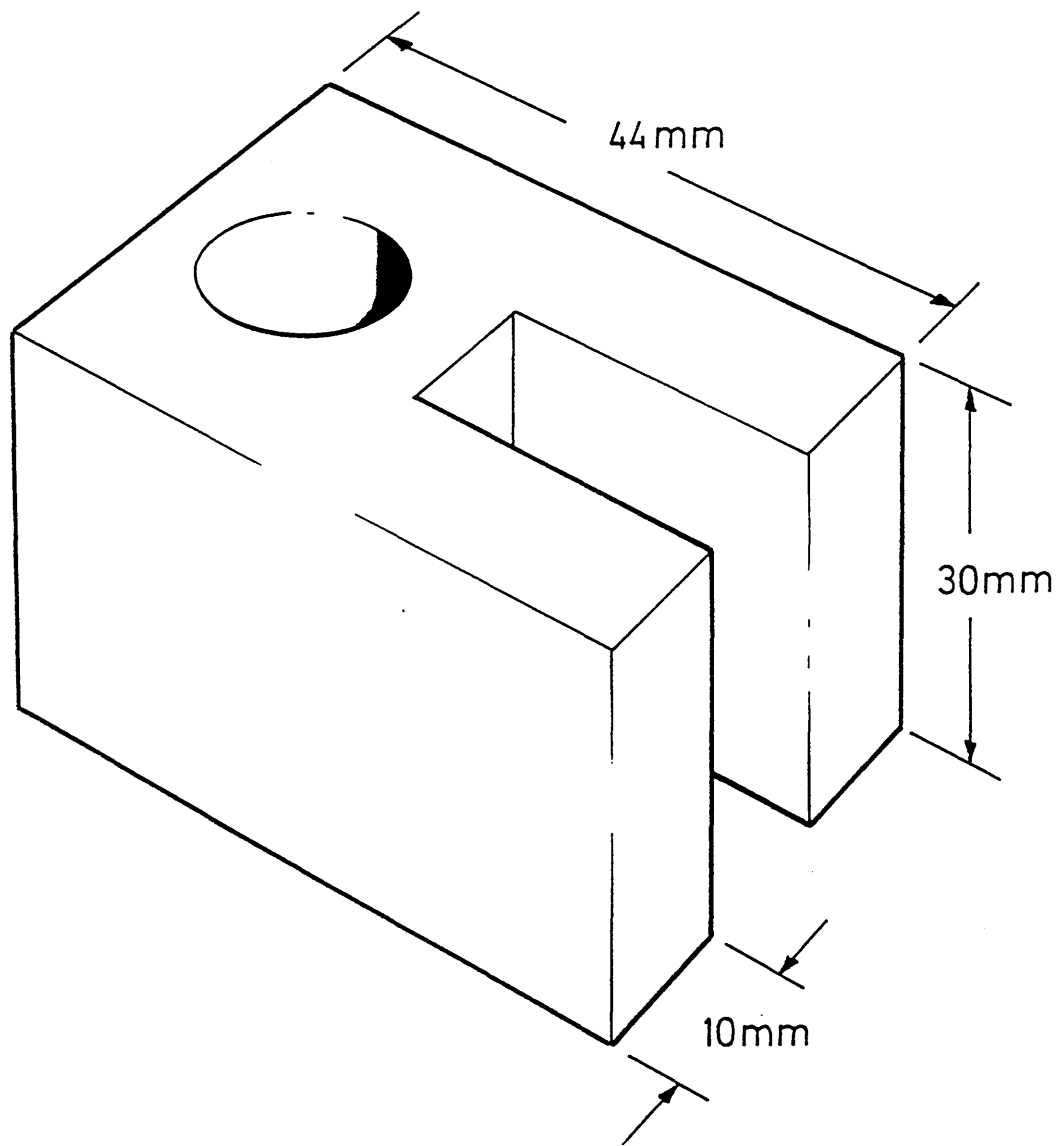


**Figure 5.3** A perspective view showing overall dimensions of the specially machined workpiece to perform the wear tests.

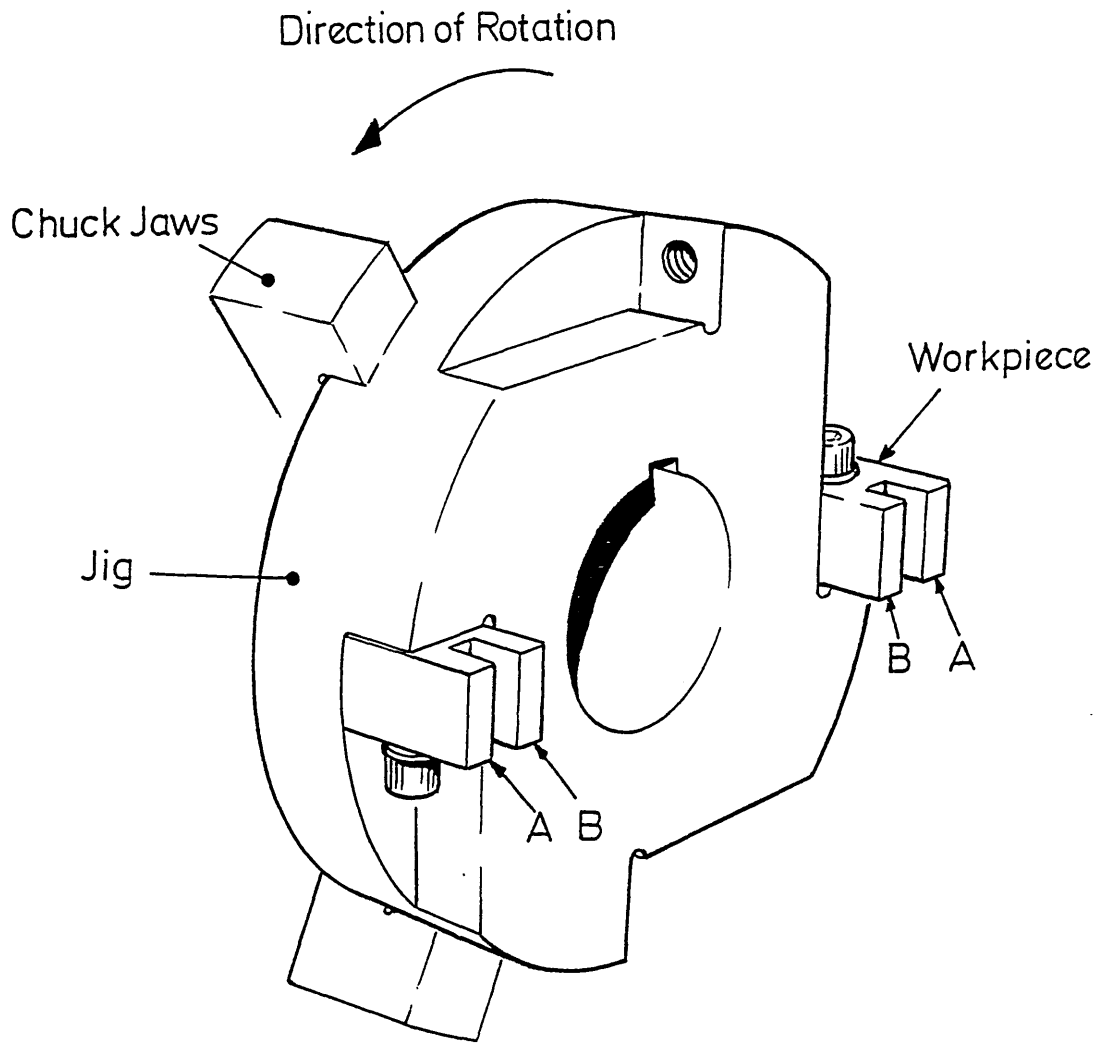


**Figure 5.4** A perspective view of the specially machined jig to hold the workpieces to carry out wear tests.

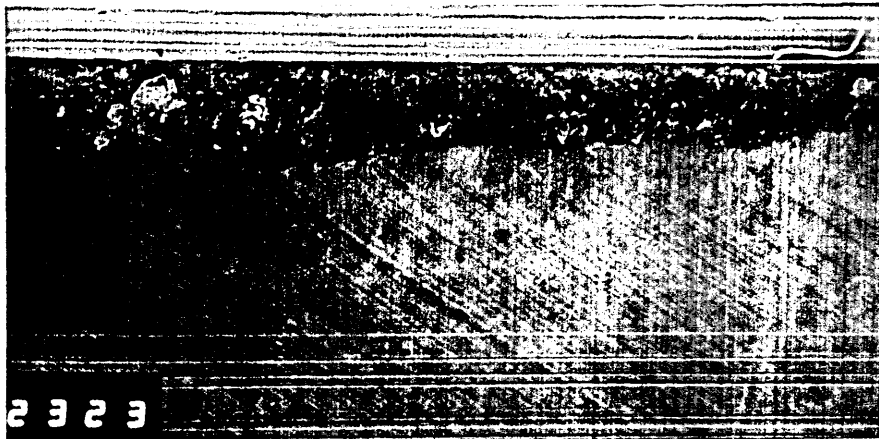


**Figure 5.5** A micrograph showing the wear scar and the adhesion of work material on the clearance face of the M2 broach sample (x25).



**Figure 5.6** A micrograph showing the wear scar on the clearance face of the ASP53 broach sample (x25).

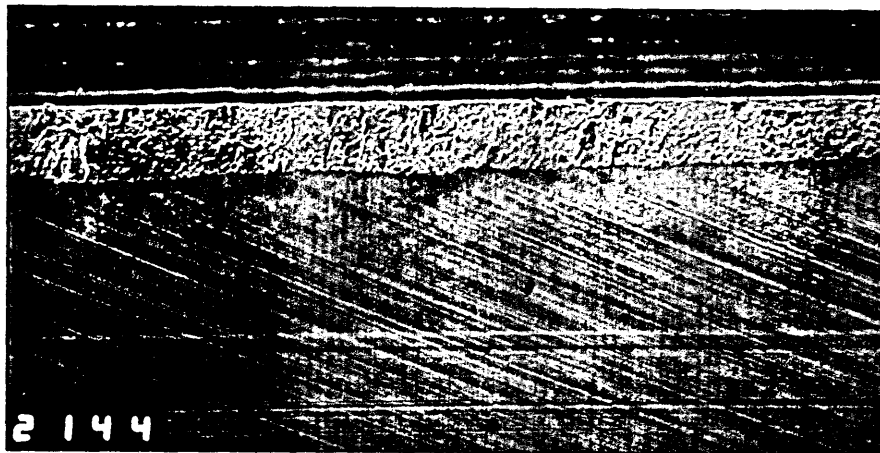


**Figure 5.7** A micrograph showing the wear scar on the clearance face of the ASP30 broach sample (x25).

### Wear tests on M2, ASP53 & ASP30 broach samples

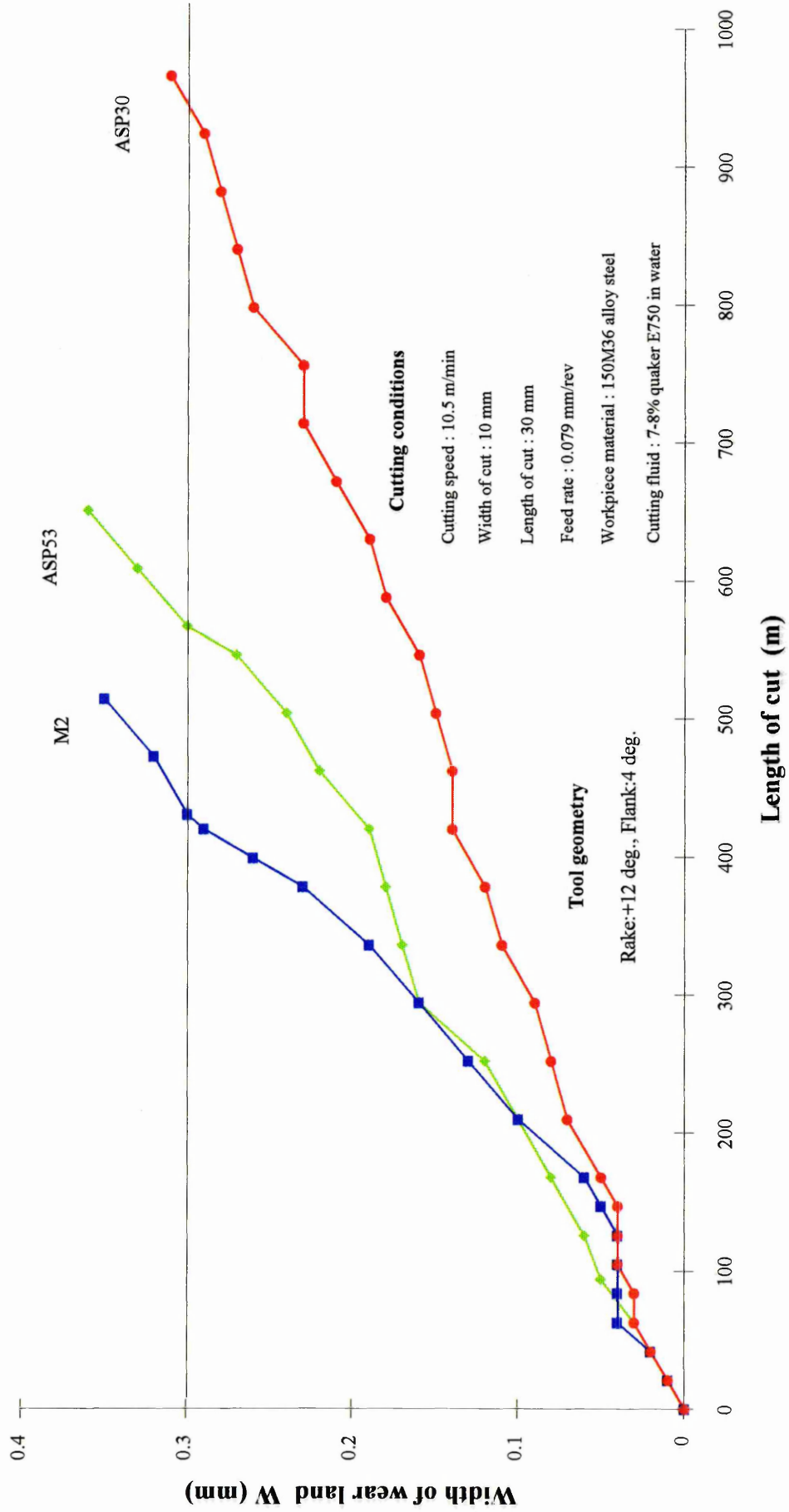
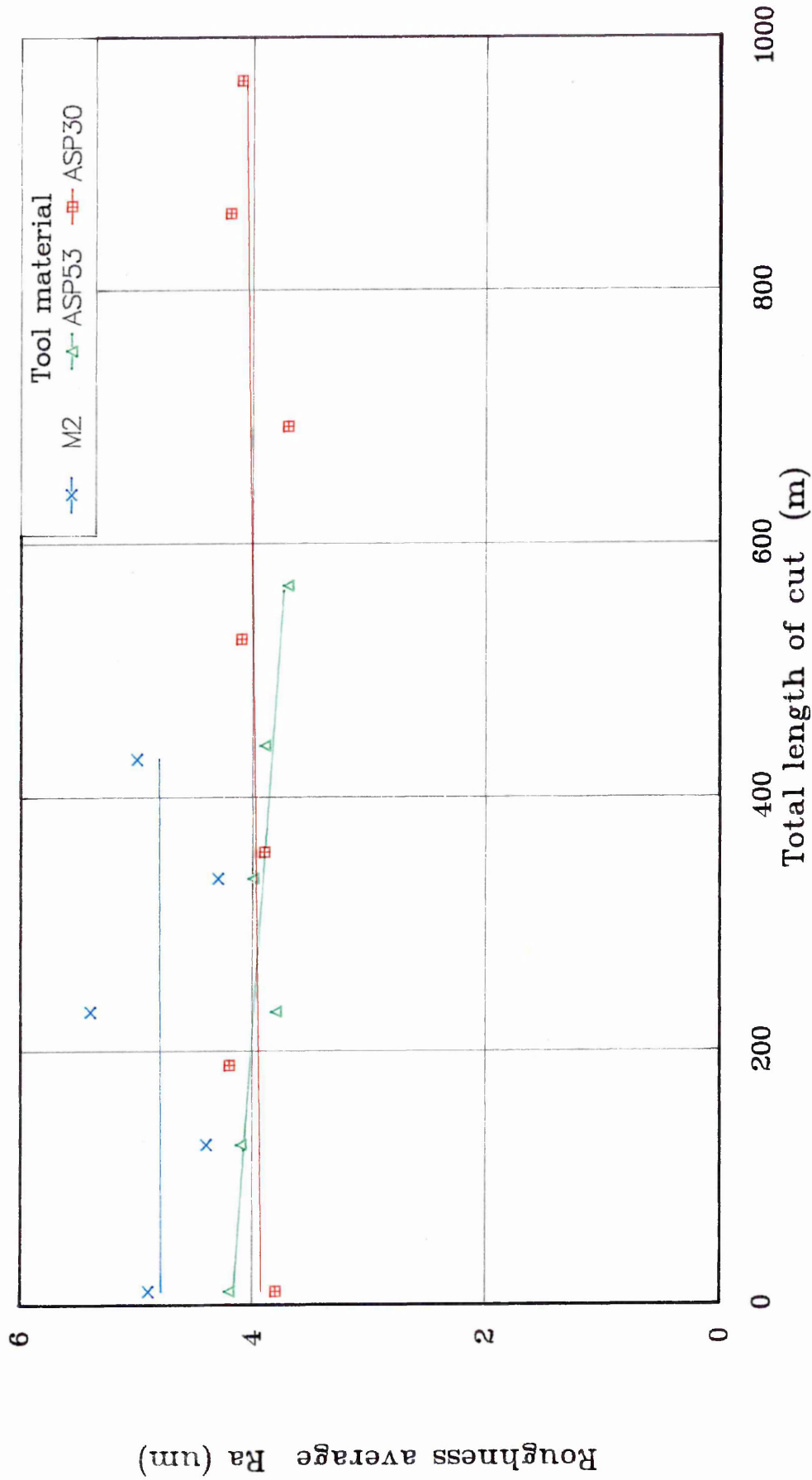


Figure 5.8

# Effect of Tool-wear on Roughness Average of Workpiece

Measured Perpendicular to the Direction of Cut (cutting speed : 10.5 m/min)

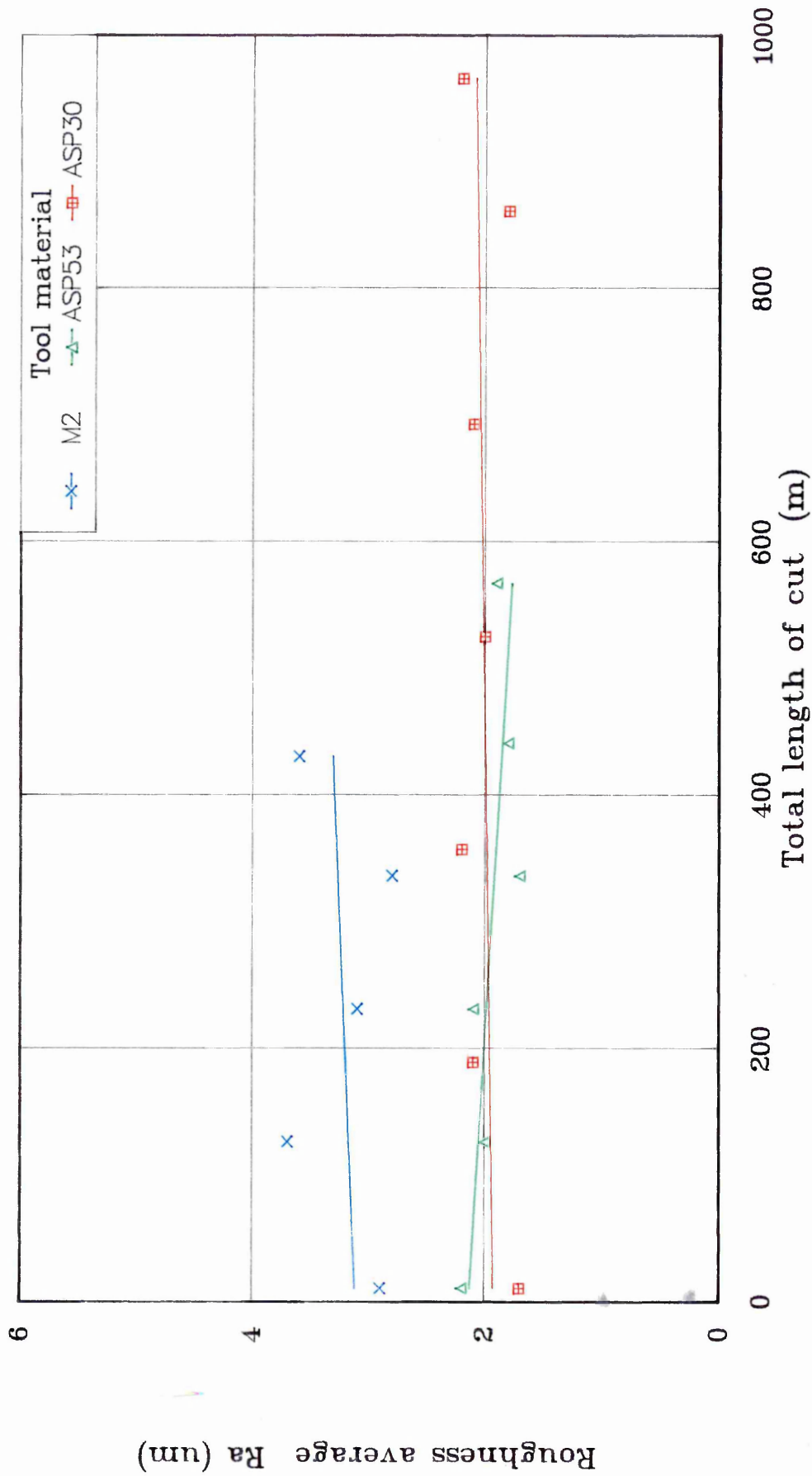


AS-131(940405)

Figure 5.9

# Effect of Tool-wear on Roughness Average of Workpiece

Measured Parallel to the Direction of Cut (cutting speed : 10.5 m/min)

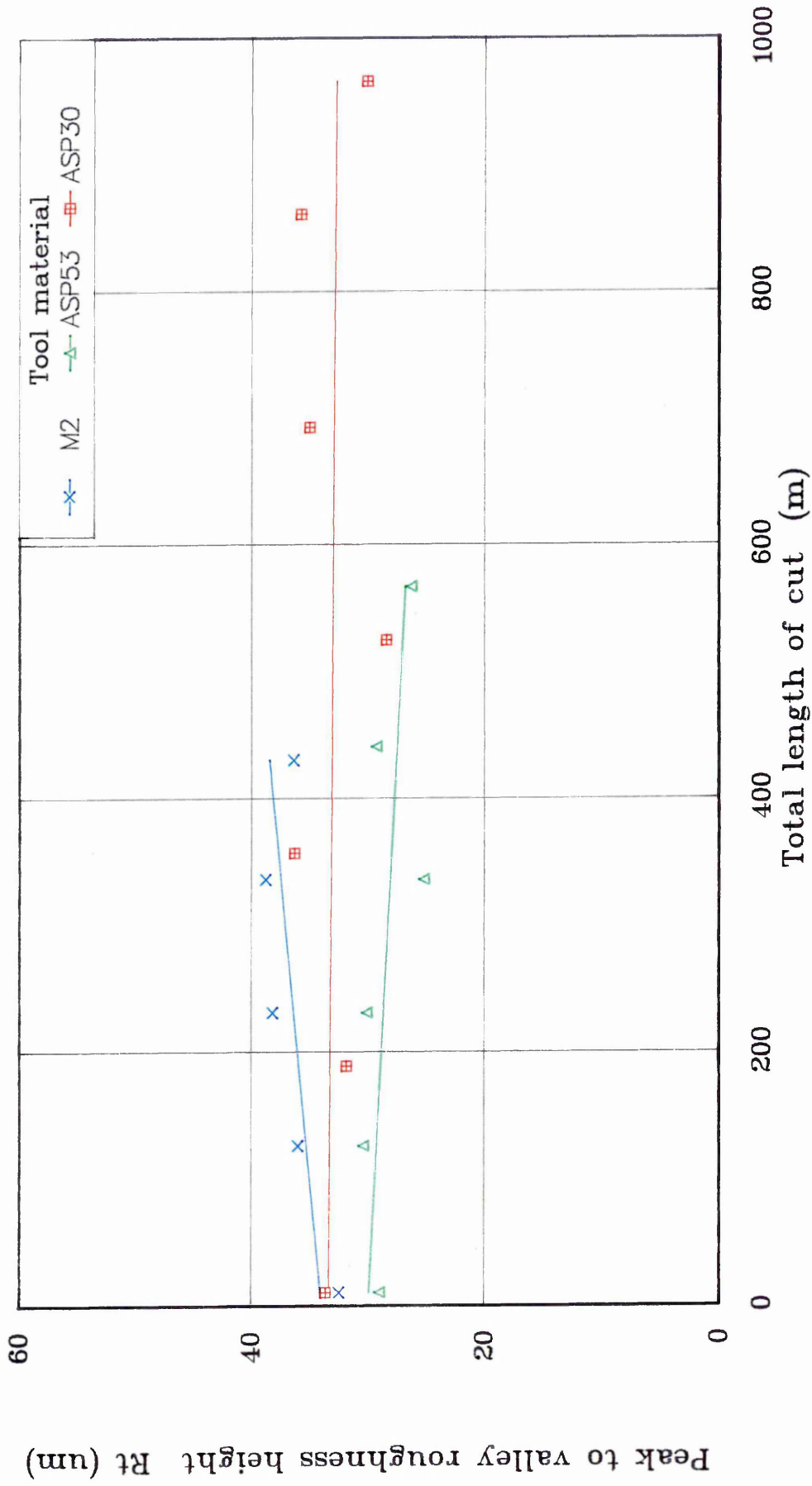


AS-131(940405)

Figure 5.10

# Effect of Tool-wear on Peak to Valley Height of Workpiece

Measured Perpendicular to the Direction of Cut (cutting speed : 10.5 m/min)

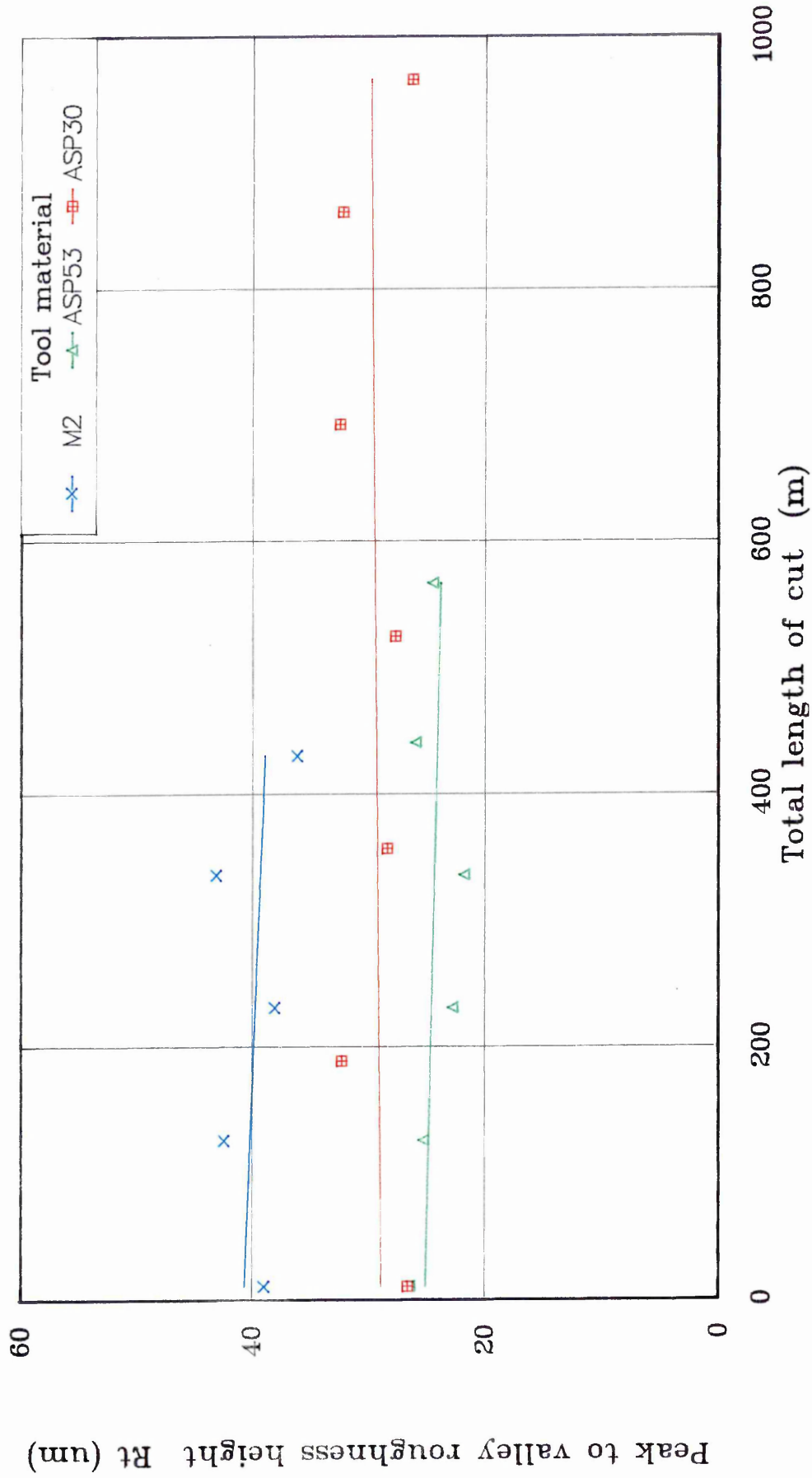


AS-13(940405)

Figure 5.11

# Effect of Tool-wear on Peak to Valley Height of Workpiece

Measured Parallel to the Direction of Cut (cutting speed : 10.5 m/min)



AS-131(940405)

Figure 5.12

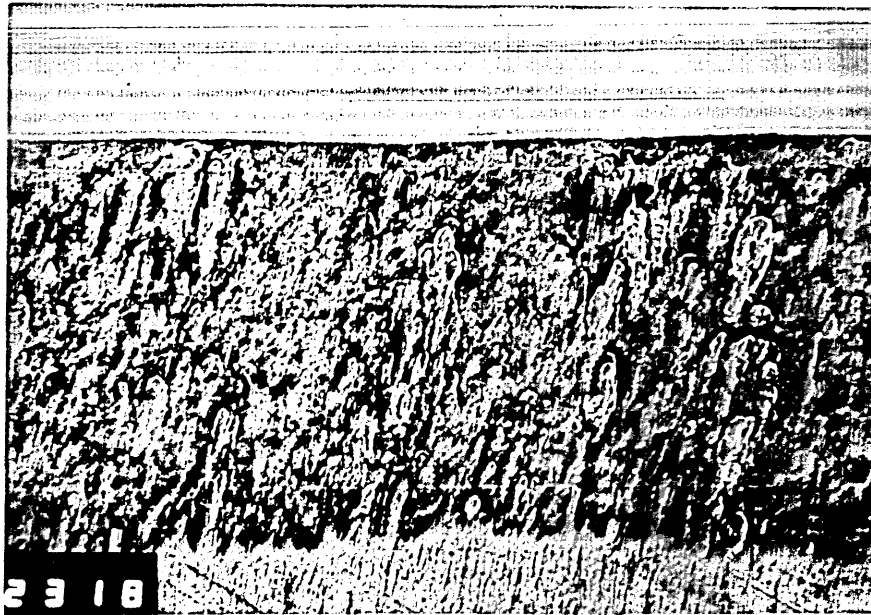


**Figure 5.13** A micrograph showing the wear scar on the clearance face of the ASP30 broach sample (x120).

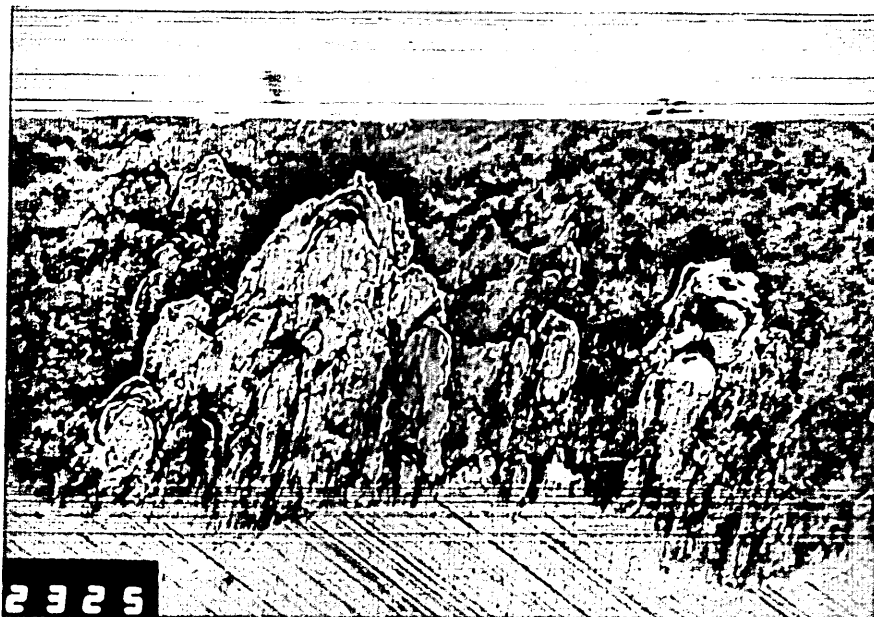


**Figure 5.14** A micrograph showing the adhesion of work material on the clearance face of the M2 broach sample (x120).

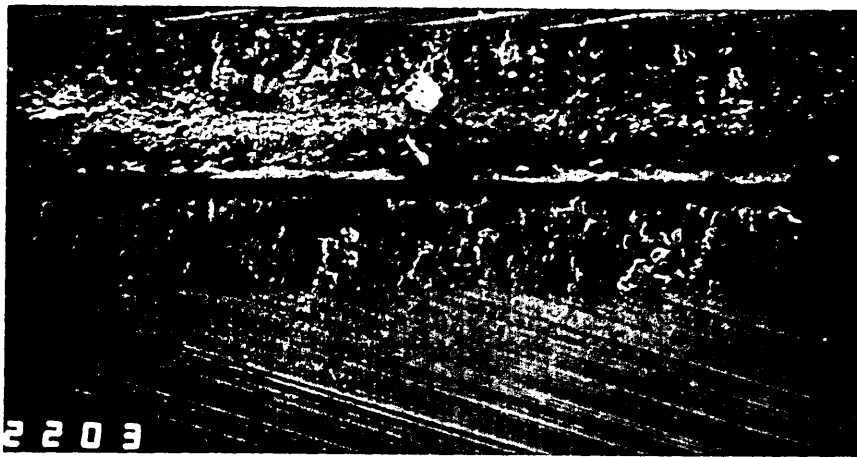


**Figure 5.15** A micrograph showing the chippings on the clearance face of the M2 broach sample (x75).



**Figure 5.16** A micrograph showing the chippings on the clearance face and adhesion of work material on the rake face of the ASP30 broach sample (x75).



**Figure 5.17** A micrograph showing the chippings on the clearance face of the ASP30 broach sample (x120).

**Table 4.1.** Clearance angle, rake angle, pitch, and depth of tooth of M2 high speed steel broach samples measured on the Hilger Universal Projector (x25).

Broach #	Clearance angle (deg.)		Rake angle (deg.)		Pitch (mm)	Depth (mm)
	Tooth 1	Tooth 2	Tooth 1	Tooth 2		
20961.1 <sup>*</sup>	3.9	3.9	11.5	11.5	9.78	4.57
20961.2	4.0	4.0	12.0	11.9	10.07	4.67
20961.3	3.9	4.2	12.0	12.2	10.0	4.91
20961.4	4.4	4.1	12.4	11.8	9.84	4.66
20961.5 <sup>•</sup>	3.7	3.5	12.0	11.5	9.45	4.65
20961.6 <sup>▪</sup>	3.8	3.4	11.7	11.9	9.43	4.64
Mean	3.9		11.9		9.76	4.68
$\sigma_n$	0.27		0.27		0.25	0.11

\* Broach sample used for wear test.

• Broach sample used for performance test at 0.7 m/min.

▪ Broach sample used for performance test at 10.5 m/min.

$\sigma_n$  = Standard deviation.

**Table 4.2.** Clearance angle, rake angle, pitch, and depth of tooth of ASP53 high speed steel broach samples measured on the Hilger Universal Projector (x25).

Broach #	Clearance angle (deg.)		Rake angle (deg.)		Pitch (mm)	Depth (mm)
	Tooth 1	Tooth 2	Tooth 1	Tooth 2		
1 <sup>▪</sup>	3.6	3.5	12.7	12.7	9.55	4.68
2	3.5	3.7	12.4	12.2	9.53	4.66
3 <sup>*</sup>	3.7	3.8	12.5	12.8	9.58	4.63
4	3.4	3.6	12.4	12.5	9.56	4.61
5 <sup>•</sup>	3.5	3.9	12.0	11.8	9.42	4.63
Mean	3.6		12.4		9.53	4.64
$\sigma_n$	0.15		0.30		0.06	0.03

<sup>▪</sup> Broach sample used for performance test at 10.5 m/min.

<sup>\*</sup> Broach sample used for wear test.

<sup>•</sup> Broach sample used for performance test at 0.7 m/min.

$\sigma_n$  = Standard deviation.

**Table 4.3.** Clearance angle, rake angle, pitch, and depth of tooth of ASP30 high speed steel broach samples measured on the Hilger Universal Projector (x25).

Broach #	Clearance angle (deg.)		Rake angle (deg.)		Pitch (mm)	Depth (mm)
	Tooth 1	Tooth 2	Tooth 1	Tooth 2		
19340.1*	3.9	3.9	12.1	12.2	9.74	4.5
19340.2 <sup>■</sup>	3.5	3.9	12.0	12.2	9.65	4.67
19340.3 <sup>•</sup>	3.9	4.0	12.2	12.0	9.46	4.66
19340.4	3.8	3.6	12.2	11.9	9.55	4.6
Mean	3.8		12.1		9.6	4.6
$\sigma_n$	0.2		0.1		0.1	0.07

\* Broach sample used for wear test.

<sup>■</sup> Broach sample used for performance test at 10.5 m/min.

<sup>•</sup> Broach sample used for performance test at 0.7 m/min.

$\sigma_n$  = Standard deviation.

**Table 4.4.** Surface roughness of M2 high speed steel broach samples measured on the rake and clearance (flank) faces in the directions perpendicular and parallel to the cutting edge. Numbers in parentheses represent Peak to Valley Roughness Height (Rt).

Broach #	Tooth #	Rake Roughness, [ $\mu\text{m}$ ]		Flank Roughness, [ $\mu\text{m}$ ]	
		Ra (Rt)	Ra (Rt)	Ra (Rt)	Ra (Rt)
		$\perp$ to edge	= to edge	$\perp$ to edge	= to edge
20961.1*	1	.80 (6.3)	.31 (2.4)	.26 (1.8)	.31 (1.8)
	2	1.2 (6.5)	.61 (2.9)	.21 (1.5)	.58 (1.6)
20961.2	1	.68 (4.9)	.38 (2.6)	.28 (2.0)	.30 (2.3)
	2	1.69 (11.0)	1.0 (5.2)	.29 (2.1)	.28 (1.9)
20961.3	1	1.26 (8.3)	.95 (5.2)	.27 (2.1)	.29 (2.0)
	2	1.54 (7.1)	.66 (4.3)	.32 (2.3)	.32 (2.2)
20961.4	1	1.9 (9.3)	1.1 (8.1)	.16 (1.3)	.16 (1.3)
	2	.85 (5.5)	.51 (3.9)	.15 (1.3)	.15 (1.1)
20961.5 <sup>•</sup>	1	.40 (3.3)	.23 (1.3)	.13 (1.2)	.12 (1.1)
	2	.65 (7.4)	.41 (5.3)	.14 (1.6)	.16 (1.5)
20961.6 <sup>■</sup>	1	.43 (3.6)	.34 (4.8)	.32 (3.1)	.25 (2.4)
	2	.75 (8.3)	.47 (5.8)	.28 (3.0)	.22 (3.1)
Mean		1.01 (6.8)	.58 (4.3)	.23 (1.9)	.26 (1.8)
$\sigma_n$		.47 (2.2)	.28 (1.7)	.07 (.6)	.12 (.5)

\* Broach sample used for wear test.

<sup>•</sup> Broach sample used for performance test at 0.7 m/min.

<sup>■</sup> Broach sample used for performance test at 10.5 m/min.

$\sigma_n$  = Standard deviation.

**TABLE 4.6.** Surface roughness of ASP30 high speed steel broach samples measured on the rake and clearance (flank) faces in the directions perpendicular and parallel to the cutting edge. Numbers in parentheses represent Peak to Valley Roughness Height (Rt).

Broach #	Tooth #	Rake Roughness, [ $\mu\text{m}$ ]		Flank Roughness, [ $\mu\text{m}$ ]	
		Ra (Rt)	Ra (Rt)	Ra (Rt)	Ra (Rt)
		$\perp$ to edge	= to edge	$\perp$ to edge	= to edge
19340.1*	1	1.54 (8.7)	.77 (5.2)	.26 (2.1)	.87 (6.6)
	2	1.1 (7.9)	1.07 (7.0)	.28 (2.2)	.27 (1.9)
19340.2 <sup>■</sup>	1	1.68 (8.1)	.98 (5.8)	.20 (1.6)	.24 (1.6)
	2	2.02 (10.7)	1.2 (8.4)	.27 (2.1)	.28 (1.9)
19340.3 <sup>•</sup>	1	1.35 (8.1)	1.07 (5.9)	.26 (2.1)	.22 (1.6)
	2	.97 (6.6)	.90 (5.1)	.24 (1.7)	.22 (1.7)
19340.4	1	1.3 (5.6)	.78 (3.6)	.25 (1.8)	.24 (1.8)
	2	1.39 (6.8)	1.02 (4.7)	.23 (1.8)	.20 (1.6)
Mean		1.42 (7.8)	.97 (5.7)	.25 (1.9)	.32 (2.3)
$\sigma_n$		.31 (1.4)	.14 (1.4)	.02 (.2)	.20 (1.6)

\* Broach sample used for wear test.

<sup>■</sup> Broach sample used for performance test at 10.5 m/min.

<sup>•</sup> Broach sample used for performance test at 0.7 m/min.

$\sigma_n$  = Standard deviation.